CSDL-T-920

FORMATIONKEEPING OF SPACECRAFT
VIA DIFFERENTIAL DRAG

by

Carolina Lee Leonard
S.B., Massachusetts Institute of Technology
(1984)

Submitted to the Department of Aeronautics
and Astronautics in partial fulfillment of the
requirements for the degree of
Master of Science

at the

Massachusetts Institute of Technology

July 1, 1986

NAS 9- 17560

The Charles Stark Draper Laboratory, Inc.

555 Technology Square
Cambridge, Massachusetts 02139

FORMATIONKEEPING
OF SPACECRAFT
VIA
DIFFERENTIAL DRAG

by

Carolina Lee Leonard

S.B., Massachusetts Institute of Technology

(1984)

SUBMITTED TO THE DEPARTMENT OF AERONAUTICS AND
ASTRONAUTICS IN PARTIAL FULFILLMENT OF THE
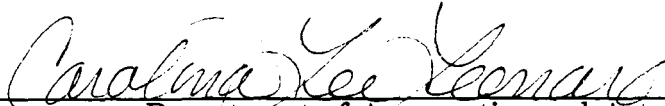REQUIREMENTS FOR THE DEGREE OF

MASTER OF SCIENCE

at the

MASSACHUSETTS INSTITUTE OF TECHNOLOGY
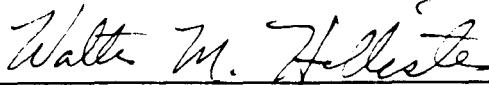
July 1, 1986

© Carolina Lee Leonard 1986

Signature of Author _____
Department of Aeronautics and Astronautics
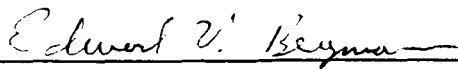July 1, 1986

Certified by _____
Professor Walter M. Hollister
Thesis Supervisor

Certified by _____
Edward V. Bergmann
CSDL Technical Supervisor

Accepted by _____
Professor Harold Y. Wachman
Chairman, Departmental Graduate Committee

i

FORMATIONKEEPING
OF SPACECRAFT
VIA
DIFFERENTIAL DRAG

by

Carolina Lee Leonard

submitted to the Department of Aeronautics and
Astronautics in partial fulfillment of the
requirements for the degree of Master of Science

ABSTRACT

This paper examines the use of differential drag in the formationkeeping of
spacecraft. In many future space missions one satellite will be required to fly
in a specific position with respect to another satellite; this action is referred to
as formationkeeping. In this study, differential drag is the difference in drag
between the two satellites. Reasons to use differential drag as an actuator for
formationkeeping include the avoidance of jet plume impingement effects on
closely spaced satellites and possible fuel savings.

The equations of relative motion between the two satellites are derived and
a mathematical transformation is made to reduce the formationkeeping problem
to the simultaneous solution of a double integrator and a harmonic oscillator.
A two-part control law is developed that simultaneously and dependently solves
the double oscillator and harmonic integrator. Results are presented of eight test
cases being driven to a target position; two different simulations are used. The
validity of assumptions made in the derivation of the control law is examined in
the comparison of similar test cases run through different simulations.

The control law developed can drive a satellite from an initial position to a
target position and maintain the satellite at that location.

Thesis Supervisor: Walter M. Hollister
Title: Professor of Aeronautics and Astronautics

ACKNOWLEDGEMENT

The production of this thesis would not have been possible without the technical and emotional support of others.

I would like to thank my Mother and Father for expecting great things from me. Thank you for giving me the strength to set my own goals and the courage to reach for them.

Professor Hollister's enthusiasm for this project was infectious. His technical abilities and intuition saved this thesis several times.

Ed Bergmann, my technical supervisor at Draper Lab, deserves acknowledgement for many things, but especially for being patient with me and for being a friend.

Bruce Persson was invaluable for his help in integrating the control law into the Draper Laboratory Space Systems Simulator.

Alex Gruzen trailblazed the way to a final thesis document; he learned the way through all the red tape (and the word processor!) and was kind enough to give me the benefit of his experience.

Contents

List of Figures

List of Tables

Chapter 1

Introduction

1.1 Formationkeeping

Several requirements exist for various spacecraft to fly in a certain position relative to a space station. Space tugs and orbital transfer vehicles may have to place themselves at certain positions with respect to the space station until they are required to perform some task. Space shuttles with replacement crews and new supplies may also have to orbit in specified positions relative to the station before they are allowed to dock. When one satellite must fly in a certain position with respect to another satellite, the two are flying in formation; the active measures taken to keep them in their relative positions is called formationkeeping. Two aspects of the formation flying problem are considered: the maneuvering of one spacecraft relative to another and the actual formationkeeping.

By convention, the satellite that takes active control measures to remain in a specific location relative to another spacecraft is called the slave satellite; the spacecraft that the slave is flying formation on is called the master satellite. When differential drag is used to formationkeep, both vehicles must take active measures to retain their relative positions. The space station will be referred to as the master satellite because the other spacecraft is flying in a certain position relative to it; the other spacecraft will then be referred to as the slave.

Controllers for formationkeeping were developed by R. Vassar and R. Sherwood [1] and D. Redding, N. Adams and E. Kukiak[2]. Both studies assumed that the actuators for formationkeeping were chemical thrusters on the slave satellite; the jets provided sufficiently high thrust to allow the control Δv's to be treated as impulsive changes in velocity. Thrust was available along all

1

three translational axes. The control laws were developed using optimal control to minimize fuel consumption. Reference [1] studied formationkeeping at equilibrium target positions and did not study large maneuvers to reach a target position. Reference [2] examined formationkeeping at both equilibrium and non-equilibrium target positions as well as maneuvers to reach a target position.

This thesis will investigate the feasiblility of formationkeeping using differential drag as the actuator. The amount of thrust that can be generated using differential drag is small and thus can not be modelled as impulsive. The use of drag as the actuator also restricts the direction of applied force to along the velocity vector. A phase plane approach to the development of the control law is used and the time to reach the target is minimized whenever possible. The reasons for examining the use of differential drag as an actuator for formationkeeping are explained in Section 1.3.

1.2   Differential Drag as an Actuator

Differential drag between a pair of satellites is the difference in drag acting upon each of the satellites. If the satellites are passing through similar density atmospheres, then any differential drag is due to different ballistic coefficients of the vehicles.

In this thesis it is assumed that the atmosphere is uniform; hence atmospheric density is the same at any location. It is also assumed that the ballistic coefficients of the satellites are initially equal. Differential drag is created through the use of drag plates attached to each of the satellites. The angle of attack of the drag plate can be changed from 0 to 90 degrees. When the drag plates of both spacecraft are at a zero angle of attack, no differential drag is created; this is referred to as zero differential drag. (Figure 1.1) Setting the angle of attack of the drag plate connected to the master satellite at 90 degrees and the angle of attack of the plate connected to the slave at 0 degrees, creates positive differential drag and acts as a thruster on the slave firing along the velocity vector. (Figure 1.2) Setting the angle of attack of the plate connected to the master at 0 degrees while the angle of attack of the plate connected to the slave at 90 degrees, creates negative differential drag and acts as a thruster on the slave firing opposite to the velocity vector. (Figure 1.3) If both the drag plates are at

a 90 degree angle of attack, no differential drag is created. (Figure 1.4) When both drag plates are at 90 degrees, the system orbit decays more rapidly than if both plates were at 0 degrees; thus if zero differential drag is desired, both drag plates will be commanded to a 0 degree angle of attack.

Different combinations of the angles of attack of the drag plates can thus act as thrusters on the slave pointed in both directions along the velocity vector.

1.3 Formationkeeping via Differential Drag

Formationkeeping can be accomplished by using either jets or differential drag as the actuators for the control scheme. Reasons to use differential drag rather than jet firings as an actuator include:

- plumes from jet firings may impinge upon the master satellite, imparting some undesired motion or contaminating solar panels.

- an impulsive jet firing may disturb a manufacturing process on the slave satellite; the accelerations created by differential drag are much smaller than those that arise from jet firings.

- possible fuel savings.

This study examines the formationkeeping of spacecraft via differential drag. Several assumptions are made in the formulation of the problem: it is assumed that the drag plates are attached to the vehicles directly behind their centers of mass so that a change of angle of attack of the drag plate does not affect the attitude of the satellite; the angle of the drag plate can be changed instantaneously; and the two vehicles are at similar altitudes so that there is no difference in atmospheric density.

The desired position of the slave satellite with respect to the master will be referred to as the target position or origin. The purpose of this thesis is to derive a control law that will use differential drag to drive a slave satellite to the target position. It is assumed that the target point is an equilibrium point not requiring thrust.

←—————— velocity vector
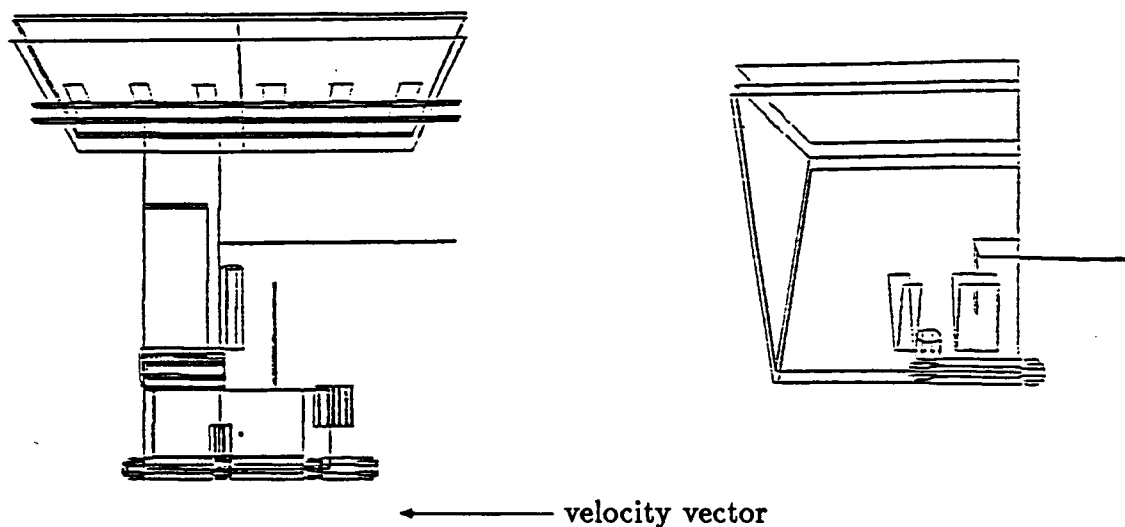
Figure 1.1: *Drag plates of both the master and slave set to 0 degree angles of attack, causing zero differential drag.*

←—————— velocity vector
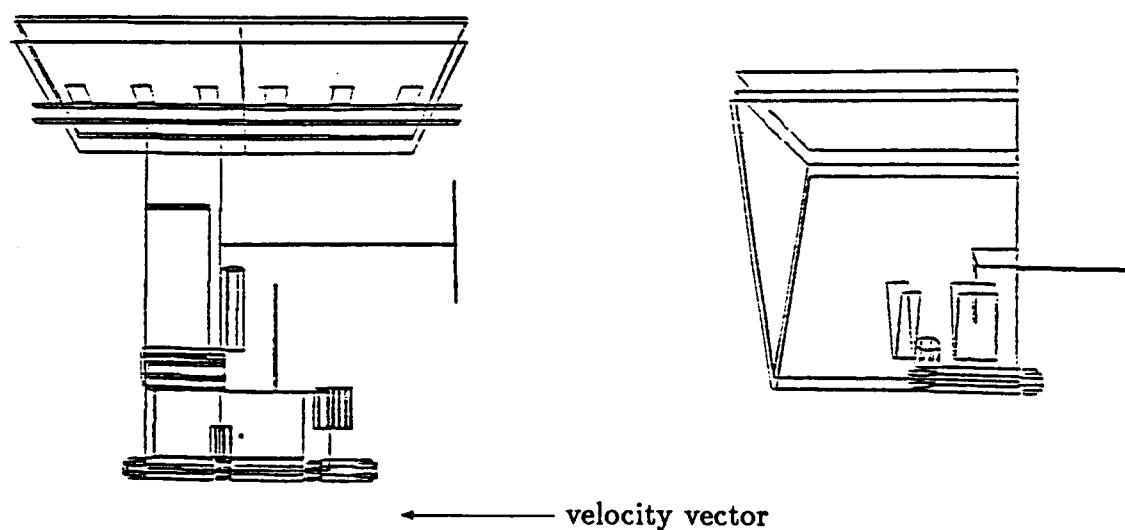
Figure 1.2: *The angle of attack of the plate connected to the master set to 90 degrees, and the angle of attack of the plate connected to the slave set to 0 degrees, causing positive differential drag.*

———————— velocity vector
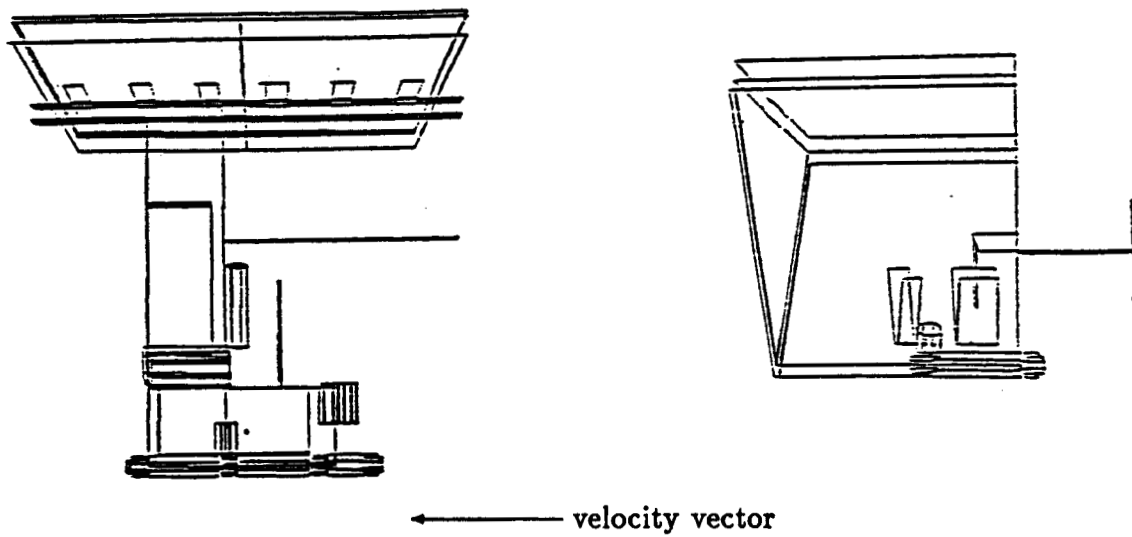
Figure 1.3: *The angle of attack of the plate connected to the master set to 0 degrees, and the angle of attack of the plate connected to the slave set to 90 degrees, causing negative differential drag.*

———————— velocity vector
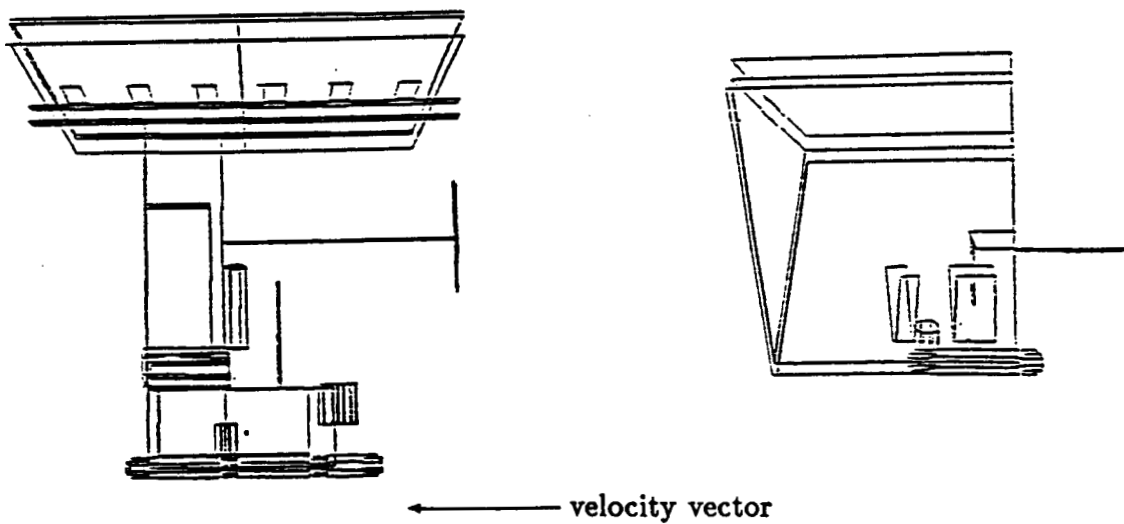
Figure 1.4: *Drag plates of both the master and slave set to 90 degree angles of attack, causing zero differential drag.*

1.4   Outline of Thesis

Chapter 2 contains the derivation of the equations of motion for the slave satellite with respect to the target. The equations of motion are then solved for a constant applied force. A transformation is derived which relates the relative position and velocity of the slave to its average relative position and eccentricity; this transformation allows the formationkeeping problem to be cast as the simultaneous solution of a double integrator and a harmonic oscillator.

Chapter 3 discusses the phase plane solutions to both the double integrator and the harmonic oscillator. Both are well known problems and are covered only briefly.

Chapter 4 explains the derivation of the two-part control law for the formationkeeping problem. The main control law is used to drive the average position of the slave to that of the target while not increasing eccentriciy any more than necessary. The object of the gamma control scheme is to reduce the eccentricity of the slave as much as possible without altering its final average position. This section describes in detail both the main and gamma control schemes and how they interact.

Chapter 5 shows the verification of the control law through simulation. The test cases are described and the simulations explained. Results are presented of eight test cases being driven to a target position; two different simulations are used. The validity of assumptions made in the derivation of the control law is examined in the comparison of similar test cases run through different simulations. The issue of how differential drag can be used to keep the slave at the target is also addressed.

The conclusions and recommendations for further work are contained in **Chapter 6.**

Chapter 2

Derivation of Equations of Motion

2.1 Introduction

This chapter describes the coordinate systems used in the formationkeeping problem and the derivation of the equations of motion. The target reference frame is discussed in Section 2.2. Hill's Equations are developed in Section 2.3 and the solutions to the force free and constant force equations are shown in Section 2.4. The transformation from target reference to $\bar{y}$ coordinates is explained in Section 2.5.

2.2 Target Reference Frame

The desired position of a satellite, also known as the target position, will be the center of the target reference coordinate system. The x direction will be measured along the radius vector to the target from the center of the earth, with the direction away from the earth being positive. The y direction will be measured along the velocity vector of the target with the positive direction corresponding to positive velocity. The third axis, z, is normal to the orbit plane, forming a right handed coordinate system. (Figure 2.1)

2.3 Derivation of Hill's Equations [3]

From Newton's second law it is known that the forces on the slave satellite,

7
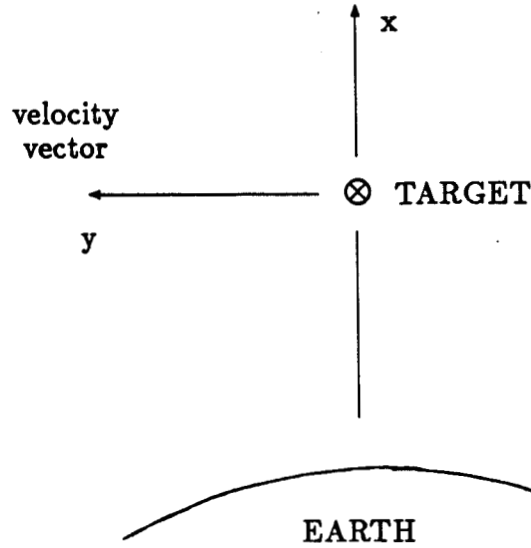
Figure 2.1: *Target reference frame.*

per unit mass, are equal to the acceleration of the slave in inertial space.

$$\ddot{R} = \frac{1}{M} \sum forces\ on\ slave\ satellite \tag{2.1}$$

where $\vec{R} = x\vec{i} + y\vec{j}$ is the position vector of the slave satellite relative to the target. The z component of the position vector is zero because it is assumed that no changes will be made to the orbital inclination; this assumption reduces the problem to a planar one. Equation 2.1 can be rewritten

$$\ddot{R} = \vec{F} - \frac{GM}{R^3}\vec{R} \tag{2.2}$$

where $\vec{F}$ constitues any non-gravitational force, per unit mass, applied to the slave and can be written as $\vec{F} = \vec{F_x} + \vec{F_y}$. The second term is due to Earth's gravitational acceleration on the slave, where G is the gravitational constant and M is the mass of the earth. Equation 2.2 can be separated into components:

$$\ddot{R} = \left(F_x - \frac{GM}{R^3}x\right)\vec{i} + \left(F_y - \frac{GM}{R^3}y\right)\vec{j} \tag{2.3}$$

$\ddot{R}$ may also be calculated by differentiating the position vector twice, which yields

$$\ddot{R} = \left(\ddot{x} - 2\dot{n}y - n^2x\right)\vec{i} + \left(\ddot{y} + 2n\dot{x} - n^2y\right)\vec{j} \tag{2.4}$$

where n is the orbital rate. Equating coordinates of the right hand sides of equations 2.3 and 2.4 produces:

$$\ddot{x} = \left(n^2 - \frac{GM}{R^3} \right) x + 2n\dot{y} + F_x \qquad (2.5)$$

$$\ddot{y} = \left(n^2 - \frac{GM}{R^3} \right) y - 2n\dot{x} + F_y \qquad (2.6)$$

The coordinates of the target are, by definition,

$$x_{target} = \rho \qquad (2.7)$$

$$y_{target} = 0 \qquad (2.8)$$

where ρ is the radius of the target from the center of the earth. Hence, the position of the slave satellite in inertial coordinates is

$$x_{slave} = x + \rho \qquad (2.9)$$

$$y_{slave} = y . \qquad (2.10)$$

It follows that the R^3 quantity in equations 2.5 and 2.6 may be rewritten as

$$R^3 = \left((x + \rho)^2 + y^2 \right)^{\frac{3}{2}} \qquad (2.11)$$

Since ρ is on the order of 270 nautical miles, x is on the order of 1000 feet, and y at most on the order of 10,000 feet, it is safe to state that $\rho \gg x, y$. With this assumption, the following approximations are valid:

$$\frac{GM}{\left((x + \rho)^2 + y^2 \right)^{\frac{3}{2}}} y \approx -\frac{GM}{\rho^3} y \qquad (2.12)$$

$$\frac{GM}{\left((x + \rho)^2 + y^2 \right)^{\frac{3}{2}}} (x + \rho) \approx -\frac{GM}{\rho^3 \left(1 + \frac{x}{\rho} \right)^3} (x + \rho) \qquad (2.13)$$

A binomial expansion of equation 2.13 leads to

$$\frac{GM}{\left((x + \rho)^2 + y^2 \right)^{\frac{3}{2}}} (x + \rho) \approx -\frac{GM}{\rho^3} (\rho - 2x) \qquad (2.14)$$

Using Kepler's Third Law and the above approximations, equations 2.5 and 2.6 may be rewritten as

$$\ddot{x} = 2n\dot{y} + 3n^2x + F_x \qquad (2.15)$$

$$\ddot{y} = -2n\dot{x} + F_y \qquad (2.16)$$

which are commonly referred to as Hill's Equations for forced motion. George William Hill used the restricted problem of three bodies in astrodynamics and rewrote the equations of motion in a rotating coordinate frame. The differential equations he derived are equivalent to an infinite number of algebraic linear equations; these results were published in 1878 in the first issue of the *American Journal of Mathematics*[4].

The assumptions used in obtaining Hill's Equations were:

- $\sqrt{x^2 + y^2}$ is small compared to ρ. With x on the order of 1000 feet, y at most on the order of 10,000 feet and ρ on the order of 270 nautical miles, this is a safe assumption.

- $\vec{F}$ is small. The magnitude of the acceleration per unit mass available from differential drag is on the order of 5.5×10^{-6} ft/sec^2.

- Eccentricity is small. In the formulation of the problem we have stated that the target is in a circular orbit and the slave satellite has a small eccentricity.

- The orbital rate is approximately constant. The target is in a circular orbit therefore this condition is met.

The errors in Hill's Equations are on the order of $\sqrt{x^2 + y^2}$. Since we have already determined that this quantity is small, the errors should be small.

2.4   Solutions to Hill's Equations

Solutions were found for Hill's Equations in the force free and constant force cases.

2.4.1 Force Free Solution

With no applied force, Hill's equations become:

$$\ddot{x} - 2n\dot{y} - 3n^2 x = 0 \tag{2.17}$$

$$\ddot{y} + 2n\dot{x} = 0 \ . \tag{2.18}$$

commonly known as the Clohessy-Wiltshire equations. The force free solution to Hill's equations appeared concurrently in two different sources. The chapter "Midcourse and Terminal Guidance" written by A. Wheelon in the book *Space Technology* contains the force free solutions; the book was published in the summer of 1959 [5]. The solutions also appeared in a paper published by W. Clohessy and R. Wiltshire in the September 1960 issue of the *Journal of Aerospace Science*; the paper was first presented at the Space Flight Session of the IAS National Summer Meeting in Los Angeles in June of 1959 [6].

Integrating equation 2.18 and substituting it into 2.17 produces the following differential equation:

$$\ddot{x} + n^2 x = 2n(\dot{y}_0 + 2n x_0) \tag{2.19}$$

where y_0 is the initial condition for y, and x_0 is the initial condition for x.

Equation 2.19 can be solved for x, and that expression substituted into equations 2.17 and 2.18 to obtain an expression for y. x and y can then be differentiated to get the values for $\dot{x}$ and $\dot{y}$.

The equations for the unforced positions and accelerations, in terms of initial conditions and accelerations, are given in state variable form below.

$$
\begin{bmatrix} x \\ y \\ \dot{x} \\ \dot{y} \end{bmatrix} =
\begin{bmatrix}
4 - 3\cos nt & 0 & \frac{1}{n}\sin nt & -\frac{2}{n}\cos nt + \frac{2}{n} \\
6\sin nt - 6nt & 1 & \frac{2}{n}\cos nt - \frac{2}{n} & \frac{4}{n}\sin nt - 3t \\
3n\sin nt & 0 & \cos nt & 2\sin nt \\
6n\cos nt - 6n & 0 & -2\sin nt & 4\cos nt - 3
\end{bmatrix}
\begin{bmatrix} x_0 \\ y_0 \\ \dot{x}_0 \\ \dot{y}_0 \end{bmatrix}
\tag{2.20}
$$

2.4.2 Constant Force Solution [7]

The solution to Hill's equations for a constant applied force was found using the method of variation of constants. It is:

$$
\vec{x}(t) = \phi \vec{x}_0 + \int_{t_0}^{t} \left\{
\begin{bmatrix} \frac{1}{n}\sin nt \\ \frac{2}{n}\cos nt - \frac{2}{n} \\ \cos nt \\ -2\sin nt \end{bmatrix} F_x +
\begin{bmatrix} -\frac{2}{n}\cos nt + \frac{2}{n} \\ \frac{4}{n}\sin nt - 3t \\ 2\sin nt \\ 4\cos nt - 3 \end{bmatrix} F_y
\right\} d\tau
\tag{2.21}
$$

where

$$\phi = \begin{bmatrix} 4 - 3\cos nt & 0 & \frac{1}{n}\sin nt & -\frac{2}{n}\cos nt + \frac{2}{n} \\ 6\sin nt - 6nt & 1 & \frac{2}{n}\cos nt - \frac{2}{n} & \frac{4}{n}\sin nt - 3t \\ 3n\sin nt & 0 & \cos nt & 2\sin nt \\ 6n\cos nt - 6n & 0 & -2\sin nt & 4\cos nt - 3 \end{bmatrix} \qquad (2.22)$$

2.5   Transformation to $\bar{y}$ Coordinates

From equations 2.21 and 2.22 it can be seen that the average value of x over time is

$$\bar{x} = 4x_0 + \frac{2\dot{y}_0}{n} + \frac{2at}{n} \qquad (2.23)$$

and that the average value for y over time is

$$\bar{y} = y_0 - \frac{2\dot{x}_0}{n} - 3\left[4x_0 + \frac{2\dot{y}_0}{n}\right]nt - \frac{3}{2}at^2. \qquad (2.24)$$

Note that

$$4x = -\left(12x_0 + 8\frac{\dot{y}_0}{n}\right)\cos nt + \left(4\frac{\dot{x}_0}{n} - 8\frac{a}{n^2}\right)\sin nt + \left(16x_0 + 8\frac{\dot{y}_0}{n}\right) + \frac{8at}{n} \quad (2.25)$$

and that

$$\frac{2\dot{y}}{n} = \frac{4}{n}\left(\frac{2a}{n} - \dot{x}_0\right)\sin nt + \frac{4}{n}(3x_0n + 2\dot{y}_0)\cos nt - \frac{6}{n}(2x_0n + \dot{y}_0) - \frac{6at}{n} \quad (2.26)$$

summing equations 2.25 and 2.26 and combining terms gives

$$4x + \frac{2\dot{y}}{n} = 4x_0 + \frac{2\dot{y}_0}{n} + \frac{2at}{n} \qquad (2.27)$$

Similarly, if we note that

$$y = \left(2\frac{\dot{x}_0}{n} - 4\frac{a}{n^2}\right)\cos nt + \left(6x_0 + 4\frac{\dot{y}_0}{n}\right)\sin nt$$

$$+ y_0 - \left(2\frac{\dot{x}_0}{n} - 4\frac{a}{n^2}\right) - \left(6x_0 + 3\frac{\dot{y}_0}{n}\right)nt - \frac{3}{2}at^2 \qquad (2.28)$$

and that

$$-\frac{2\dot{x}}{n} = \left(-6x_0 - 4\frac{\dot{y}_0}{n}\right)\sin nt + \left(-2\frac{\dot{x}_0}{n} + 4\frac{a}{n^2}\right)\cos nt - \frac{4a}{n^2} \qquad (2.29)$$
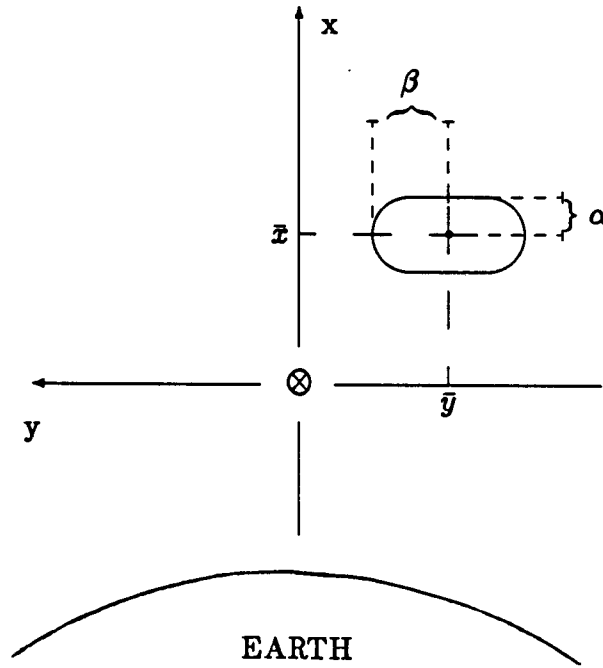
Figure 2.2: $\bar{y}$ coordinate frame.

summing equations 2.28 and 2.29 and combining terms gives

$$y - \frac{2\dot{x}}{n} = y_0 - \frac{2\dot{x}_0}{n} - 3\left(4x_0 + \frac{2\dot{y}_0}{n}\right)nt - \frac{3}{2}at^2. \tag{2.30}$$

Combining equations 2.23 and 2.27 gives the average value for x,

$$\bar{x} = 4x + \frac{2\dot{y}}{n} \tag{2.31}$$

and combining equations 2.24 and 2.30 gives the average value for y

$$\bar{y} = y - \frac{2\dot{x}}{n} \tag{2.32}$$

With the average values for x and y known, α is defined as the difference between the actual x position and $\bar{x}$ at any point in time,

$$\alpha = x - \bar{x} \tag{2.33}$$

and β is defined as the difference between the actual y position and $\bar{y}$ at any point in time. (Figure 2.2)

$$\beta = y - \bar{y} \tag{2.34}$$

It follows that

$$\alpha = -3x - \frac{2\dot{y}}{n} \tag{2.35}$$

and

$$\beta = \frac{2\dot{x}}{n} \tag{2.36}$$

Differentiating $\bar{y}$ twice:

$$\ddot{\bar{y}} = \ddot{y} - \ddot{\beta} \tag{2.37}$$

Substituting in the value of $\ddot{y}$ from equation 2.16 gives

$$\ddot{\bar{y}} + \ddot{\beta} = a - n^2\beta \tag{2.38}$$

Differentiating equation 2.26 twice:

$$\ddot{\beta} = \frac{2\ddot{x}}{n} \tag{2.39}$$

Differentiating equation 2.15 and substituting in for the value of $\ddot{x}$ gives

$$\ddot{\beta} = 4\ddot{y} + 6n\dot{x} \tag{2.40}$$

Substituting equation 2.27 into the above equation leads to

$$4\ddot{\bar{y}} = -3\ddot{\beta} - 3n^2\beta \tag{2.41}$$

The substitution of equation 2.28 into 2.31 keeping $\bar{y}$ produces

$$\ddot{\bar{y}} = -3a \tag{2.42}$$

where the substitution of equation 2.28 into 2.31 keeping β yields

$$\ddot{\beta} + n^2\beta = 4a \tag{2.43}$$

Noting that

$$\dot{\beta} = -2n\alpha \tag{2.44}$$

and that

$$\dot{\bar{y}} = -\frac{3n\bar{x}}{2} \tag{2.45}$$

allows us to solve two equations, 2.42 and 2.43, and drive four states, β, α, $\bar{y}$ and $\bar{x}$, to the origin. Driving β, α, $\bar{y}$ and $\bar{x}$ to the origin correspondingly drives x, y, $\dot{x}$ and $\dot{y}$ to the origin. Equation 2.42 corresponds to a double integrator and equation 2.43 corresponds to a harmonic oscillator.

Chapter 3

Control Laws for the Double Integrator and Harmonic Oscillator

3.1 Introduction

Control laws must be developed for the simultaneous control of two separate and different equations. A phase plane approach is used for the control of each. The two phase planes must then be combined in such a way that a single control law can drive all four states to the origin.

The two equations for which phase plane control laws are developed were derived in Section 2.5. They are

$$\ddot{y} = -3a \tag{3.1}$$

$$\ddot{\beta} + n^2\beta = 4a \tag{3.2}$$

Equation 3.1 is a double integrator which describes the average position of the slave with respect to the target. Section 3.2 will develop the solution for the double integrator. Section 3.3 will discuss equation 3.2 which is a harmonic oscillator and describes the eccentricity of the slave with respect to the target. Both problems are well known and will not be covered extensively in this chapter. The reader not familiar with optimal control techniques is referred to references [8] and [9]. The two control laws will be combined in Chapter 4.

Three major assumptions were used in the development of these control laws:

- The switch curves for equations 3.1 and 3.2 were developed so that the systems would be time optimal. It was assumed that the required level of drag is essentially free and does not contribute greatly to the degradation of the system orbit.

- It was assumed that the value of the differential drag was either a, 0 or $-a$, in essence a bang-bang controller. Here, a is the amount of drag produced by the drag plate at 90 degrees to the relative wind. Because the value of the acceleration due to the drag plates is quite small, 54×10^{-6} ft/s^2, it was assumed that the entire available commanded acceleration would be used to execute maneuvers.

- The change of angle of attack of a drag plate was assumed to be instantaneous and not to impart any change of attitude to the vehicle to which it is attached.

3.2   Control of the Double Integrator [8]

From the equation for the double integrator,

$$\ddot{\bar{y}} = -3a \tag{3.3}$$

define

$$x_1 = \bar{y} \tag{3.4}$$

$$x_2 = \dot{\bar{y}} \tag{3.5}$$

It follows that

$$\dot{x}_1 = x_2 \tag{3.6}$$

$$\dot{x}_2 = -3a \tag{3.7}$$

A unique time optimal control exists for a double integrator. The cost function associated with a minimum time trajectory is

$$J = \int dt \tag{3.8}$$

Thus the Hamiltonian for this system may be written

$$H = 1 + x_2 p_1 - 3a p_2 \tag{3.9}$$

For H to be a minimum it follows that

$$a = sign(p_2) = \Delta \tag{3.10}$$

The *Euler-Lagrange equations* produce

$$\dot{p}_1 = -\frac{\partial H}{\partial x_1} = 0 \tag{3.11}$$

$$\dot{p}_2 = -\frac{\partial H}{\partial x_2} = -p_1 \tag{3.12}$$

Solving these,

$$p_1 = const = \pi_1 \tag{3.13}$$

and

$$p_2 = -p_1 t + const = \pi_2 - \pi_1 t \tag{3.14}$$

where $p_1(0) = \pi_1$ and $p_2(0) = \pi_2$. Thus in a plot of p_2 vs t, p_2 is a straight line. The control, a, is dependent on the sign of p_2. Since p_2 is a straight line, then the optimal control can switch at most once.

Let

$$x_1(0) = \varsigma_1 \tag{3.15}$$

$$x_2(0) = \varsigma_2 \tag{3.16}$$

Then

$$x_1(t) = \varsigma_1 + \varsigma_2 t + \frac{3}{2}\Delta t^2 \tag{3.17}$$

$$x_2(t) = \varsigma_2 + 3\Delta t \tag{3.18}$$

Solving equation 3.18 for t gives

$$t = \frac{x_2 - \varsigma_2}{3\Delta} \tag{3.19}$$

Substituing equation 3.19 into equation 3.17 gives

$$x_1 = \varsigma_1 + \frac{x_2^2}{6\Delta} - \frac{\varsigma_2^2}{6\Delta} \tag{3.20}$$

Equation 3.20 describes parabolic trajectories in the x_1, x_2 plane that originate at ς_1 and ς_2, subject to the control action Δ. (Figure 3.1.)
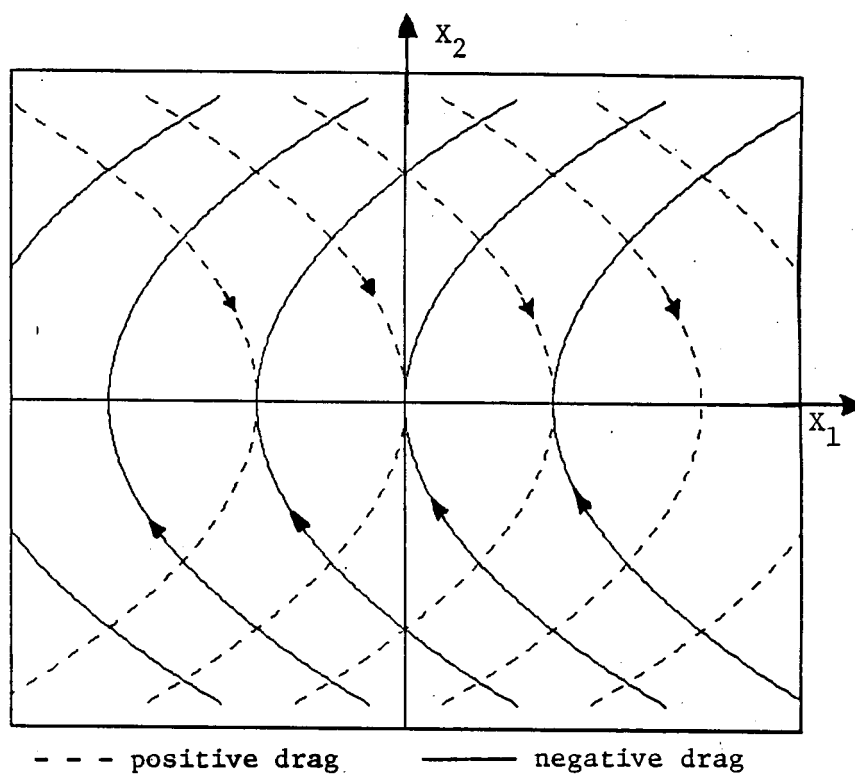
Figure 3.1: *Trajectories in the x_1, x_2 plane for control action Δ*
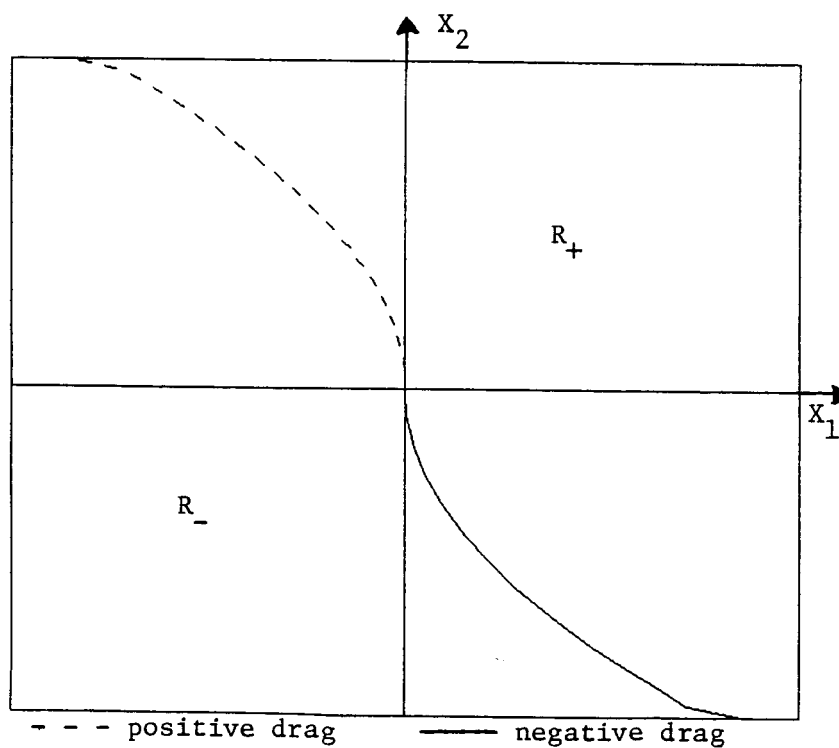
Figure 3.2: *Switch curve for the double integrator.*

The initial conditions for which a constant control drives the state to the origin are shown in Figure 3.2. For time optimal control, the commanded differential drag for any initial position on the dotted line or in the R_+ region would be positive a (along the velocity vector). Negative a (opposite to the velocity vector), would be the commanded differential drag for an initial position on the solid switch curve or in the R_- region.

3.3 Control of the Harmonic Oscillator [9]

From the equation for the harmonic oscillator

$$\ddot{\beta} + n^2\beta = 4a \tag{3.21}$$

define

$$y_1 = \beta \tag{3.22}$$

$$y_2 = \dot{\beta} \tag{3.23}$$

Then define

$$x_3 = \frac{n}{4}y_1 \tag{3.24}$$

$$x_4 = \frac{1}{4}y_2 \tag{3.25}$$

Equations 3.24 and 3.25 may be written as

$$\dot{\vec{x}} = \begin{bmatrix} 0 & n \\ -n & 0 \end{bmatrix} \vec{x} + \begin{bmatrix} 0 \\ 1 \end{bmatrix} a \tag{3.26}$$

The eigenvalues for the above A matrix are complex, which implies an oscillating state; this suggests that the appropriate control is also oscillating.

The state transition matrix for the unforced system is given by

$$\Phi(t) = \begin{bmatrix} \cos nt & \sin nt \\ -\sin nt & \cos nt \end{bmatrix} \tag{3.27}$$

If $x_3(0) = \varsigma_3$ and $x_4(0) = \varsigma_4$, then

$$\begin{bmatrix} x_3(t) \\ x_4(t) \end{bmatrix} = \begin{bmatrix} \cos nt & \sin nt \\ -\sin nt & \cos nt \end{bmatrix} \begin{bmatrix} \varsigma_3 \\ \varsigma_4 \end{bmatrix} \tag{3.28}$$

Squaring the equations for $x_3(t)$ and $x_4(t)$ in equation 3.28 and summing gives

$$x_3^2(t) + x_4^2(t) = \varsigma_3^2 + \varsigma_4^2 = const \tag{3.29}$$

Equation 3.29 shows that the trajectories of the unforced system are circles of radius $\sqrt{\varsigma_3^2 + \varsigma_4^2}$ centered at the origin of the $x_3 n, x_4 n$ plane.

A time optimal control exists for a harmonic oscillator. The cost function associated with a minimum time trajectory is

$$J = \int dt \tag{3.30}$$

Thus the Hamiltonian for the forced equation is

$$H = 1 + x_4 n p_3 - x_3 n p_4 + a p_4 \tag{3.31}$$

It follows that the control to minimize H is

$$a = -sign(p_4) = \Delta \tag{3.32}$$

The *Euler-Lagrange equations* produce

$$\dot{p_3} = -\frac{\partial H}{\partial x_3} = n p_4 \tag{3.33}$$

$$\dot{p_4} = -\frac{\partial H}{\partial x_4} = -n p_3 \tag{3.34}$$

Equations 3.33 and 3.34 can be written in state space form as

$$\vec{p} = \begin{bmatrix} 0 & n \\ -n & 0 \end{bmatrix} \vec{p} \tag{3.35}$$

The solution the equation 3.35 is

$$\begin{bmatrix} p_3(t) \\ p_4(t) \end{bmatrix} = \begin{bmatrix} \cos nt & \sin nt \\ -\sin nt & \cos nt \end{bmatrix} \begin{bmatrix} \pi_1 \\ \pi_2 \end{bmatrix} \tag{3.36}$$

where $p_3(0) = \pi_1$ and $p_4(0) = \pi_2$.

The time optimal control a goes as minus the sign of p_4. It can be seen from equation 3.36 that p_4 is the sum of two sinusoids, or equivalently,

$$p_4(t) = r \sin(nt + \varsigma) \tag{3.37}$$

It follows that the time optimal control can remain constant for no more than π/n units of time.

The solution to the forced equation 3.26 is

$$\begin{bmatrix} x_3(t) \\ x_4(t) \end{bmatrix} = \Phi x_0 + \int_0^\tau \Phi(t - \tau) B\Delta \ d\tau \tag{3.38}$$

Noting that both B and Δ are independent of time, let

$$Q = \begin{bmatrix} q_1 \\ q_2 \end{bmatrix} = B\Delta \int_0^\tau \Phi(t-\tau) \ d\tau \tag{3.39}$$

$$\Phi(t-\tau) = \begin{bmatrix} \cos n(t-\tau) & \sin n(t-\tau) \\ -\sin n(t-\tau) & \cos n(t-\tau) \end{bmatrix} \tag{3.40}$$

Using trigonometric addition formulas, it follows that

$$\Phi(t-\tau) = \begin{bmatrix} \cos nt \cos n\tau + \sin nt \sin n\tau & \sin nt \cos n\tau - \cos nt \sin n\tau \\ -\sin nt \cos n\tau + \cos nt \sin n\tau & \cos nt \cos n\tau + \sin nt \sin n\tau \end{bmatrix} \tag{3.41}$$

Integrating equation 3.41 produces

$$\int \Phi(t-\tau) = \frac{1}{n} \begin{bmatrix} \cos nt \sin n\tau - \sin nt \cos n\tau & \sin nt \sin n\tau + \cos nt \cos n\tau \\ -\sin nt \sin n\tau - \cos nt \cos n\tau & \cos nt \sin n\tau - \sin nt \cos n\tau \end{bmatrix} \tag{3.42}$$

Substitution of equation 3.42 into equation 3.39 gives that

$$Q = \begin{bmatrix} 0 & \frac{1}{n}\left(\sin^2 nt + \cos^2 nt\right) \\ -\frac{1}{n}\left(\sin^2 nt + \cos^2 nt\right) & 0 \end{bmatrix} \begin{bmatrix} 0 \\ \Delta \end{bmatrix}$$
$$- \begin{bmatrix} -\sin nt & \cos nt \\ -\cos nt & -\sin nt \end{bmatrix} \begin{bmatrix} 0 \\ \frac{\Delta}{n} \end{bmatrix} \tag{3.43}$$

which simplifies to

$$Q = \begin{bmatrix} \Delta/n \\ 0 \end{bmatrix} - \frac{\Delta}{n} \begin{bmatrix} \cos nt \\ -\sin nt \end{bmatrix} \tag{3.44}$$

Substituting equation 3.44 into equation 3.38 gives

$$\begin{bmatrix} x_3(t) \\ x_4(t) \end{bmatrix} = \Phi x_0 + Q \tag{3.45}$$

The separate equations for x_3 and x_4 are

$$x_3(t) = \left(\varsigma_3 - \frac{\Delta}{n}\right) \cos nt + \varsigma_4 \sin nt + \frac{\Delta}{n} \tag{3.46}$$

$$x_4(t) = -\left(\varsigma_3 - \frac{\Delta}{n}\right) \sin nt + \varsigma_4 \cos nt \tag{3.47}$$

Multiplying equations 3.46 and 3.47 by n gives

$$x_3 n(t) = (n\varsigma_3 - \Delta)\cos nt + n\varsigma_4 \sin nt + \Delta \tag{3.48}$$

- - - positve drag   ———— negative drag
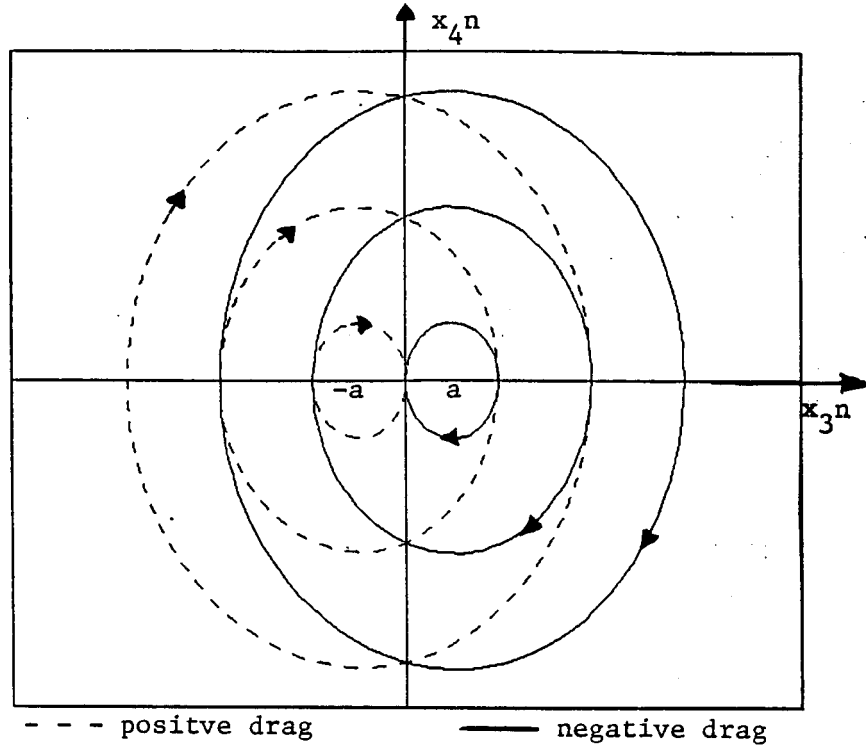
Figure 3.3: *Trajectories in the x_3n, x_4n plane for control action Δ*

$$x_4n\left(t\right) = -\left(n\varsigma_3 - \Delta\right)\sin nt + n\varsigma_4\cos nt \tag{3.49}$$

Squaring both sides of equations 3.48 and 3.49 and rearranging produces

$$\left(x_3n\left(t\right) - \Delta\right)^2 = \left(n\varsigma_3 - \Delta\right)^2\cos^2 nt + \left(n\varsigma_4\right)^2\sin^2 nt \tag{3.50}$$

$$\left(x_4n\left(t\right)\right)^2 = \left(n\varsigma_3 - \Delta\right)^2\sin^2 nt + \left(n\varsigma_4\right)^2\cos^2 nt \tag{3.51}$$

Summing equations 3.50 and 3.51 gives

$$\left(x_3n\left(t\right) - \Delta\right)^2 + \left(x_4n\left(t\right)\right)^2 = \left(n\varsigma_3 - \Delta\right)^2 + \left(n\varsigma_4\right)^2 \tag{3.52}$$

Equation 3.52 represents circles in the x_3n, x_4n plane with centers displaced along the x_3n axis. (Figure 3.3.) The time necessary to travel from $(\varsigma_3n, \varsigma_4n)$ to (x_3n, x_4n) when the control is Δ may be determined graphically by measuring the angle $\theta = nt$ of the circular arc centered at $(\Delta, 0)$, from point $(\varsigma_3n, \varsigma_4n)$ to (x_3n, x_4n). (Figure 3.4) By knowing the angular rate n, the time needed to travel a certain angular distance θ can be found from

$$t = \frac{\theta}{n} \tag{3.53}$$
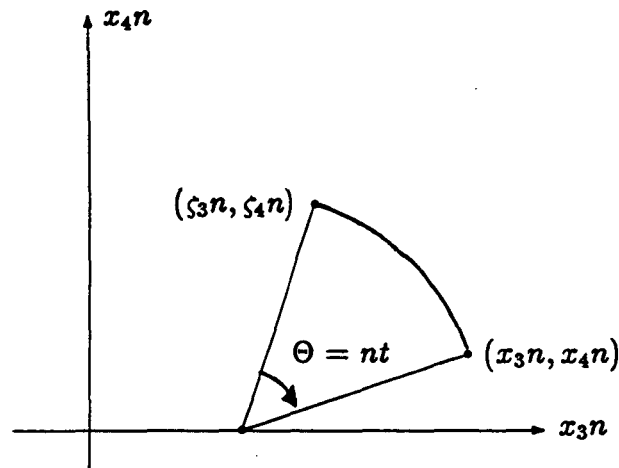
Figure 3.4: *Graphical means by which to figure the time necessary to travel from* $(\varsigma_3 n, \varsigma_4 n)$ *to* $(x_3 n, x_4 n)$ *when the control is* Δ

The above method for measuring time is only valid through a constant control segment or continuous circular arc.

There exist two circles G_+ and G_- which pass through the origin of the $x_3 n, x_4 n$ plane. G_+ is centered at $(-a, 0)$ and any point on G_+ can be driven to the origin with the control $\Delta = a$, positive commanded differential drag. G_- is centered at $(a, 0)$ and any point on G_- can be driven to the origin with negative differential drag. (Figure 3.5)

On G_+, the point $(-2a, 0)$ can be forced to the origin in π/n units of time $(\theta = nt = \pi)$. The point $(-a, a)$ can be forced into the origin in $\pi/2n$ units of time. The point $(-a, -a)$ on the G_+ curve could be forced to the origin in $3\pi/2n$ units of time; this last example would not be optimal as the optimal control can remain constant for no more than π/n units of time. On G_+, the points that can be driven to the origin in less than π/n units of time are represented by the semi-circle above the $x_3 n$ axis. On G_-, the points that can be driven to the origin in less than π/n units of time are represented by the semi-circle below the $x_3 n$ axis.

The optimal switch curve for any point in the $x_3 n, x4 n$ plane is shown in Figure 3.6. In the region G_+ a control of positive a should be used; a control of negative a should be used in the G_- region.
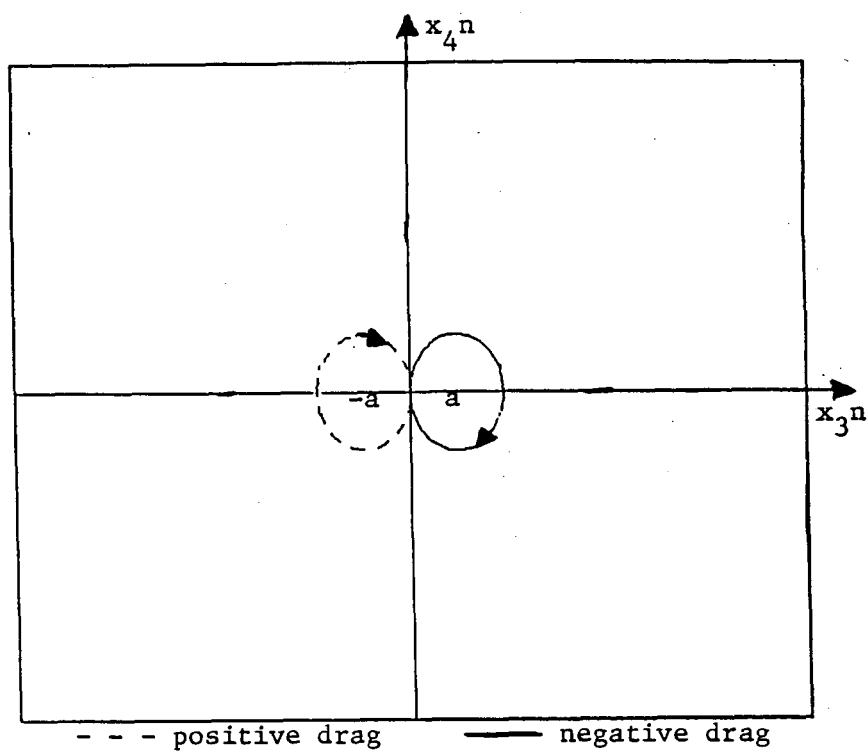
Figure 3.5: *Constant control switch curves for the harmonic oscillator.*
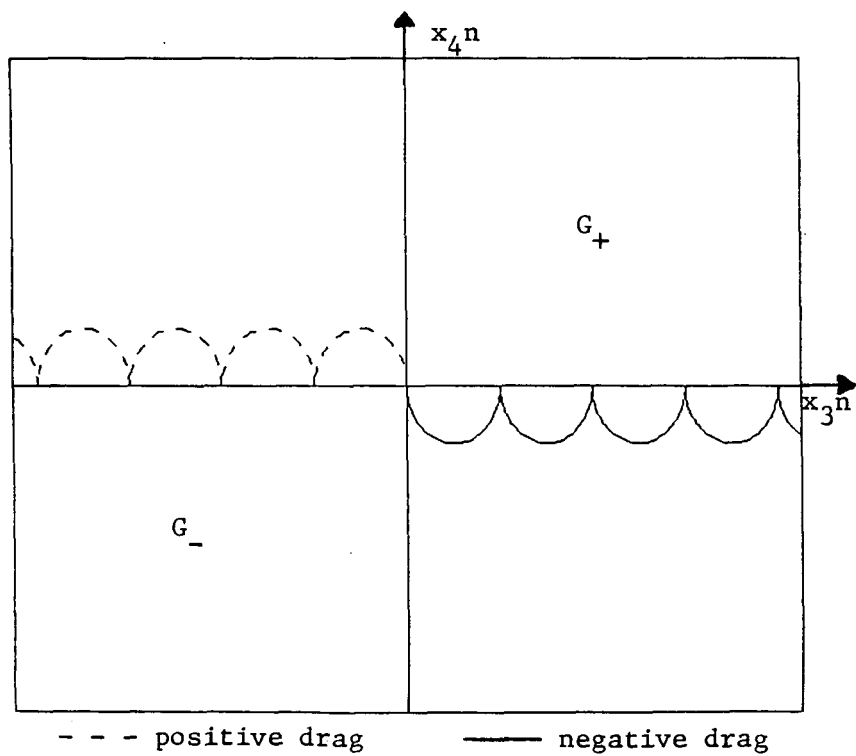
Figure 3.6: *Optimal switch curve for any point in the $x_3 n, x_4 n$ plane.*

$- - -$ positive drag　　　$---$ negative drag
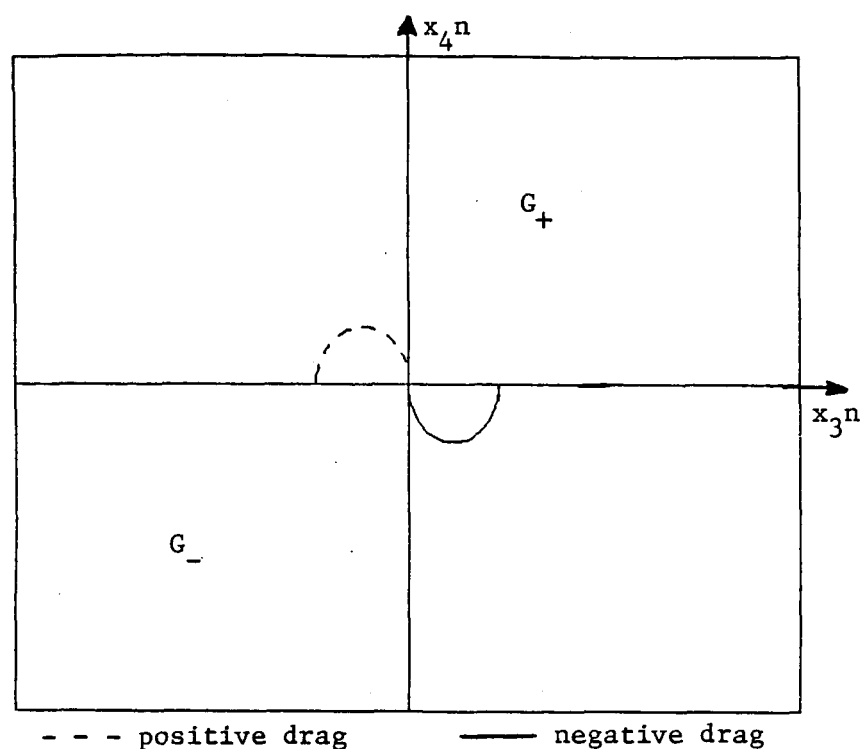
Figure 3.7: *Simplified sub-optimal switch curve for any point in the $x_3 n, x_4 n$ plane.*

The engineering realization of the optimal switch curve in the $x_3 n, x_4 n$ is not simple. A simplified, sub-optimal switch curve was presented by Athans and is shown in Figure 3.7. As before, in the region G_+ a positive differential drag should be commanded; in the region G_- a control of negative a should be used. The maximum increase in time-to-origin with the sub-optimal switch curve is 4.3% above the optimal system.

The simplified switch curve for the harmonic oscillator is used in the formationkeeping problem rather than the optimal switch curve because it is much easier to realize in the engineering sense and does not greatly reduce performance.

Chapter 4

Consolidation of the Double Integrator and Harmonic Oscillator Control Schemes

4.1 Introduction

Both the double integrator and the harmonic oscillator controls must be used to drive the position and eccentricity of the slave to that of the target. The double integrator control determines the behavior of the average position of the slave, while the harmonic oscillator control determines its eccentricity. Solving them concurrently leads to the positioning of the slave at the target.

The two controls intrinsically differ. The double integrator control will switch sign at most once; the harmonic oscillator control must switch every half revolution period of the target. Therefore, solving them simultaneously and independently is impossible. Solving them independently, one before the other, would not control the composite system. Once one pair of states is at the desired point, bringing the other pair to its commanded point would drive the original pair out of its designated spot.

The solution lies in solving the double integrator and harmonic oscillator simultaneously and dependently. A simultaneous and dependent control scheme uses the control law for either the position or the eccentricity, whichever is deemed more important at the time, without causing the uncontrolled quantity to move farther from its goal. In order to implement this control scheme, position and eccentricity must be prioritized as discussed in Section 4.2. The final control

law consists of two parts: the main control law, discussed in Section 4.3, and the gamma control scheme, discussed in Section 4.4. The switch curves developed in the final control law are named in Section 4.5.

4.2 Relative Importance of Position and Eccentricity Errors

An error in position is more important than an error in eccentricity, because an error in eccentricity does not diverge, while in most cases an error in position does.

For example, if the average position of the slave were at the target with some error in eccentricity, the average position would remain at the target indefinitely and the eccentricity would stay fixed. An error in eccentricity is a stable error; it does not increase by itself, nor does it cause the average position of the slave to grow away from the target. This example assumes that eccentricity is small enough that differences in atmospheric density between the target altitude and the slave perigee altitude would not cause the orbit of the slave to degrade more rapidly than that of the target.

An error in the radial position of the slave causes an error in position along the velocity vector. As Kepler's second law states, if the slave is in a lower average orbit than the target, it will have a larger orbital rate; if the slave is in a higher average orbit, it will have a smaller orbital rate. Thus if the slave were at a different altitude than the target, it would have a non-zero velocity in the y direction with respect to the target.

The orbital motion described by Kepler's second law can actually decrease the average position error along the velocity vector if certain conditions exist: if the average radial position of the slave is larger than that of the target and the average position along the velocity vector of the slave is ahead of the target, or if the average radial position is smaller than that of the target, and the average position along the velocity vector is behind the target. This unthrusted orbital motion will be used in the gamma control scheme. If the slave were allowed to drift for a long duration of time, it would eventually move away from the origin. Thus in the unrestricted time case, an error in the radial direction would cause an error in the velocity vector position that would grow steadily over time. (It

is assumed that the difference in true anomaly of the slave and the target is less than 180 degrees.)

The only position error that generates another error is a difference in radial position. A radial position error produces an error in the position only along the velocity vector, it does not get worse radially nor does it affect eccentricity. A position error along the velocity vector does not affect future position or eccentricity errors. In most cases the average position of the slave includes an error in the radial position.

4.3   Formulation of the Main Control Law

The main control law depends upon the notion that position errors are more important than eccentricity errors and that an error in the radial direction is more important than an error along the velocity vector.

The object of the main control law is to drive the average position of the slave to that of the target while not increasing eccentricity any more than necessary. Both the switch curve for the double integrator and the switch curve for the harmonic oscillator must be considered to achieve this goal. Because the switch curves are given in x_1, x_2, x_3n and x_4n coordinates, it will be in those coordinates that the control law is derived.

In order to understand the control actions taken by the main control law in the x_1, x_2 plane, the reader must first understand what is meant by favorable switching conditions in the x_3n, x_4n plane.

4.3.1   Favorable Switching Conditions in the x_3n, x_4n Plane

Favorable switching conditions in the x_3n, x_4n plane depend on the size of x_2, the desired control, and the magnitude of the eccentricity.

The Magnitude of x_2

The state x_2 relates to $\bar{x}$. A large $\bar{x}$ is undesirable for two reasons: first, a large $\bar{x}$ jeopardizes the accuracy of the equations of relative motion; second, a large $\bar{x}$ causes gross movements in $\bar{y}$. Although large movements in $\bar{y}$ may be desirable at certain areas in the $\bar{x}, \bar{y}$ plane, they are generally undesirable and

will be avoided in the control law. Therefore an $\bar{x}$ with large magnitude should be reduced as soon as possible.

If the absolute value of $\bar{x}$ is larger than a certain quantity, which corresponds to a similar restriction on the value of x_2, the control should be switched to the desired drag command as soon as the switch will not enlarge the eccentricity. If the absolute value of x_2 is smaller than the given value, then the switch to the desired drag should occur where it would decrease the eccentricity the most.

The value of x_2, therefore, dictates whether favorable switching conditions in the $x_3 n, x_4 n$ plane minimize the eccentricity as much as possible or merely bound its magnitude.

The time that it would take x_2 to reach the x_1 axis under constant control for one orbital period represents the cutoff value for x_2. This cutoff value will be referred to as one orbital period away from the x_1 axis. This value was chosen because it limited the relative velocity in the $\bar{y}$ direction, but allowed significant movement of the slave toward the target.

The Desired Control

Two factors determine the locations on the $x_3 n, x_4 n$ plane where a switch to a certain drag is considered favorable: the desired control and whether the eccentricity is being decreased by the largest amount possible or merely bound.

If the eccentricity is being decreased by the largest possible amount, then the switch to a new drag will occur at the shortest line segment connecting the circle due to the present drag in the $x_3 n, x_4 n$ plane, and the origin of the circular trajectory of the desired drag.

In the switch from positive or zero commanded drag to negative drag, the switch must occur on the $x_3 n$ axis and have a value greater than $-a$. The line segment connecting the circle due to the present drag in the $x_3 n, x_4 n$ plane, and the origin of the circular trajectory due to the desired drag will be a minimum on this locus of points. (Figure 4.1) Similarly, a switch from negative or zero drag to positive drag would cause the locus of favorable switching points to lie on the $x_3 n$ axis with a value less than a.

If the eccentricity is simply being bound, then the switch to a new drag will occur when the line segment connecting the circle due to the present drag in the $x_3 n, x_4 n$ plane, and the origin of the circular trajectory of the desired drag, is
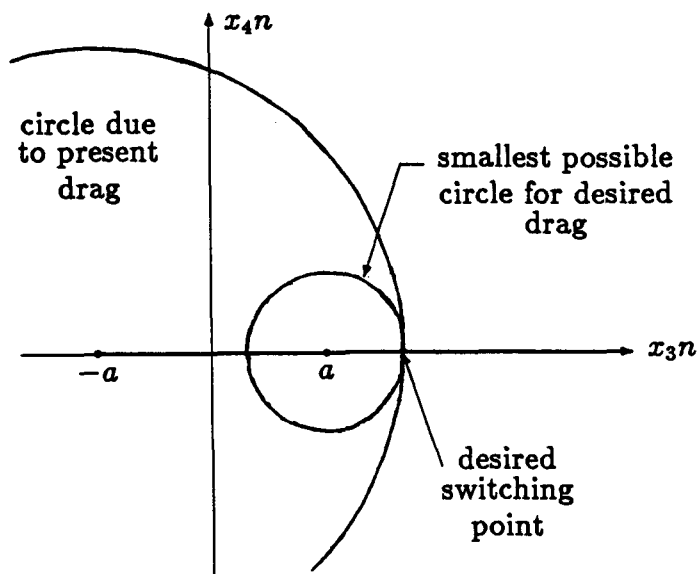
Figure 4.1: *The locations on the x_3n, x_4n plane for a favorable switch from positive or zero to negative drag for the eccentricity minimizing case.*

smaller than or equal to the radius of the circle due to the present drag.

Figure 4.2 shows the locus of points for a favorable switch from zero to negative drag for the case in which the eccentricity is bound. In the area where the value for x_3n is greater than or equal to $a/2$, the line segment connecting the circle due to the present drag, and the origin of the circular trajectory of the desired drag, is smaller than or equal to the radius of the circle due to the present drag. Similarly, the region in the x_3n, x_4n plane where it is favorable to switch from zero to positive drag for the eccentricity bound case lies where x_3n is smaller than or equal to $-a/2$.

There is no point in the control law where a switch to simply bound the eccentricity would be made from a non-zero drag. The desire to bound the eccentricity rather than minimize it implies that the slave is in a position such that there is only one appropriate commanded control, as will be further explained in Section 4.3.3. A switch from zero drag would be possible in the start-up procedure of the control law, where it is assumed that the system starts with a zero commanded drag.
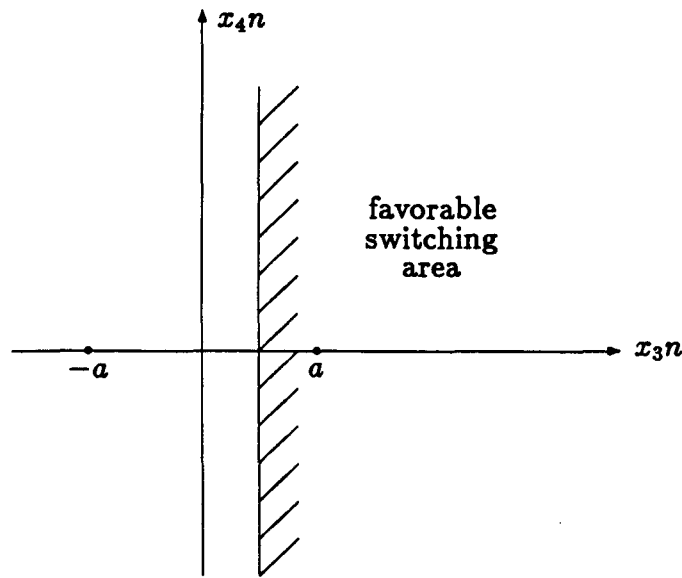
Figure 4.2: *The locations on the x_3n, x_4n plane for a favorable switch from zero to negative drag for the eccentricity bound case.*

The Magnitude of the Eccentricity.

Bounding or reducing the size of the eccentricity is contingent upon the eccentricity's having at least a certain minimum magnitude.

In bounding the eccentricity it is assumed that the radius of a circle due to zero drag about the origin will be greater than or equal to the radius of a circle centered at a or $-a$ on the x_3n axis. For this to be true, the initial magnitude of the eccentricity must be larger than or equal to $a/2$.

If the initial magnitude of the eccentricity is smaller than $a/2$, then the switch to the desired command is made immediately. Given a position error large enough to warrant bounding rather than minimizing the eccentricity, it is assumed that there will be opportunities to further reduce the eccentricity before the origin is reached, as will be explained in more detail in Section 4.3.3.

The magnitude of the original eccentricity would have to be larger than $2a$ to minimize the eccentricity for a switch from a non-zero drag to the opposite drag, and larger than a for a switch from zero drag. The favorable switching conditions for minimizing eccentricity described above will still be used when the original eccentricity is not large enough to validate the minimization process. This action will no longer reduce the eccentricity but will keep it in a cycle in the shape of an eight about the origins of the circles for the two commanded
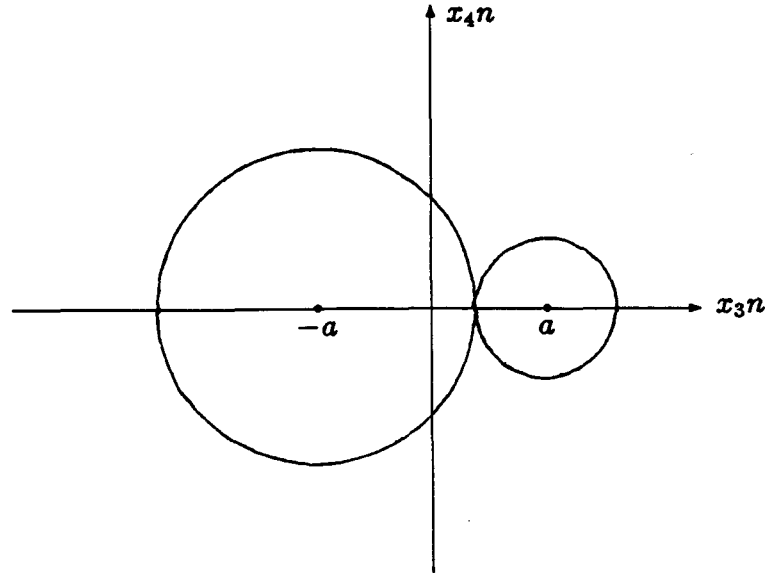
Figure 4.3: *Sample trajectory in the x_3n, x_4n plane for the case to minimize eccentricity when the original magnitude of the eccentricity is smaller than $2a$.*

drags. (Figure 4.3) To further reduce the eccentricity, the gamma control scheme described in Section 4.4 will be employed.

4.3.2   Control Regions in the x_1, x_2 Plane

The x_1, x_2 plane can be thought of as two switch curves and four control regions. (Figure 4.4) The switch curve above the x_1 axis is referred to as S1 while the switch curve below this axis is called S2. Area A occupies the region above the x_1 axis and to the left of the switch curve S1. The region above the x_1 axis and to the right of the switch curve S1 will be called area B. The region below the x_1 axis and to the right of the switch curve S2 is area C, while the region below the x_1 axis and to the left of the switch curve S2 is called area D.

4.3.3   The Main Control Law

The main control law first asks if the position of the slave is on one of the switch curves in the x_1, x_2 plane. If the state is on a switch curve, then the control that would take the x_1 and x_2 states to the origin is exercised immediately, no matter what the consequences to the eccentricity are. This is the only case in the main control law in which action will be taken without considering the effects on eccentricity.
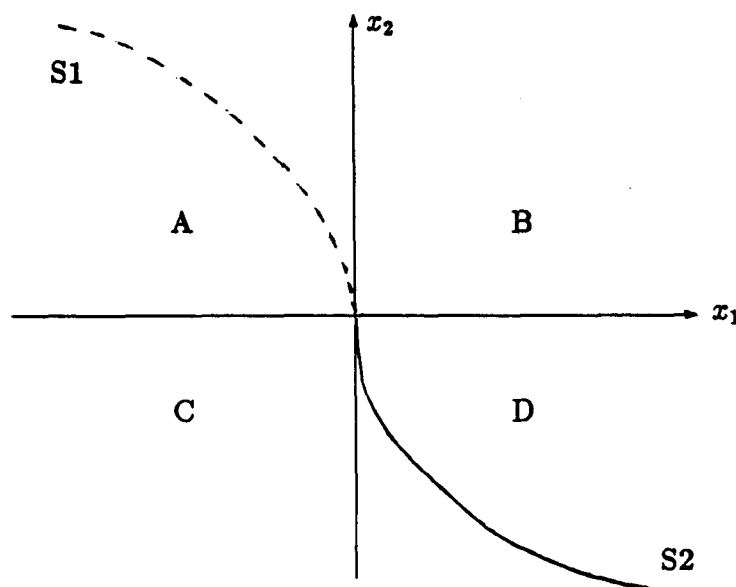
Figure 4.4: *Control decision areas in the x_1, x_2 plane.*

As the control actions for areas B and D are simpler than those for areas A and C, they will be explained first.

Control Actions for Areas B and D

If the position of the satellite correlates to area B, the desired control action will be to command a negative a. A command of negative drag in the B region will cause the position of the satellite to move toward the switch curve in the C region. If the existing drag is negative, then the proper control is to do nothing, leaving the negative drag as negative drag. If the existing control is zero, then the control must be switched to a negative drag as soon as the conditions are favorable in the x_3n, x_4n plane. If the current control is positive, then the slave must be in part of a sawtooth maneuver as explained in **Control Actions for Areas A and C**; in this case, the control must be switched to a negative drag as soon as the conditions are favorable to reduce the eccentricity.

If the position of the slave correlates to area D, the desired control action will be to command a positive drag, which will cause the position of the satellite to move toward the switch curve in the A region. If the existing drag is positive, then the proper control is to do nothing, leaving the positive drag as positive drag. If the existing control is zero, then the control must be switched to a positive drag as soon as the conditions are favorable in the x_3n, x_4n plane. If

the current control is negative, then the slave must be in part of a sawtooth maneuver; in this case, the control must be switched to a positive drag as soon as the conditions are favorable to minimize the eccentricity.

Control Actions for Areas A and C

There are three different ways for a slave in the A area to reach the switch curve S1. First, a command of zero drag would allow the slave to drift into the switch curve S1. Second, a command of positive drag would force the slave along a parabolic arc to the switch curve. Third, a command of positive or negative drag that switched to the opposite drag (when it was favorable to do so in the x_3n, x_4n plane) would sawtooth the slave toward the switch curve. (Figures 4.5, 4.6 and 4.7)

A command of zero drag which would let the slave drift into the switch curve is not time optimal. In general, the switch curve could be reached more rapidly by commanding a positive drag. Remembering the assumption that drag is free and that the time to reach the origin is to be minimized, letting the slave drift into the switch curve is not desirable.

A command of positive drag which would place the slave on a parabolic path toward the switch curve is the time optimal solution to reach the switch curve S1 from any point in the A area. If the problem to be solved were simply to control the average position of the slave then this would be the control action to choose.

A command of either positive or negative drag that switched to the opposite drag when it was favorable to do so in the x_3n, x_4n plane, moves the slave toward the switch curve in a sawtooth pattern. This control pattern has the benefit of moving the average position of the slave toward the switch curve while reducing eccentricity.

The formationkeeping problem involves both the control of the average position of the slave and its eccentricity, thus the sawtooth control approach to reaching the switch curve was chosen as the best control for area A.

Two restrictions limit the use of the sawtooth control action in this region; both are concerned with the size of x_2.

The reduction of the magnitude of x_2, when it is large, will take precedence over sawtooth control. If the present drag is negative or zero, and it is favorable
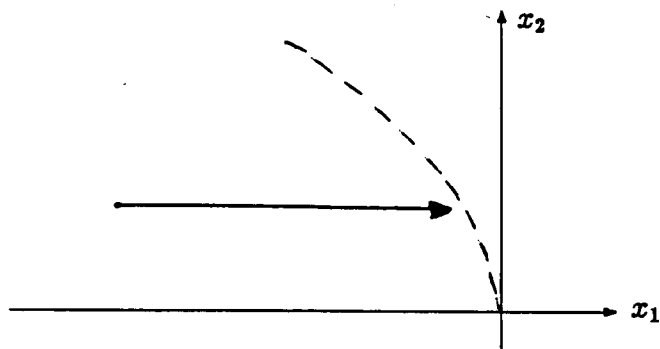
Figure 4.5: *The path of a slave in area A with a commanded drag of zero drifting in to the switch curve S1.*
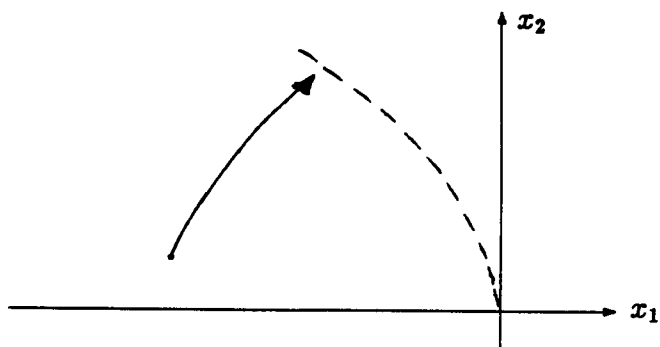
Figure 4.6: *The parabolic path of a slave in area A with a commanded positive drag moving toward the switch curve S1.*
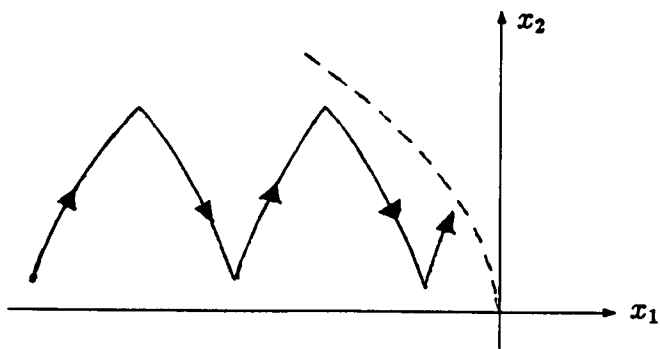
Figure 4.7: *The sawtooth path of a slave in area A with a commanded drag that switches between positive and negative drag when it is favorable to do so in the x_3n, x_4n plane.*

to switch to a positive drag, the system will only do so if x_2 is less than one revolution away from the x_1 axis.

For the sawtooth action to move the slave toward the target the average value of x_2 over the duration of a sawtooth maneuver must stay in the A region.

Figure 4.8 shows the case in which the average value of x_2 is zero. Figure 4.9 shows a case in which the average value of x_2 is positive or in the A region, while Figure 4.10 shows the trajectory of the slave when the average value of x_2 is in area D or negative.

The maximum duration of constant control for a leg of the sawtooth is one orbital revolution, corresponding to the case in which the eccentricity is small and is kept in a cycle the shape of an eight in the x_3n, x_4n plane. For sawtooth maneuvers to move the slave toward the origin, any switch from positive or zero drag to negative drag must occur when x_2 is larger than one half revolution away from the x_1 axis. The larger x_2 is, the faster the slave will move in toward the target. To ensure an acceptable closing rate, the minimum value of x_2 for which a switch to negative drag could occur is set at three-fourths of a revolution away from the x_1 axis.

Thus the control actions to be taken in the A region are:

- The sawtooth control will be used when it is favorable to switch to positive drag and x_2 is less than one revolution away from the x_1 axis, or when a switch to negative drag is favorable and x_2 is greater than three-fourths of a revolution away from the x_1 axis.

- If x_2 is larger than one revolution away from the origin, a negative drag is desired. If the current drag is negative, the system will not make a switch; if the current drag is zero, the system will switch to a negative drag as soon as it is favorable to do so. If the current drag is positive, it implies that the slave is in a sawtooth maneuver since this is the only way to have a commanded positive drag in this region. In this case, the switch will be made to negative drag only when the switch is favorable in the x_3n, x_4n plane to minimize eccentricity.

- If x_2 is smaller than three-fourths of a revolution away from the axis, then a positive drag is wanted. If the current drag is zero, then the system will switch to a positive drag as soon as it is favorable to do so; if the current
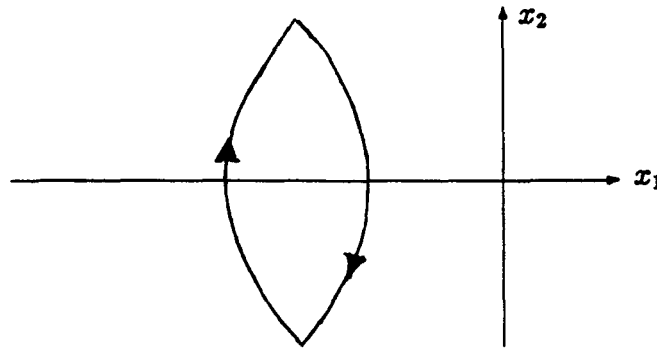
Figure 4.8: *The trajectory of the slave in the* x_1, x_2 *plane during a sawtooth maneuver when the average value of* x_2 *over the duration of the sawtooth is zero. The sawtooth control does not move the slave closer to or father away from the origin.*
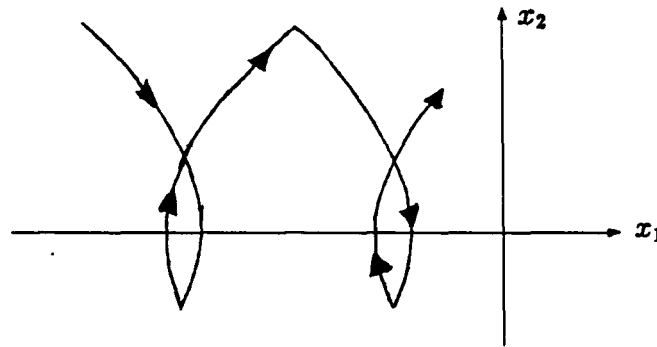
Figure 4.9: *The trajectory of the slave in the* x_1, x_2 *plane during a sawtooth maneuver when the average value of* x_2 *over the duration of the sawtooth is positive. The sawtooth control moves the slave closer to the origin.*
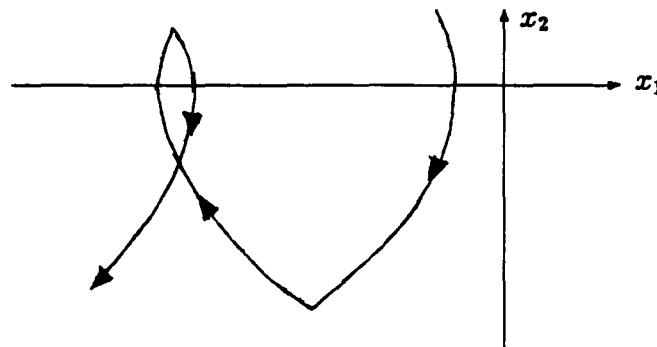
Figure 4.10: *The trajectory of the slave in the* x_1, x_2 *plane during a sawtooth maneuver when the average value of* x_2 *over the duration of the sawtooth is negative. The sawtooth control moves the slave father away from the origin.*

drag is positive, no switch will be made. A current negative drag implies that the slave is in a sawtooth maneuver since this is the only way to have a commanded negative drag in area A. In this case, the switch to positive drag will occur when it is favorable to minimize eccentricity.

The control actions to be taken in area C use similar logic:

- The sawtooth control will be used when it is favorable to switch to negative drag and the magnitude of x_2 is less than one revolution away from the x_1 axis, or when a switch to positive drag is favorable and the magnitude of x_2 is greater than three-fourths of a revolution away from the x_1 axis.

- If the magnitude of x_2 is larger than one revolution away from the origin, positive drag is desired. If the current drag is positive, the system will not make a switch; if the current drag is zero, the system will switch to a positive drag as soon as it is favorable to do so. If the current drag is negative, it implies that the slave is in a sawtooth maneuver since this is the only way to have a commanded negative drag in this region. In this case, the switch will be made to positive drag only when the switch is favorable to minimize eccentricity.

- If the magnitude of x_2 is smaller than three-fourths of a revolution away from the axis, then a negative drag is wanted. If the current drag is zero, then the system will switch to a negative drag as soon as it is favorable to do so; if the current drag is negative no switch will be made. If the current drag is positive, it implies that the slave is in a sawtooth maneuver since this is the only way to have a commanded positive drag in this section. In this case the switch to negative drag will occur when it is favorable to minimize eccentricity.

Execution of the Main Control Law

If the slave is in the B or D area, then it will drive itself in a parabolic arc into the C or A region. Once in the A or C area, the slave will sawtooth to the switch curve. Up to this point, the main control law has been consulting the x_3n, x_4n plane and reducing the eccentricity as much as possible. Once the switch curve is reached, the proper control to drive the average position

to the origin is exercised immediately, no matter what the consequence is to the eccentricity. The main control law has completed its goal when the average position is at that of the target. The gamma control scheme is used to reduce any remaining eccentricity.

4.4   Formulation of the Gamma Control Scheme

The gamma control scheme begins when the average position of the slave is at the target. The object of this scheme is to reduce the eccentricity as much as possible without altering the final average position of the slave. If the eccentricity is already zero then the control law has completed its task because all four states have been driven to the origin.

The strategy to reduce eccentricity is shown in Section 3.3. If the eccentricity is large, then the proper procedure to reduce it is to switch drag twice each orbit, at the x_3n axis. When the eccenticity is less than $2a$, the switch curves are defined by two semi-circles of radius a centered at $-a$ and a on the x_3n axis.

Given the switch curves which drive the eccentricity to zero, a method of using them without compromising the average position must be found. The control applied to reduce eccentricity moves the average position of the slave away from the target; thus a sequence of controls must be developed to reduce eccentricity and place the slave at its original average position by the end of the sequence.

Either a hat shaped maneuver or a sawtooth shaped maneuver in the x_1, x_2 plane could reduce eccentricity without altering the final average position of the slave.

The Choice of the Hat Shaped Maneuver

The hat shaped maneuver allows only two switches that reduce eccentricity before the average position of the slave must be returned to the origin; the maneuver repeats itself until the desired eccentricity is reached. (Figure 4.11) The sawtooth shaped maneuver performs all the switches to reduce eccentricity before returning the average position of the slave to the origin. (Figure 4.12) Each tooth of the sawttooth maneuver would correspond to a hat in the hat shaped maneuver; the small tooth would correspond to the hat for maneuver small ec-
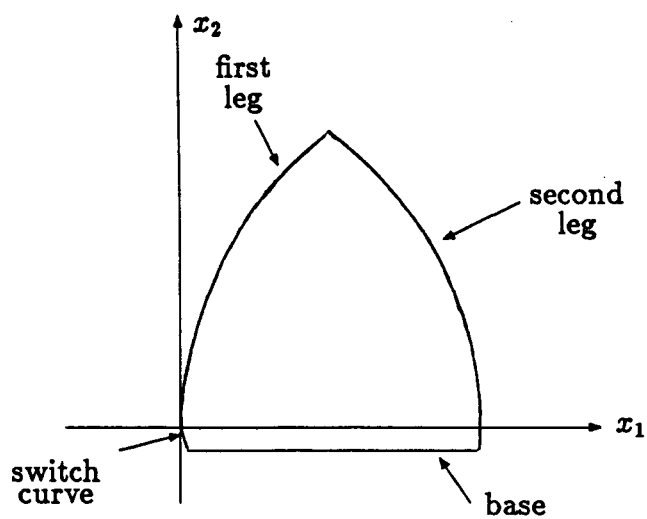
Figure 4.11: *The hat maneuver of the gamma control scheme in the x_1, x_2 plane.*
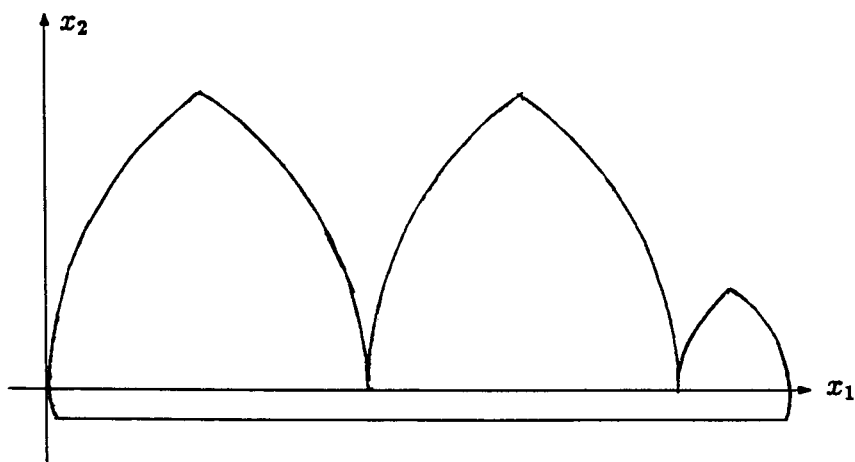
Figure 4.12: *A sawtooth shaped maneuver in the x_1, x_2 plane.*

centricity. Reducing any given eccentricity to an acceptable level would take roughly the same time for both control configurations. The hat shaped maneuver bounds the average position error of the slave, while the sawtooth maneuver lets the error in position grow until the eccentricity reaches an acceptable level; thus the hat shaped maneuver was chosen over the sawtooth maneuver.

The hat shaped maneuver is slightly different for cases of large eccentricity and for cases in which $sqrt(x_3n)^2 + (x_4n)^2$ is less than $2a$. The procedure for large eccentricities will be explained first; the process for small eccentricities will follow.

The Hat Shaped Maneuver for Large Eccentricity

The x_3n axis is the switch curve for reducing large eccentricity. Let Θ_0 be the angle which the state makes with the negative x_3n axis while the drag is zero. The angle Θ_0-switch is the angle Θ_0 at which the switch from zero drag to non-zero drag should be made. The angle traversed by the state during the first interval of non-zero commanded drag will be referred to as Θ_1; the angle corresponding to the subsequent opposite drag will be known as Θ_2. Figure 4.13 shows that Θ_2 is larger than Θ_1. For the gamma control scheme to work the second leg of the hat must be longer than the first leg of the hat, so that unthrusted orbital motion will bring the state back toward the origin. This unthrusted motion forms the third leg or base of the hat. For the second leg of the hat shaped maneuver in the x_1, x_2 plane to be longer than the first leg, the drag that corresponds to the second leg must be on longer than the corresponding interval for the first leg. Equation 3.53 shows that the duration of a certain control is related to the angle that it passes through in the x_3n, x_4n plane; hence the angle that the second leg transverses must be larger than the angle of the first leg.

The angle Θ_2 is set to the optimum value of 180 degrees. The angle Θ_1 was selected as 20 degrees smaller than Θ_1. The difference of 20 degrees between Θ_2 and Θ_1 was chosen to insure a large closing rate of the average position of the slave toward the target in the unthrusted or drift phase of the hat maneuver. The larger the difference in angles, the larger the separation distance between the slave and the x_1 axis in the drift phase. The difference in position between the slave and the x_1 axis is proportional to the closing rate; the larger the
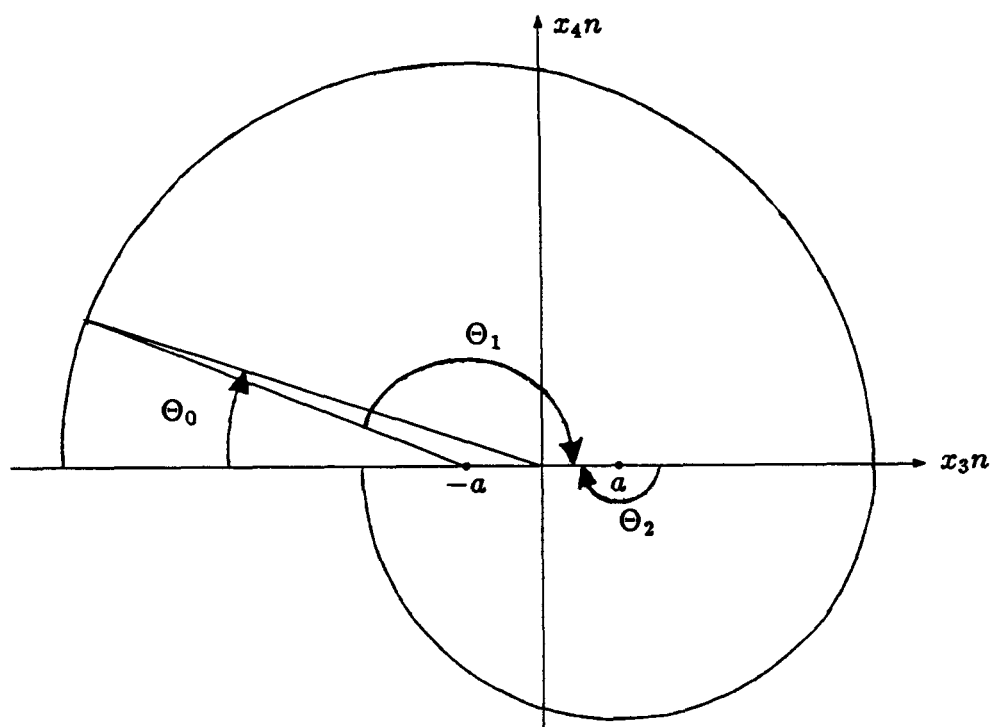
Figure 4.13: *The switch decision process for large eccentricity in the* $x_3 n, x_4 n$
plane.

separation distance, the faster the closing rate. The Θ_0-switch corresponding to the chosen values of Θ_1 and Θ_2 is then 20 degrees, which is similar to a value of Θ_0-switch equalling 200 degrees because the control law is symmetric about the x_3n axis.

In gamma control the commanded differential drag is initially zero, which keeps the average position of the slave at the target and results in the state circling about the origin in the x_3n, x_4n plane.

When Θ_0 equals 20 degrees, the commanded drag will switch from zero to the proper value. For x_4n larger than zero the proper drag will be a, otherwise negative drag is selected. This first switch will reduce the eccentricity and form the first leg of the hat in the x_1, x_2 plane. The next switch will occur at the x_3n axis after the angle Θ_1 has been passed; it will command a change in sign of drag. This action will reduce the eccentricity once again and form the second leg of the hat in the x_1, x_2 plane. When the x_3n axis is reached again (corresponding to to a transferred Θ_2 of 180 degrees), the drag is commanded to be zero. The states in the x_3n, x_4n plane will then circle about the origin and the states in the x_1, x_2 plane will drift toward the origin, forming the base of the hat.

When the drifting slave encounters the switch curve in the x_1, x_2 plane, the appropriate drag control will drive the average position of the slave to the target. The strategy will be repeated until the eccentricity has been reduced enough to go through the gamma control scheme for small eccentricities.

The Switch Decision Process for a Small Eccentricity

The difference between Θ_1 and Θ_2 chosen for the small eccentricity case determines the minimum achievable eccentricity. In the decision process for this situation, Θ_2 was chosen to be 10 degrees larger than Θ_1.

The difference between Θ_1 and Θ_2 affects the closing rate of the slave during the drift phase of the hat maneuver and the minimum eccentricity that the control law can achieve. The larger the closing rate the farther the slave is away from the x_1 axis. During the drift phase of the gamma control scheme for small eccentricity, the eccentricity of the system is zero. The eccentricity becomes non-zero when the drag becomes non-zero in order to drive the average position of the slave along the switch curve to the origin. The longer the non-zero control is on, the larger the final eccentricity of the system will be (the control will be
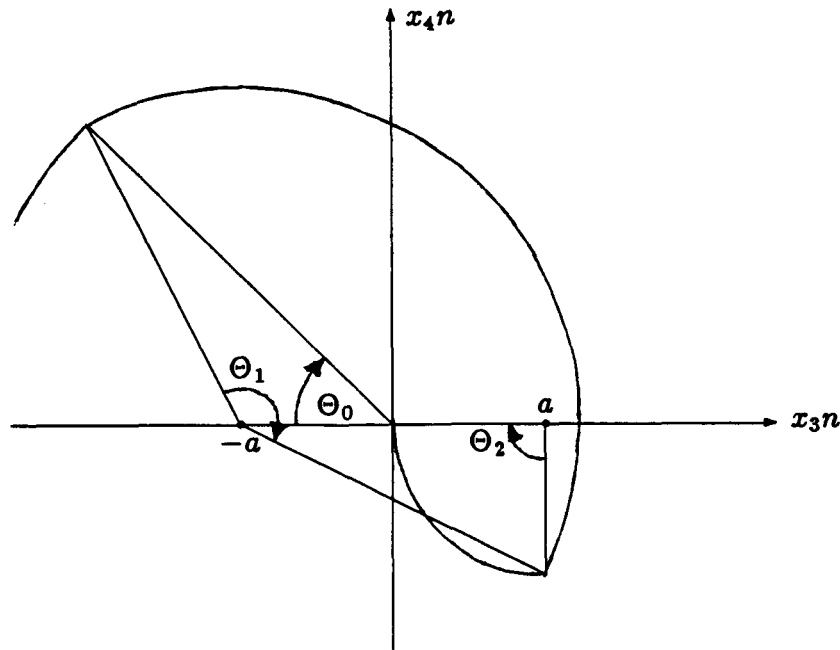
Figure 4.14: *The angles Θ_1 and Θ_2 in the switch decision process for small eccentricities in the x_3n, x_4n plane.*

on for less than one half orbital period as the slave is near the x_1 axis in the drift phase of the gamma control scheme). There is, thus, a trade off between the closing rate and the acceptable final eccentricity of the system.

In the decision process for large eccentricity the closing rate was given priority over the final eccentricity since the gamma process would have to be repeated again at some point for the smaller eccentricity. For small eccentricity, Θ_2 was chosen to be 10 degrees larger than Θ_1 as this difference allows for an acceptable compromise between closing rate and final eccentricity. Theoretically, the closing rate would be 1.532 feet per minute and the maximum error in position due to eccentricity would be 15.37 feet. For the simulation, which allows certain errors in the position of the slave at the start of gamma control and has a discrete time step, the difference of 10 degrees guarantees that the slave will reach a favorable position to drift toward the origin after the second leg of the hat has been completed.

The two semi-cirlces of radius a centered at $-a$ and a on the x_3n axis are the switch curves for eccentricities smaller than $2a$. The optimum Θ_2 is no longer
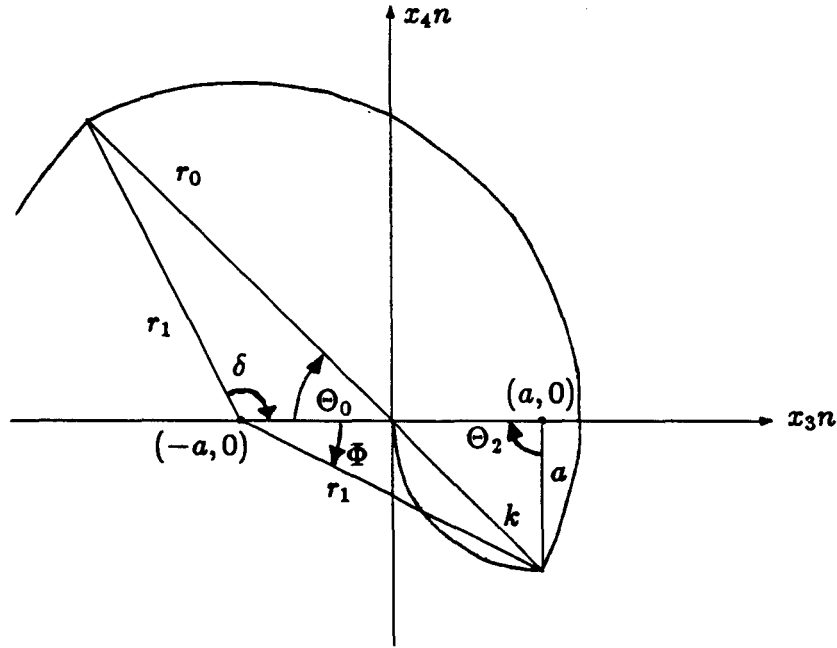
Figure 4.15: *Geometry in the x_3n, x_4n plane for the switch algorithm in the decision making process for small eccentricities .*

180 degrees, as it was for the large eccentricity case. The optimum Θ_2 is now defined as the angle on the switch curve from where the state encounters the curve, to the origin. (Figure 4.14)

The initial zero drag commanded by the gamma control keeps the average position of the slave at the origin and results in the eccentricity circling about the origin in the x_3n, x_4n plane.

The eccentricity of the system dictates the values of Θ_0-switch, Θ_1 and Θ_2. An algorithm was developed for evaluating the current position of the slave in the x_3n, x_4n plane, and the corresponding values of Θ_1 and Θ_2; if Θ_2 is 10 degrees larger than Θ_1, the first switch is made. The algorithm is as follows; the necessary geometry is shown in Figure 4.15.

1. r_0 is related to the eccentricity of the system.

$$r_0 = \sqrt{(x_3n)^2 + (x_4n)^2} \tag{4.1}$$

2. Θ_0 can be obtained from x_3n and x_4n.

$$\Theta_0 = \arctan\left(\frac{-x_4n}{x_3n}\right) \tag{4.2}$$

3. r_1 can then be computed from r_0, Θ_0 and a using the law of cosines.

$$r_1 = \sqrt{(r_0^2 + a^2 - 2r_0 a \cos \Theta_0)} \qquad (4.3)$$

4. δ can be found from r_0, r_1 and Θ_0 using the law of sines.

$$\delta = \arcsin \left(\frac{r_0 \sin \Theta_0}{r_1} \right) \qquad (4.4)$$

5. Φ can be found using the law of cosines and a and r_1.

$$\Phi = \arccos \left(\frac{3a^2 + r_1^2}{4ar_1} \right) \qquad (4.5)$$

6. Θ_1 is equal to the sum of δ and Φ.

$$\Theta_1 = \delta + \Phi \qquad (4.6)$$

7. Θ_2 may be found from r_1, a and Φ using the law of sines.

$$\Theta_2 = \arcsin \left(\frac{r_1 \sin \Phi}{a} \right) \qquad (4.7)$$

8. At this point a check is made. If Θ_2 is 10 degrees larger than Θ_1 then the values for Θ_1 and Θ_2 are retained in memory and the first switch is made; if $x_4 n$ is positive the switch is to a positive drag; otherwise the switch is to a negative drag. This switch starts the first leg of the hat in the x_1, x_2 plane. If Θ_2 is not 10 degrees larger than Θ_1 then the drag is left at zero and the switch determining algorithm is repeated as the state circles about the origin until the proper time to switch is found.

Once the switching point has been reached, the quantity k is calculated.

$$k = \sqrt{2a^2 - 2a^2 \cos \Theta_2} \qquad (4.8)$$

Drag is switched to the opposite sense when the eccentricity of the system is equal to k, and $x_4 n$ has changed sign since the initial switch. This second switch will put the states in the $x_3 n, x_4 n$ plane on the final switch curve to the origin; it also begins the second leg of the hat in the x_1, x_2 plane.

When the eccentricity reaches zero, the drift phase of the gamma control scheme begins . A switch is made to zero commanded drag; the eccentricity stays at zero and the unthrusted motion of the slave corresponds to the base of the hat in the x_1, x_2 plane.

When the state crosses the switch curve in the x_1, x_2 plane, the appropriate drag control will drive the average position of the slave to the target. After the average position reaches that of the target, the final eccentricity should be acceptable as determined by the choice of the 10 degree difference between Θ_1 and Θ_2. The four states will in essence have been driven to zero - the object of the final control law which combines the main and gamma control schemes.

4.5   Naming of Switch Curves

The switch curves were named in order to clarify the results of the simulations presented in Chapter 5.

Switch curves in the main control law begin with the letter S. The curve above the x_1 axis is called S1 and dictates that the control switch to a positive drag. Below the axis, the curve is called S2 and commands a negative drag. The origin of the x_1, x_2 plane is referred to as GA and signifies the start of the gamma control scheme. (Figure 4.16)

The switch curve S3, which commands a negative drag, is the line on the x_3n axis greater than or equal to $-a$. A positive commanded drag corresponds to the switch curve S4 which is the line segment of the x_3n axis less than or equal to a.(Figure 4.17)

The switch curves in the gamma control scheme begin with the letter G. The line forming a 20 degree angle with the negative x_3n axis is GO1; this is the switch curve at which the first switch to a non-zero drag is made in the gamma control scheme for large eccentricities. The positive x_3n axis is called GO2; at this curve the non-zero drag switches to the opposite sign. The last switch curve in the gamma control scheme for large eccentricities is GO3, corresponding to the negative x_3n axis; this switch curve is where the drag is commanded to zero to begin the drift phase of the hat maneuver. (Figure 4.18)

The eccentricity defines the switch curve GI1 for the first switch to a non-zero drag in the gamma control scheme for small eccentricities. Once the states
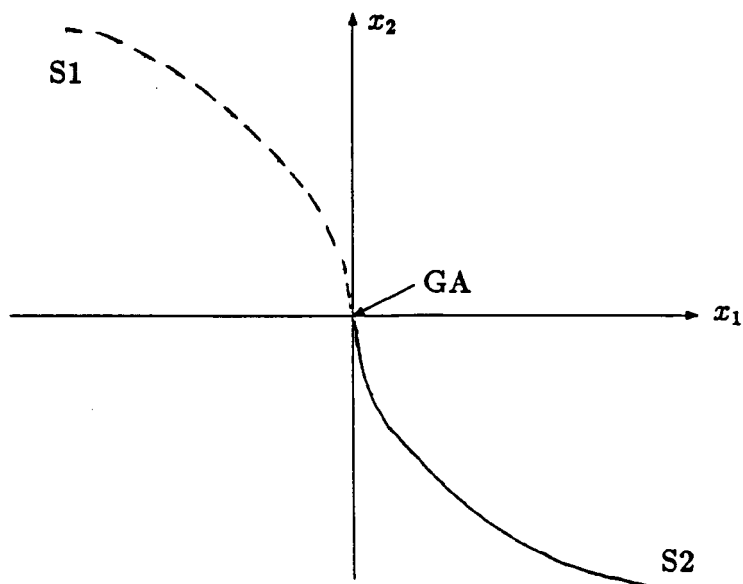
Figure 4.16: *Switch curves in the x_1, x_2 plane for the main control law.*

S4 is the line segment
where $x_3n \leq a$

S3 is the line segment
where $x_3n \geq -a$
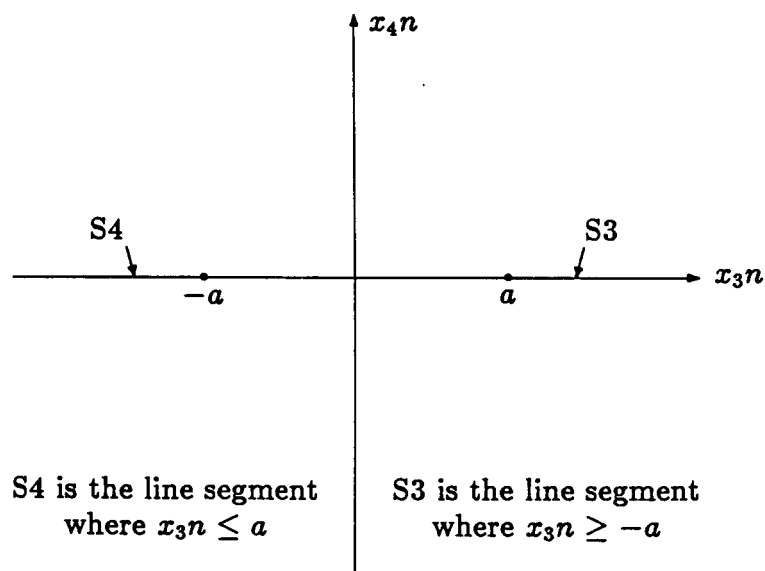
Figure 4.17: *Switch curves in the x_3n, x_4n plane for the main control law.*
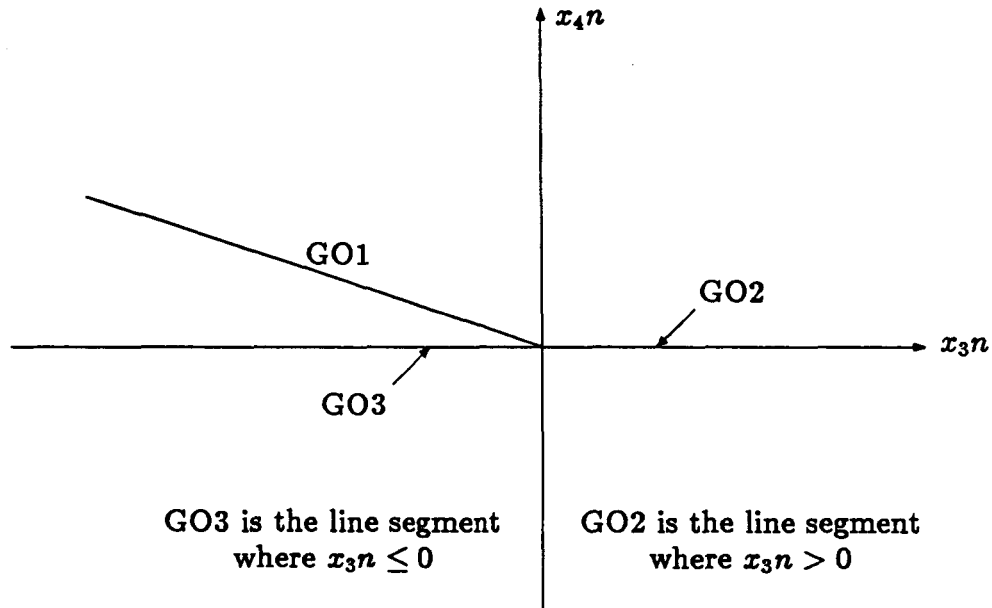
Figure 4.18: *Switch curves in the x_3n, x_4n plane for large eccentricities in the gamma control scheme.*

have encountered GI1, it is ignored if it is met again before the GI2 curve is reached. The semi-circlular switch curve GI2 is where the switch is made from a non-zero drag to a drag of the opposite sign. The origin of the x_3n, x_4n plane is referred to as GI3; the arival of the states at GI3 marks the beginning of the drift phase of the control law for small eccentricities. At GI3 the eccentricity of the system is zero. (Figure 4.19)

The switch curve names are used in the explanation of the plots generated by the test case simulations.
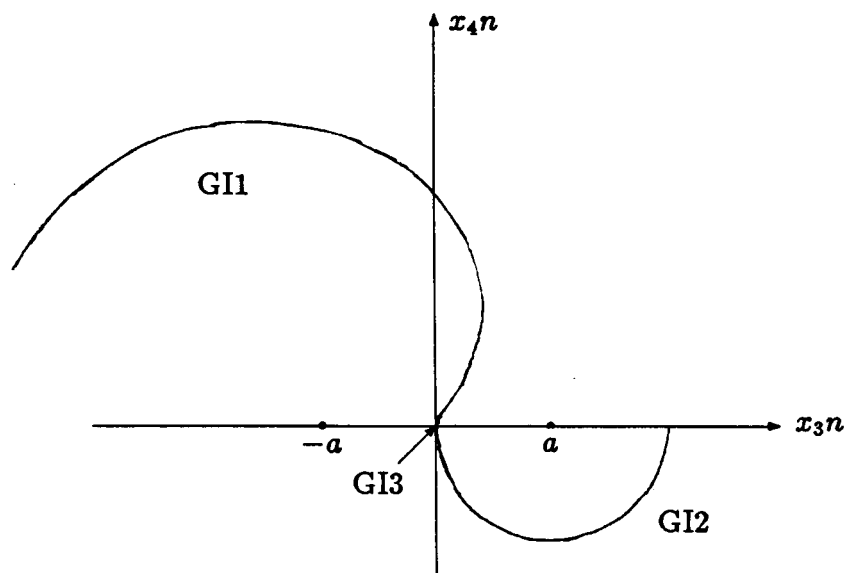
Figure 4.19: *Switch curves in the x_3n, x_4n plane for small eccentricities in the gamma control scheme.*

Chapter 5

Verification by Simulation

5.1   Introduction

The object of the control law developed in Chapter 4 is to move a slave satellite from a given position and eccentricity to that of the target. The validation of the control law is shown in Section 5.2; the slave is driven to the origin from a combination of eight different initial positions and eccentricities. A comparison of the main control law and the gamma control scheme using identical initial conditions will be made in Section 5.3. Section 5.4 will address the issue of how differential drag can be used to keep the slave at the target.

5.2   Validation of the Final Control Law

The final control law is validated by running eight representative test cases on two separate simulations. The test cases will be presented in Section 5.2.1 and the simulations will be discussed in Section 5.2.2. The results of the simulations will be covered in Section 5.2.3. Section 5.2.4 will show examples of a specific test case being driven to the origin for various values for differential drag.

5.2.1   Initial Conditions for the Test Cases

The switch curve in the $\bar{y}, \bar{x}$ plane divides the plane into two different control regions. A point chosen in each control region would have been sufficient for testing the control law. For a more rigorous testing, each control region was divided into two parts, one above the $\bar{x}$ axis and the other below it, for a total
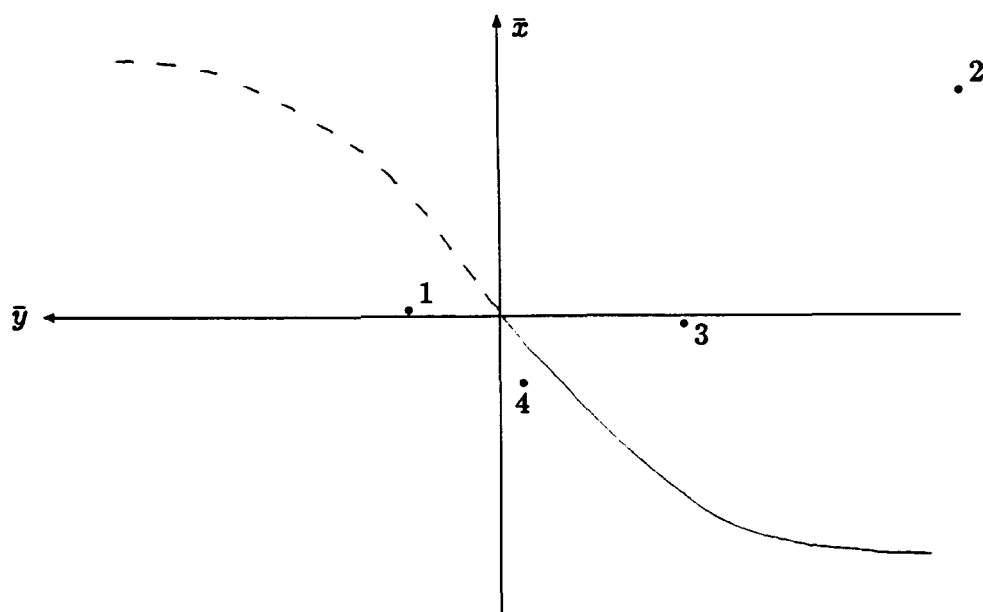
Figure 5.1: *The four areas chosen in the $\bar{y}, \bar{x}$ plane as representative of different control regions.*

point	$\bar{y}$ in feet	$\bar{x}$ in feet
1	400	25
2	-2000	1000
3	-800	-40
4	-10	-300

Table 5.1: *Values for points chosen as representative of control areas in the $\bar{y}, \bar{x}$ plane.*

of four test areas in the $\bar{y}, \bar{x}$ plane. (Figure 5.1)

A point was chosen in each area as being representative of that region. Table 5.1 shows the values given for each point.

The gamma control scheme reaction varies with the magnitude of eccentricity. Figure 5.2 shows the two different regions associated with small and large eccentricities; the values assigned to the points that were chosen as representative of those areas are given in Table 5.2.

Combinations of the points chosen in each control plane define the test cases. Table 5.3 gives the resulting test cases and their values in $\bar{y}$, $\bar{x}$, β and α.
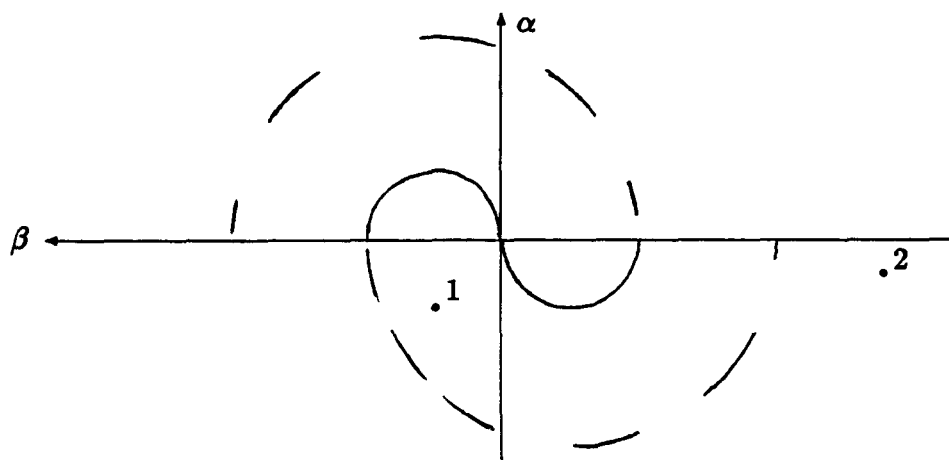
Figure 5.2: *The two areas chosen in the β, α plane as representative of different control schemes.*

point	β in feet	α in feet
1	90	-90
2	-500	-45

Table 5.2: *Values for points chosen as representative of control areas in the β, α plane.*

test case	$\bar{y}$ in feet	$\bar{x}$ in feet	β in feet	α in feet
A	400	25	90	-90
B	-2000	1000	90	-90
C	-800	-40	90	-90
D	-10	-300	90	-90
E	400	25	-500	-45
F	-2000	1000	-500	-45
G	-800	-40	-500	-45
H	-10	-300	-500	-45

Table 5.3: *The eight test cases and their corresponding initial conditions in $\bar{y}$, $\bar{x}$, β and α.*

5.2.2   The Separate Simulations

The first simulation is based on the equations of motion developed in Chapter 2; thus the assumptions considered valid in the development of the control law are also assumed valid in the first simulation. This simulation will be referred to as the ideal simulation; if all the assumptions made in the development of the control law were completely valid, the behavior of the slave will be exactly that produced by the ideal simulation. The quantity for differential drag was given a constant value of .1944 ft/min^2 based on skylab data [10] and a masters thesis written by T. F. Vargas [11].

The second simulation is based on a pre-existing Space Systems Simulator at the Charles Stark Draper Laboratory. The Space Systems Simulator is an engineering tool used in support of shuttle, space station and Department of Defense payloads. This simulation will be referred to as the detailed simulation. The motion of both the target and the slave is integrated in spherical then converted into inertial coordinates; the position and velocity of the target and slave are differenced to calculate $\bar{y}$, $\bar{x}$, β and α. Differential drag calculations use a Jacchia atmosphere and the size of the drag plate; the value of drag for a 90 degree deflection of the drag plate is computed once, then assumed constant thereafter. The altitude of the orbit was adjusted so that the value calculated in the detailed simulation for differential drag would be .1944 ft/min^2, the same value used in the ideal simulation; this was done so that any differences in the ideal and detailed plots would not be due to differences in drag. Though the results from the detailed simulation can not exactly duplicate what would happen to the slave in orbit, they are more precise than the ideal simulation.

The validity of the assumptions made in the development of the control law will be found in the comparison the the results of the ideal and detailed simulations.

5.2.3   Test Results

The results of the ideal and detailed simulations will be presented first as a plot of y vs. x, which represents the physical coordinates of the slave over time. To clarify the switch curve encounters during the simulations, plots of x_1 vs. x_2, and $x_3 n$ vs. $x_4 n$ will then be shown. Significant points in a simulation are

marked on its plots; the points are then explained in a table corresponding to that simulation.

To help understand the movement of the slave versus time throughout a simulation, tic marks are on the plots for the ideal simulations at approximately every half orbital period.

The results from test cases A, B and C will be presented in this section with the remainder of the results shown in Appendix A.

Case A

The plot of y vs. x for case A using the ideal simulation is shown in Figure 5.3. Table 5.4 aides in the understanding of the control actions taken in the ideal simulation of case A. (The switch curves mentioned in this table are defined in Section 4.5.) The slave is considered driven to the origin after the simulation has been running 294.4 minutes; positive drag is commanded 52.4 minutes, negative drag for 48.8 minutes, and the remaining 193.2 minutes are at zero differential drag. Figure 5.4 is a plot of y vs. x for case A using the detailed simulation. Table 5.5 explains the significant points encountered in this simulation. The slave is considered driven to the origin after 349.2 minutes; 50.8 of those minutes use positive drag, 48.4 minutes use negative drag, and the remaining 250.0 minutes command zero differential drag.

The only difference in the plots is between points F and G; in the ideal case it is a straight line and in the detailed case it oscillates in x. The straight line signifies that the slave has zero eccentricity while the oscillations result from a small eccentricity. The switch curves and durations of control for the two cases match closely except for the drift time between points F and G. In the detailed case the control drives the slave closer to the y axis than in the ideal case; this causes the slave to drift toward the origin at a slower rate and increases the total simulation time proportionately.

A plot of x_1 vs. x_2 for the ideal case is shown in Figure 5.5 and the corresponding plot for the detailed case is shown in Figure 5.6; x_3n vs. x_4n for the ideal case is shown in Figure 5.7 with the corresponding plot for the detailed case is shown in Figure 5.8. The plots of x_1 vs. x_2 for the ideal and detailed simulations are basically identical. The plots for x_3n vs. x_4n show the differences in eccentricity that cause the straight and oscillating lines in Figures 5.3

and 5.4; the points F and G are shown at the origin in the ideal simulation
while they are shown to be on a circle with small eccentricity about the origin
in the detailed case. The small eccentricity in the detailed simulation is the only
significant difference between the two cases.

Case B

The plot of y vs. x for case B using the ideal simulation is shown   in Fig-
ure 5.9; Table 5.6 explains the significant points encountered in this simulation.
Figure 5.10 shows the corresponding plot for the detailed simulation and its sig-
nificant points are explained by Table 5.7. The slave is considered driven to the
origin in the ideal simulation after 1020.8 minutes; 458.8 of those minutes are
spent commanding positive drag, 288.8 minutes are at negative drag, and the
remaining 273.2 minutes are at zero differential drag. For the detailed simula-
tion, the time until the slave reaches the origin is 1026.0 minutes; 462.0 minutes
spent are with positive drag, and 285.8 minutes with negative drag.

The plots of y vs. x for the ideal and detailed cases for case B do not match
as well as the plots for case A. The overall shape and total simulation time of
the two cases are similar, but the magnitude of the plots and the behavior of the
slave near the origin are not. A clue to the discrepancies is found in the plots
for the switch curves.

A plot of x_1 vs. x_2 for the ideal case is shown in Figure 5.11.; the corre-
sponding plot for the detailed case is shown in Figure 5.12. The ideal plot shows
the theoretical projected motion of the slave. The final hat maneuver drives the
state in different directions in the ideal and detailed simulations. Slight differ-
ences in the position of the slave when it arrives in the gamma scheme could
cause hat maneuvers to use different controls. The detailed plot is not smooth
from the start of the simulation until shortly after point B; this behavior cannot
be explained using the control law.

The plot of $x_3 n$ vs. $x_4 n$ for the ideal case is shown in Figure 5.13; the
corresponding plot for the detailed case is shown in Figure 5.14. The plot of $x_3 n$
vs. $x_4 n$ for the detailed case is quite disturbing. Not only does it differ from
the ideal plot greatly, but it also containes trajectory segments that appear as
ellipses; in the ideal simulation, the same trajectory segments appear as circles.
The tilted ellipses were not explainable using the control law.
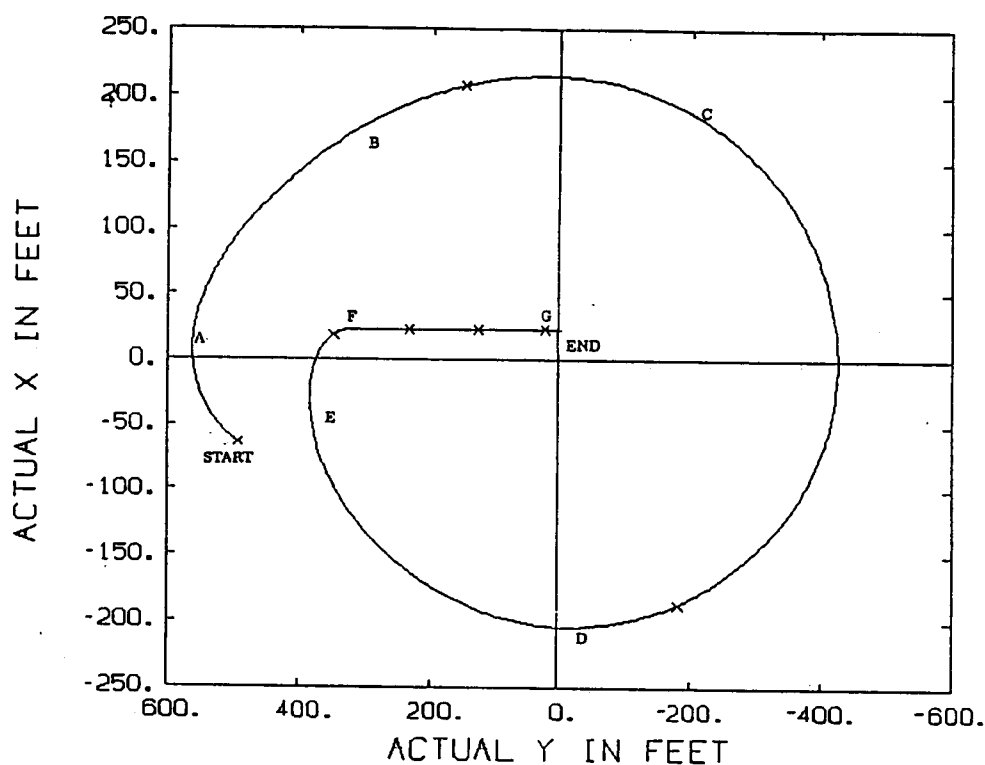
Figure 5.3: *y vs. x for case A using the ideal simulation.*

position	simulation time (min)	switch curve	commanded control	duration of control (min)
START	0.0	–	$a = 0$	16.8
A	16.8	S3	$a < 0$	20.8
B	37.6	S2	$a > 0$	24.4
C	62.0	GA	$a = 0$	37.6
D	99.6	GI1	$a > 0$	24.8
E	124.4	GI2	$a < 0$	28.0
F	152.4	GI3	$a = 0$	138.8
G	291.2	S2	$a > 0$	3.2

Table 5.4: *Points of importance in the ideal simulation for case A.*
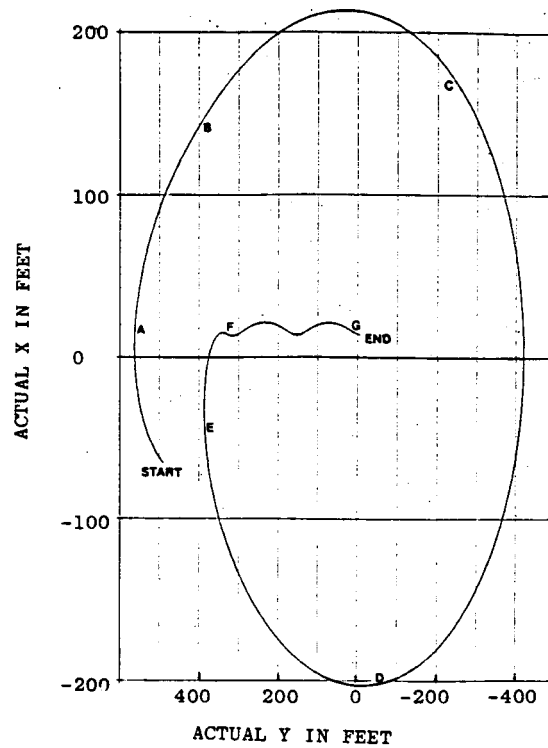
Figure 5.4: *y vs. x for case A using the detailed simulation.*

position	simulation time (min)	switch curve	commanded control	duration of control (min)
START	0.0	–	$a = 0$	17.2
A	17.2	S3	$a < 0$	20.8
B	38.0	S2	$a > 0$	24.4
C	62.4	GA	$a = 0$	37.6
D	100.0	GI1	$a > 0$	25.2
E	125.2	GI2	$a < 0$	27.6
F	152.8	GI3	$a = 0$	195.2
G	348.0	S2	$a > 0$	1.2

Table 5.5: *Points of importance in the detailed simulation for case A.*

Figure 5.5: x_1 vs. x_2 for case A using the ideal simulation.

Figure 5.6: x_1 vs. x_2 for case A using the detailed simulation.

Figure 5.7: x_3n vs. x_4n for case A using the ideal simulation.

Figure 5.8: x_3n vs. x_4n for case A using the detailed simulation.
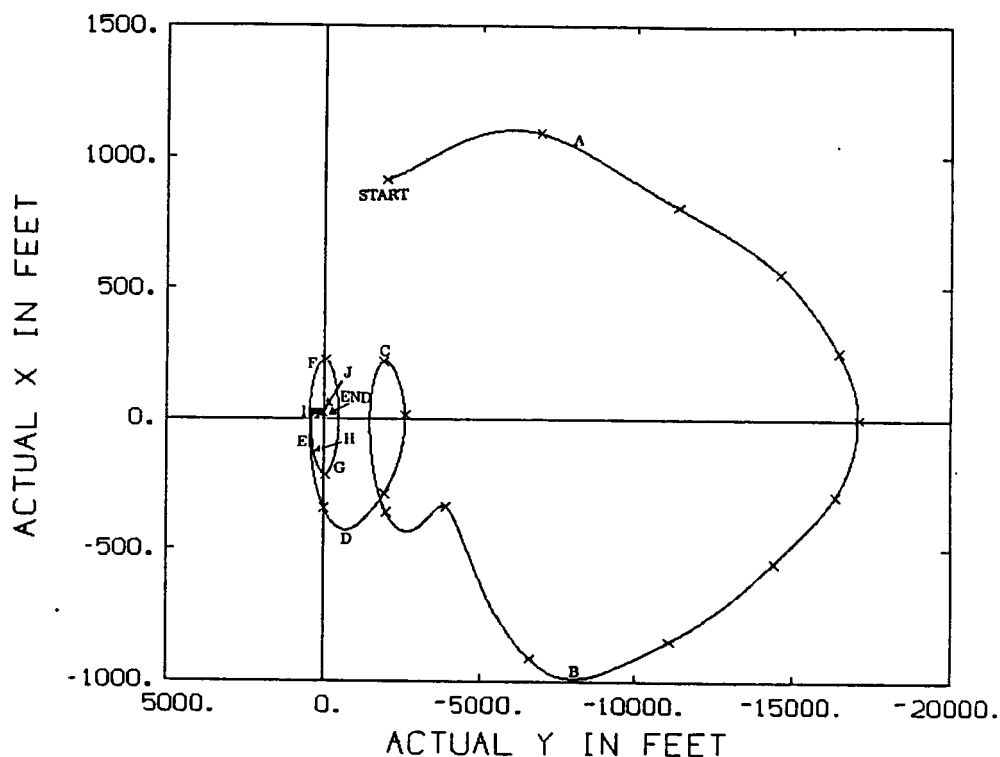
Figure 5.9: *y vs. x for case B using the ideal simulation.*

position	simulation time (min)	switch curve	commanded control	duration of control (min)
START	0.0	–	$a = 0$	64.0
A	64.0	S4	$a > 0$	331.2
B	395.2	S3	$a < 0$	189.6
C	584.8	S4	$a > 0$	93.2
D	678.0	S1	$a < 0$	70.4
E	748.4	S2	$a > 0$	5.6
F	754.0	GA	$a = 0$	46.0
G	800.0	GI1	$a > 0$	26.0
H	826.0	GI2	$a < 0$	28.8
I	854.8	GI3	$a = 0$	163.2
J	1018.0	S2	$a > 0$	2.8

Table 5.6: *Points of importance in the ideal simulation for case B.*

Figure 5.10: *y vs. x for case B using the detailed simulation.*

position	simulation time (min)	switch curve	commanded control	duration of control (min)
START	0.0	–	$a = 0$	63.2
A	63.2	S4	$a > 0$	338.0
B	401.2	S1	$a < 0$	190.0
C	591.2	S2	$a > 0$	60.0
D	651.2	S1	$a < 0$	40.0
E	691.2	S2	$a > 0$	2.4
F	693.6	GA	$a = 0$	8.4
G	702.0	GO1	$a < 0$	37.2
H	739.2	GO2	$a > 0$	46.8
I	786.0	GO3	$a = 0$	145.2
J	931.2	S1	$a < 0$	5.4
K	936.6	GA	$a = 0$	40.6
L	977.2	GI1	$a < 0$	12.0
M	989.2	GI2	$a > 0$	14.8
N	1004.0	GI3	$a = 0$	22.0
O	1026.0	S1	$a < 0$	1.2

Table 5.7: *Points of importance in the detailed simulation for case B.*
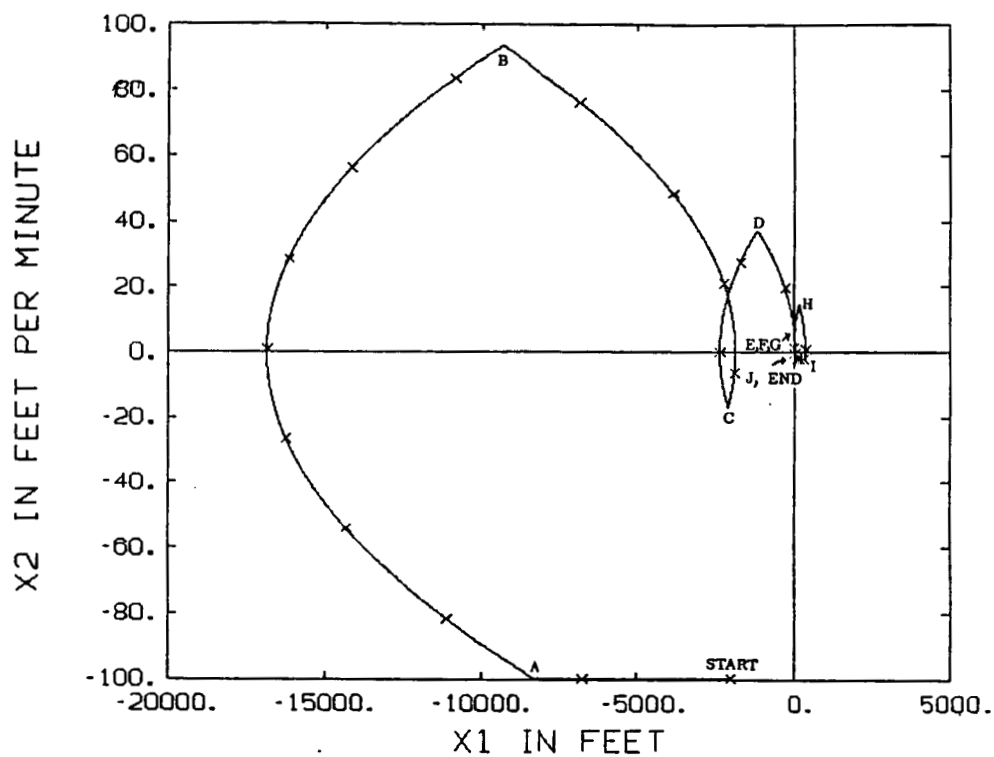
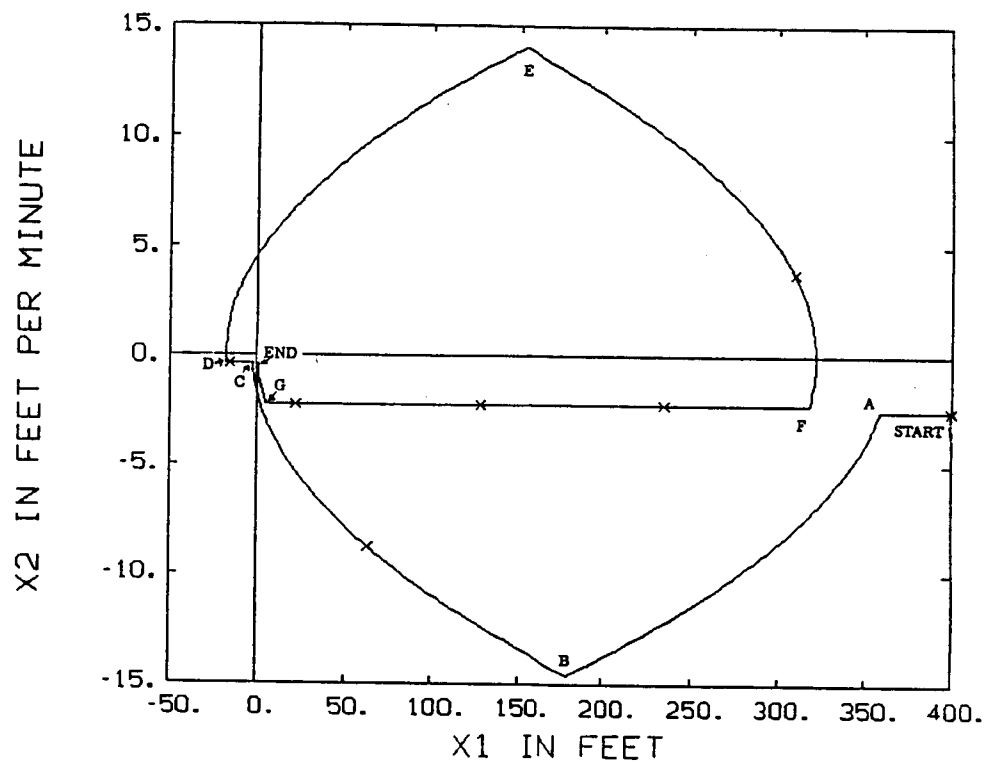Figure 5.11: x_1 vs. x_2 for case B using the ideal simulation.
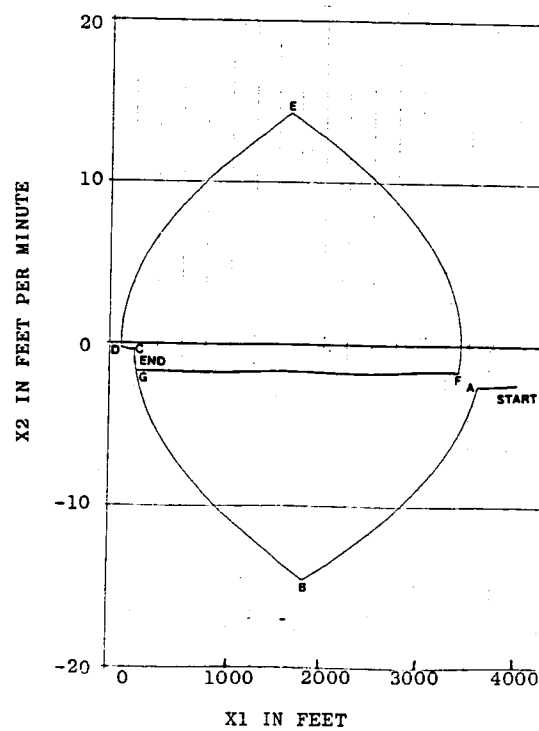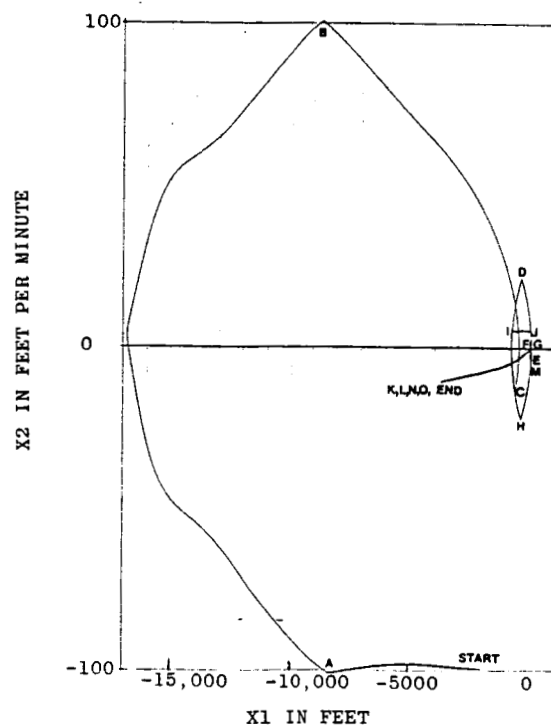

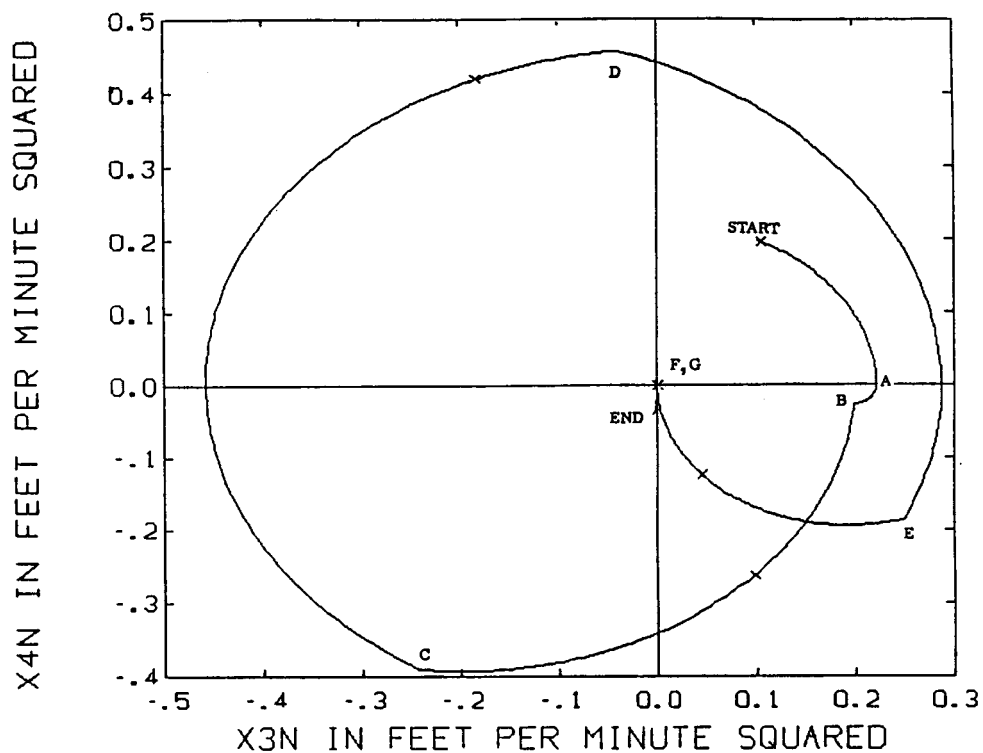Figure 5.12: x_1 vs. x_2 for case B using the detailed simulation.
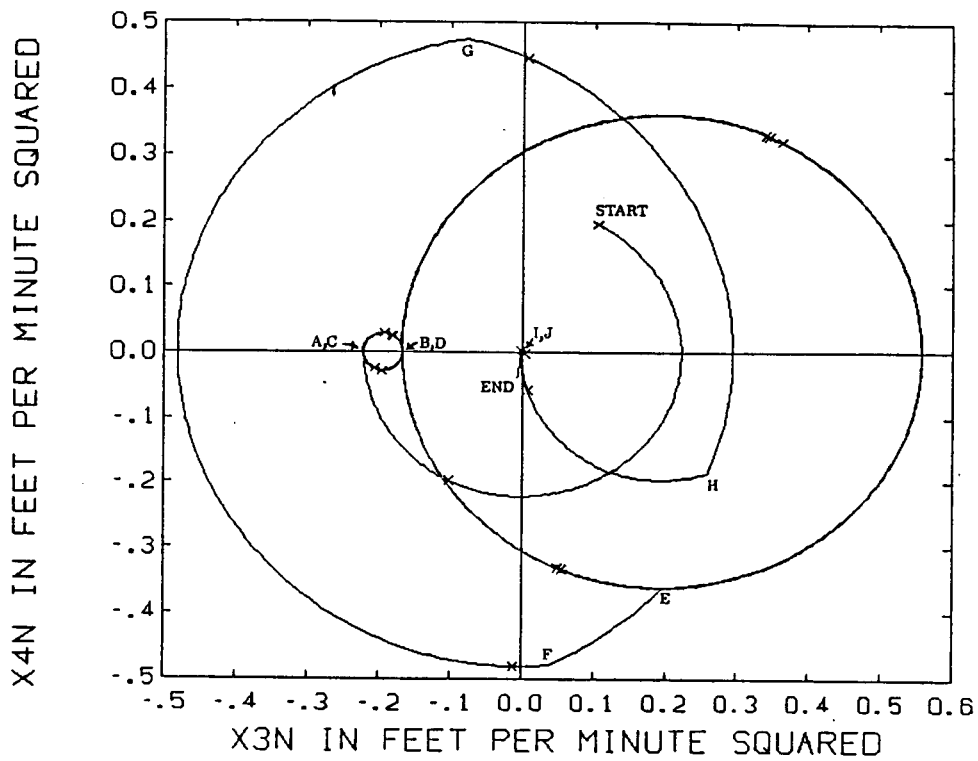
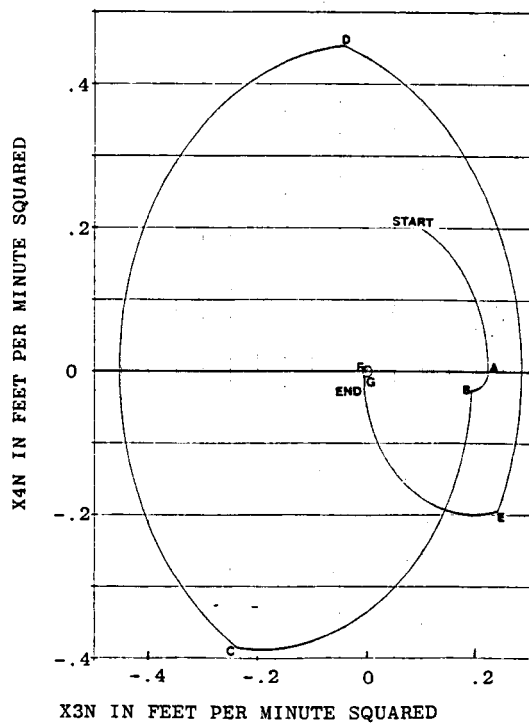Figure 5.13: x_3n vs. x_4n for case B using the ideal simulation.

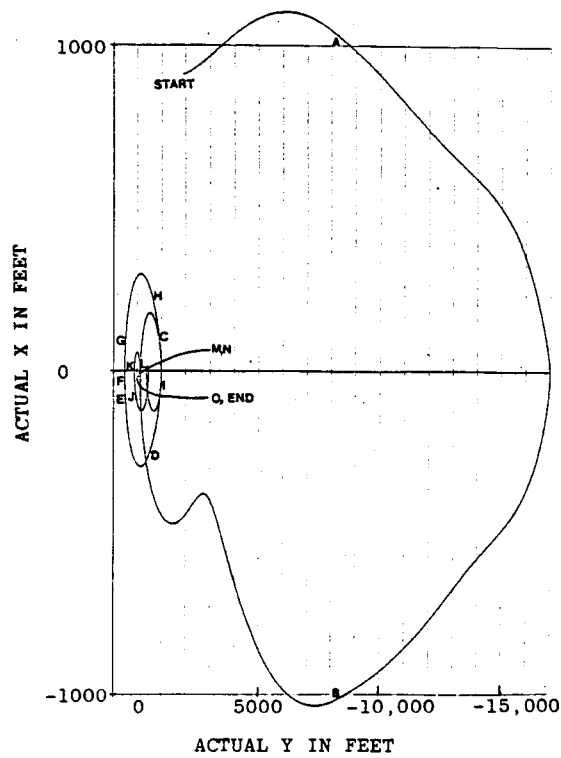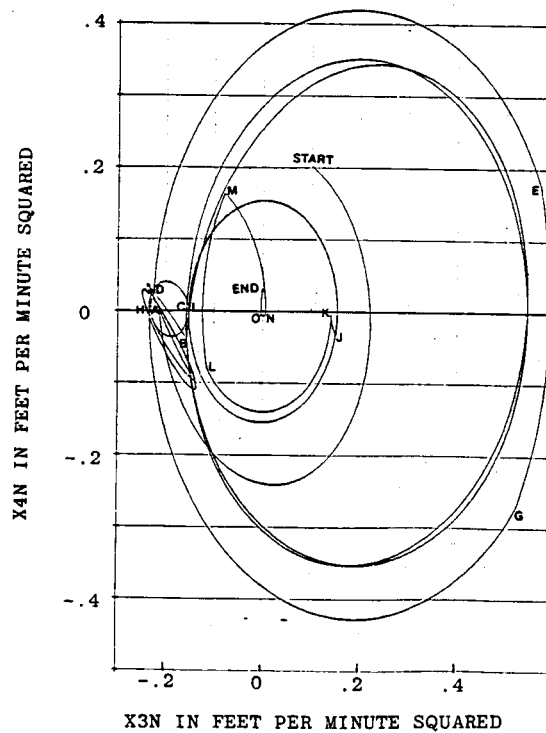Figure 5.14: x_3n vs. x_4n for case B using the detailed simulation.
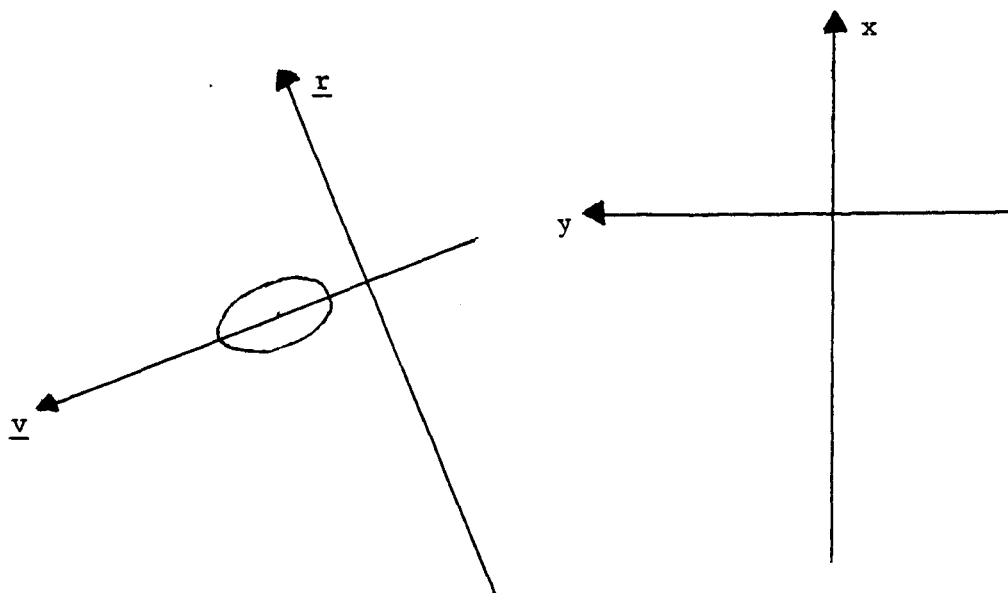
Figure 5.15: *Eccentricity as seen by the detailed simulation at a large value of* $\bar{y}$.

The tilted curves exist in the plot for the detailed simulation because of the rectilinear coordinate system used. The detailed simulation integrates the motion of both the target and the slave in spherical coordinates, then converts the states into inertial coordinates. The position and velocity of the target and slave are then differenced to calculate $\bar{y}$, $\bar{x}$, β and α. The eccentricity of the slave is a two by one ellipse in the rectilinear coordinate system. With a substantial difference in y between the slave and the target, an ellipse with its major axis horizontal in the spherical frame appears as a similar ellipse with its major axis tilted from the horizontal in the rectilinear frame. (Figure 5.15) When the mathematical transformation to change a two by one ellipse in the x, y plane to a circle in the $x_3 n, x_4 n$ plane occurs, the tilted two by one ellipse is accentuated.

In order to verify the above explanation for the tilted ellipse in the $x_3 n, x_4 n$ plane, case B was tested using the detailed simulation with curvilinear rather than rectilinear coordinates. The plot of y vs. x for this simulation is shown in Figure 5.16, x_1 vs. x_2 is shown in Figure 5.17 while Figure 5.18 shows the

plot of x_3n vs. x_4n.   The significant points in the simulation are explained in Table 5.8. The slave is considered driven to the origin after 1340 minutes; 654.8 of those minutes are spent commanding positive drag, 484.8 minutes are with negative drag, and the remaining 200.4 minutes are at zero differential drag.

The plot of y vs. x is not similar to the ideal case but does resemble what theoretically could occur for the initial conditions. The plot of x_1 vs. x_2 is smooth and the sawtooth maneuver used to reduce eccentricity is clear in this plot. The tilted ellispes in the plot of x_3n vs. x_4n have disappeared with the use of the curvilinear coordinate system; this plot almost identically matches the ideal one. The trajectory spirals in the x_3n vs. x_4n plot due to the slave geting closer to the origin.

Case C

The plot of y vs. x for case C using the ideal simulation is shown in Figure 5.19; Table 5.9 explains the significant points encountered in this simulation. Figure 5.20 shows the corresponding plot for the detailed simulation and its significant points are explained by Table   5.10. The slave is considered driven to the origin in the ideal·simulation after 912.0 minutes; 58.4 of those minutes are spent commanding positive drag, 64.4 minutes are with negative drag, and the remaining 789.2 minutes are at zero differential drag. For the detailed simulation, the time until the slave reaches the origin is 372.8 minutes; 60.0 minutes under positive drag, and 63.6 minutes with negative drag.

The plots for the two simulations are quite similar. The ideal simulation places the slave closer to the y axis; this causes the slave to take longer to drift toward the origin and thus increases the total simulation time. The final eccentricities are the same; the final eccentricity for the ideal case may appear more pronounced as the slave moves more slowly toward the origin and more cycles of eccentricity are shown.

A plot of x_1 vs. x_2 for the ideal case is shown in Figure 5.21.; the corresponding plot for the detailed case is shown in Figure 5.22. The plots of x_1 vs. x_2 are similar. The final leg of the hat maneuver places the slave closer to the x_1 axis in the ideal case, resulting in the slave's slower movement toward the origin. This plot depicts one of the problems encountered using a large time step; point B is not actually on the switch curve S1, thus the origin is missed,
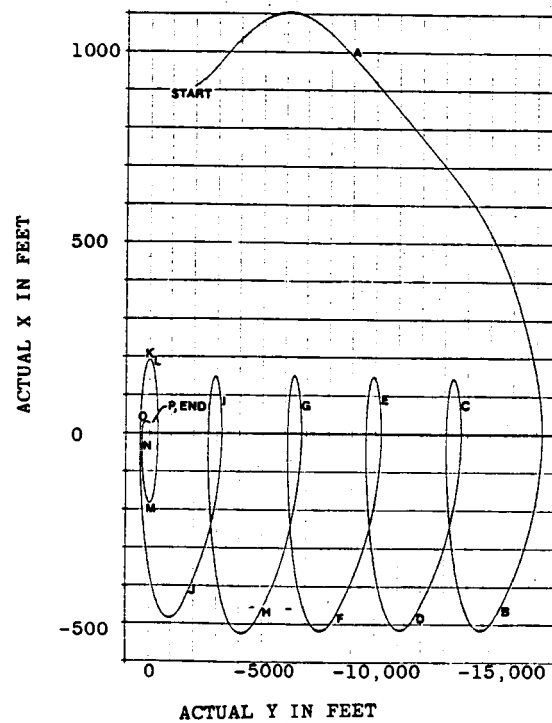
Figure 5.16: *y vs. x for case B using the detailed simulation with curvilinear coordinates.*

position	simulation time (min)	switch curve	commanded control	duration of control (min)
START	0.0	–	$a = 0$	65.6
A	65.6	S4	$a > 0$	250.0
B	315.6	S3	$a < 0$	95.2
C	410.8	S4	$a > 0$	94.8
D	505.6	S3	$a < 0$	95.2
E	600.8	S4	$a > 0$	95.2
F	696.0	S3	$a < 0$	95.2
G	791.2	S4	$a > 0$	96.0
H	887.2	S3	$a < 0$	95.2
I	982.4	S4	$a > 0$	88.0
J	1070.4	S1	$a < 0$	77.2
K	1147.6	S2	$a > 0$	4.0
L	1151.6	GA	$a = 0$	46.0
M	1197.6	GI1	$a > 0$	22.8
N	1220.4	GI2	$a < 0$	26.8
O	1247.2	GI3	$a = 0$	88.8
P	1336.0	S2	$a > 0$	4.0

Table 5.8: *Points of importance for case B using the detailed simulation with curvilinear coordinates.*
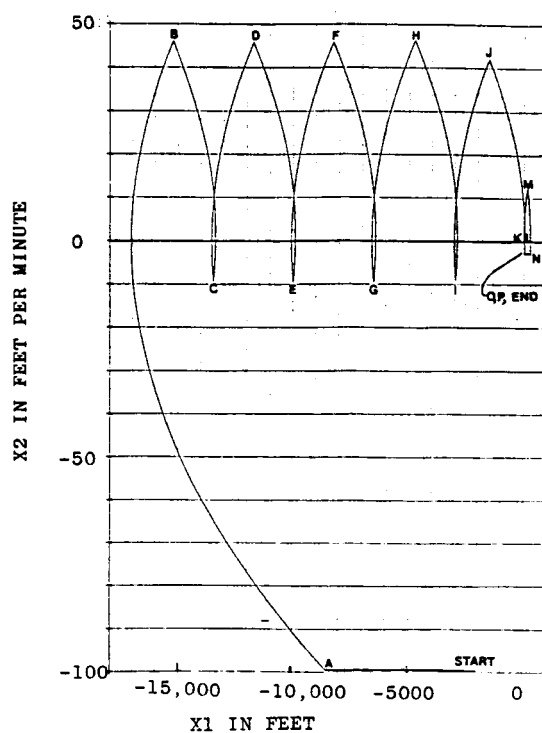
Figure 5.17: x_1 vs. x_2 for case B using the detailed simulation with curvilinear coordinates.
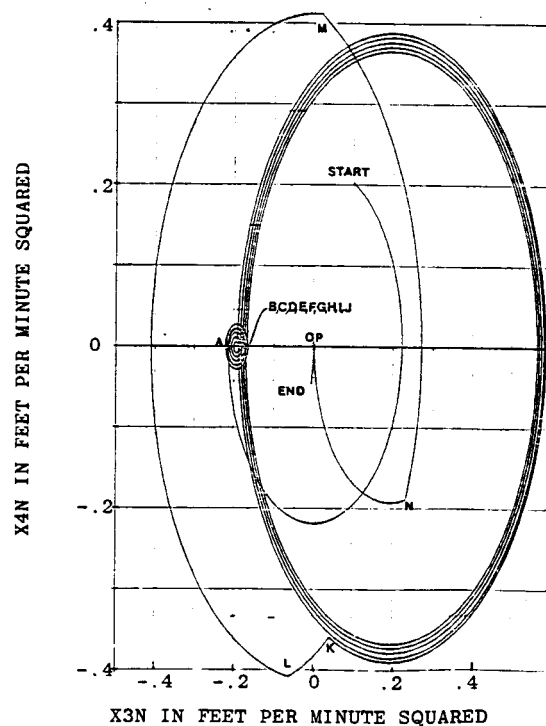
Figure 5.18: $x_3 n$ vs. $x_4 n$ for case B using the detailed simulation with curvilinear coordinates.
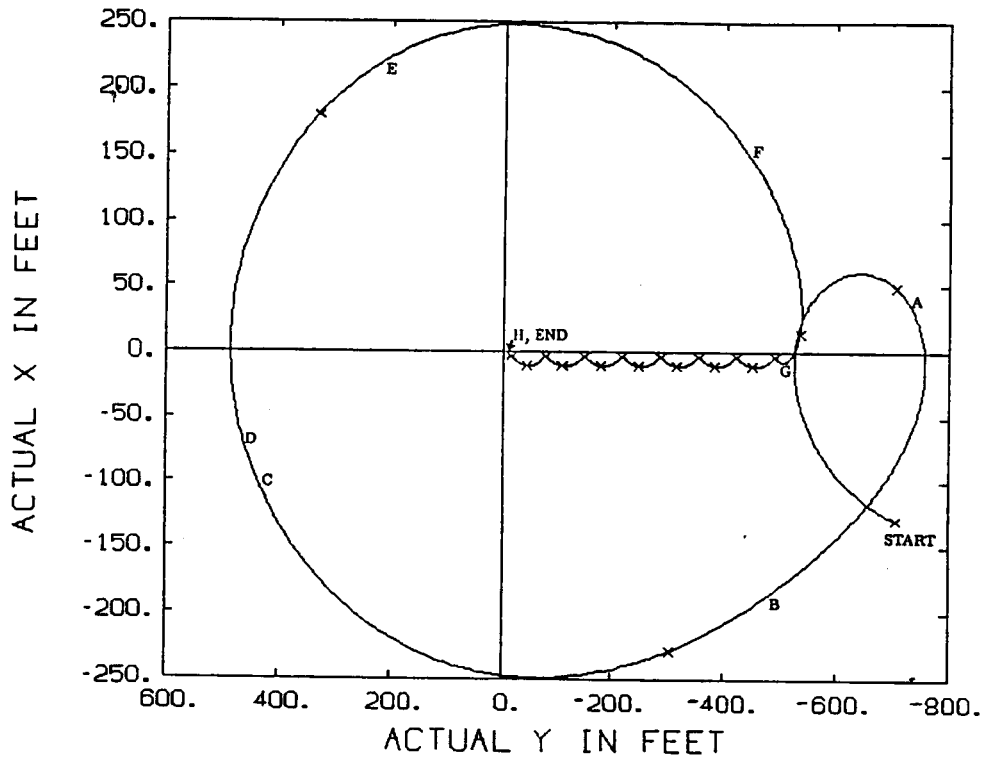
Figure 5.19: *y vs. x for case C using the ideal simulation.*

position	simulation time (min)	switch curve	commanded control	duration of control (min)
START	0.0	–	$a = 0$	64.0
A	64.0	S4	$a > 0$	24.4
B	88.4	S1	$a < 0$	35.6
C	124.0	S2	$a > 0$	3.6
D	127.6	GA	$a = 0$	21.2
E	148.8	GI1	$a < 0$	28.4
F	177.2	GI2	$a > 0$	30.4
G	207.6	GI3	$a = 0$	704.0
H	911.6	S1	$a < 0$	0.4

Table 5.9: *Points of importance in the ideal simulation for case C.*
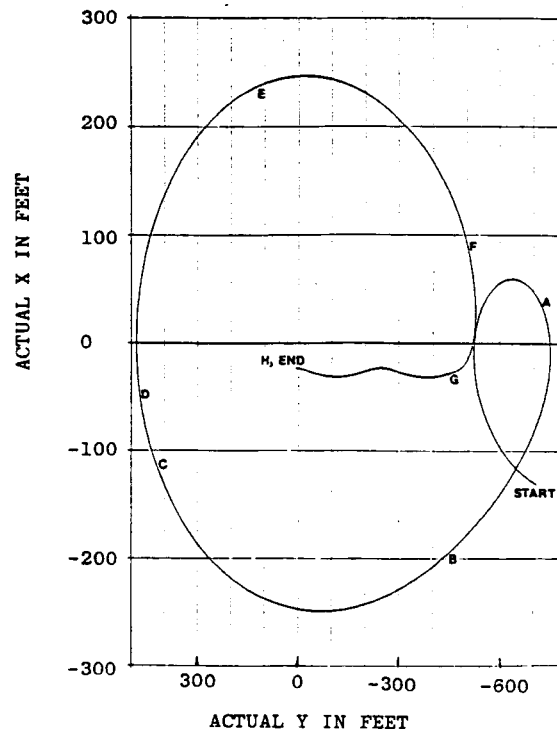
Figure 5.20: *y vs. x for case C using the detailed simulation.*

position	simulation time (min)	switch curve	commanded control	duration of control (min)
START	0.0	–	$a = 0$	64.0
A	64.0	S4	$a > 0$	24.0
B	88.0	S1	$a < 0$	35.2
C	123.2	S2	$a > 0$	3.6
D	126.8	GA	$a = 0$	22.0
E	148.8	GI1	$a < 0$	27.2
F	176.0	GI2	$a > 0$	32.4
G	208.4	GI3	$a = 0$	163.2
H	371.6	S1	$a < 0$	1.2

Table 5.10: *Points of importance in the detailed simulation for case C.*
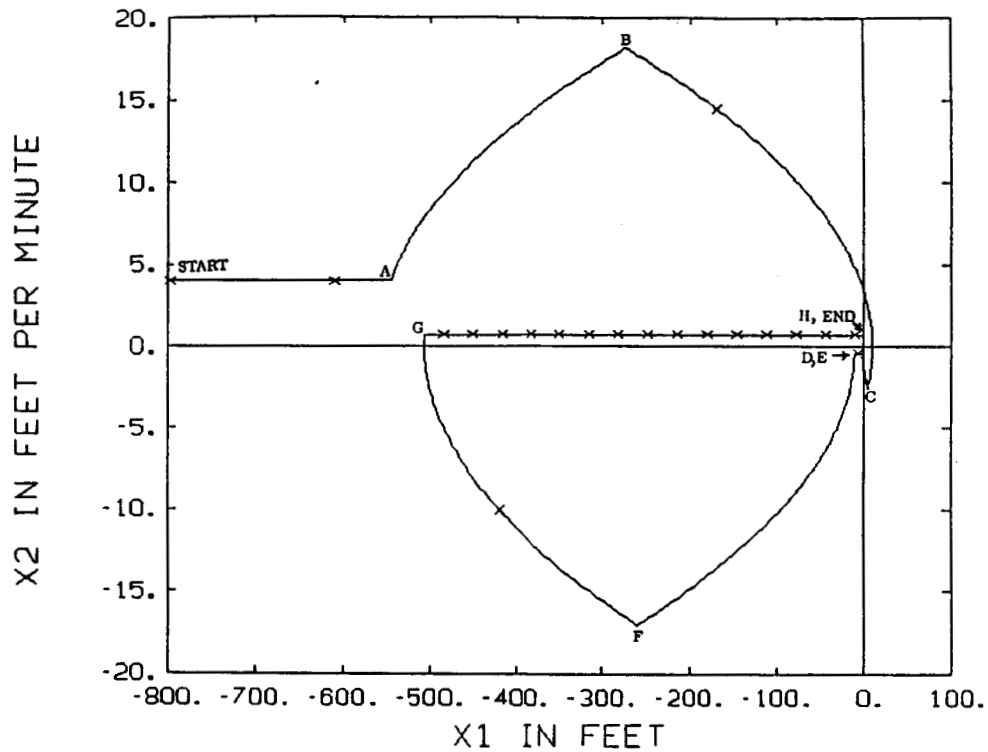
Figure 5.21: x_1 vs. x_2 for case C using the ideal simulation.
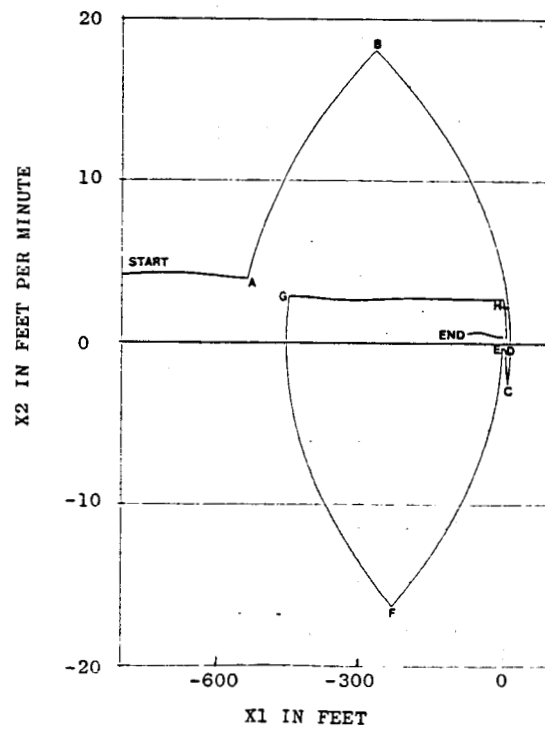
Figure 5.22: x_1 vs. x_2 for case C using the detailed simulation.
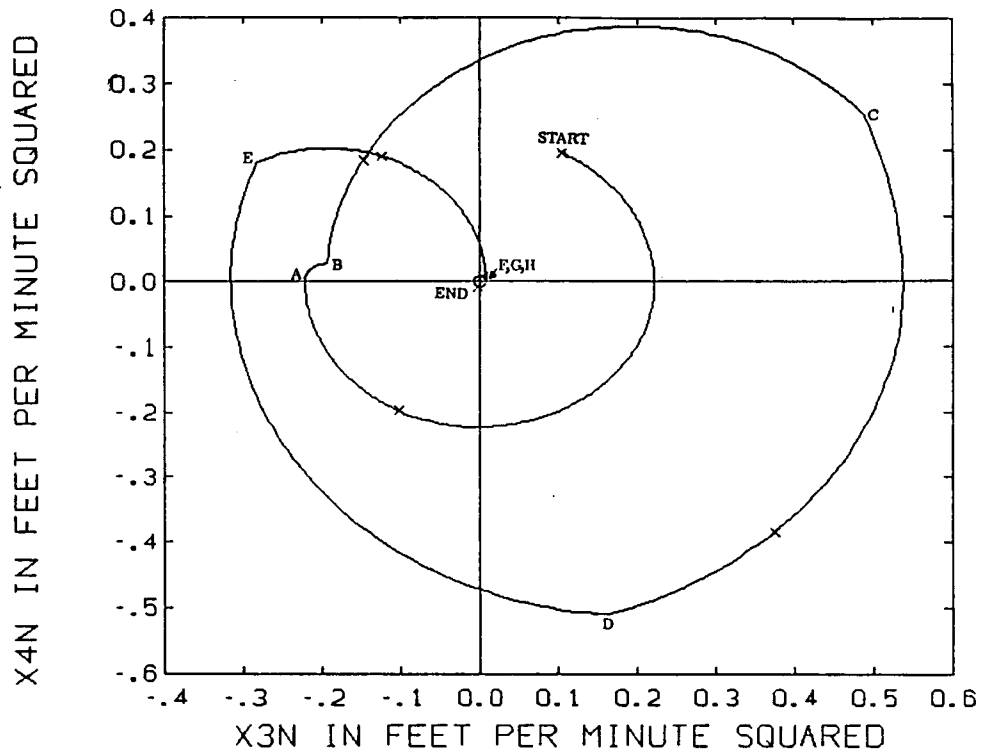
Figure 5.23: x_3n vs. x_4n for case C using the ideal simulation.
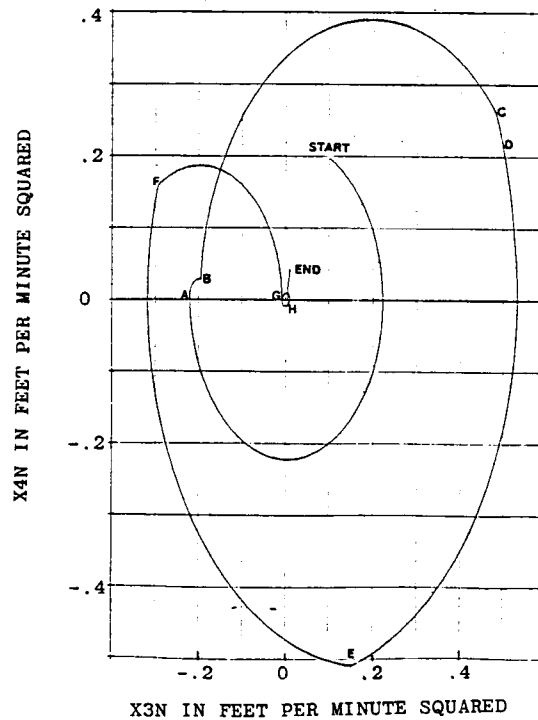
Figure 5.24: x_3n vs. x_4n for case C using the detailed simulation.

and the switch at point C to the switch curve S2 is used to reach the origin.

The plot of $x_3 n$ vs. $x_4 n$ for the ideal case is shown in Figure 5.23; the corresponding plot for the detailed case is shown in Figure 5.24. The two simulations have simular plots for $x_3 n$ vs. $x_4 n$. The plots show the trade off between the closing rate of the drift phase of the final hat maneuver and the final eccentricity. The ideal case, which has a very slow closing rate, does not need to move its eccentricity far from the origin at the end of the simulation; in the detailed case, which has a relatively fast closing rate, it is necessary to move the eccentricity farther from the origin in order to get the average position of the slave to the target.

Verification for Differing Values for Differential Drag

A differential drag value of .1944 ft/min^2 was used in the ideal and detailed simulations. In order to verify that the control law works for different values of differential drag, case C was tested using the ideal simulation with a differential drag of .1388 ft/min^2 in one case and .2500 ft/min^2 in the other.

Figure 5.25 shows y vs. x for the simulation where the differential drag used was .1388 ft/min^2; Figure 5.26 shows x_1 vs. x_2 and Figure 5.27 shows $x_3 n$ vs. $x_4 n$. Table 5.11 explains the significant points in this simulation. The slave is considered driven to the origin after 352.0 minutes; positive drag is commanded for 59.6 minutes, 65.6 minutes are at negative drag, and the remaining 226.8 minutes are at zero differential drag.

During the main control scheme of the control law, the slave using smaller drag does not drift as far from the target as does the one using nominal drag. The maximum and minumum x for the simulation using a smaller drag are 178 ft and -214 ft; the maximum and minimum x for the nominal drag are 246 and -249 ft. The slave using the smaller drag only moves 360 ft in front of the target while with the nominal drag it moves 480 ft in front of the target. The hat shaped maneuver is thinner in the case with the smaller drag and the centers of the non-zero drag circles in the $x_3 n, x_4 n$ plane have moved closer to the origin. The total non-zero drag time for the simulation using smaller drag is 125.2 minutes compared to 123.6 minutes for the simulation with nominal drag.

Figure 5.28 shows y vs. x for the simulation where the differential drag used was .2500 ft/min^2; Figure 5.29 shows x_1 vs. x_2 and Figure 5.30 shows $x_3 n$

vs.x_4n. Table 5.12 explains the significant points in this simulation. The slave is considered driven to the origin after 552.0 minutes; 58.0 of those minutes are spent commanding positive drag, 62.4 minutes are at negative drag, and the remaining 431.6 minutes are at zero differential drag.

During the main control scheme of the control law, the slave using larger drag goes farther from the target than the one using nominal drag. The simulation using the larger drag has a maximum and minumum x of 335 ft and -338 ft and moves 670 ft in front of the target. The hat shaped maneuver is wider in the case with the larger drag and the centers of the non-zero drag circles in the x_3n, x_4n plane have moved farther from the origin. The total non-zero drag time for the case using larger drag is 120.4 minutes.

The control law is able to drive the slave to the origin in all cases. Though there are differences in magnitude, the basic shape of all corresponding plots are similar. The smaller the drag, the closer the slave tends to stay to the origin and the longer the duration of non-zero drag used to get the slave to the target. The larger the drag, the shorter the duration of non-zero drag and the farther the slave strays from the target.

The results of cases D through H are presented in Appendix A. Case F is similar in nature to case B, hence both the linear and curvilinear cases for the detailed simulation are shown.

5.3   Test Cases Started in the Gamma Control Scheme

The initial conditions for test cases A and D are such that they could be in the drift phase of a hat maneuver. This section examines what happens to the slave when the control law is started in the drift phase of the hat maneuver, rather than at the beginning of the control law, for cases A and D; the corresponding test cases will be called I and J.

The plot of y vs. x for case I is shown in Figure 5.31. The plot of x_1 vs. x_2 is shown in Figure 5.32; x_3n vs. x_4n is plotted in Figure 5.33. The important points of this simulation are explained in Table 5.13. The simulation ends after 489.2 minutes. The total times of positive and negative drag are 23.6 and 18.0 minutes respectively; the duration of zero differential drag is 247.6 minutes.

Figure 5.25: *y vs. x for case C using the detailed simulation with a differential drag lower than the nominal value.*

position	simulation time (min)	switch curve	commanded control	duration of control (min)
START	0.0	–	$a = 0$	64.0
A	64.0	S4	$a > 0$	26.8
B	90.8	S1	$a < 0$	35.6
C	126.4	GA	$a = 0$	22.8
D	149.2	GI1	$a < 0$	28.8
E	178.0	GI2	$a > 0$	32.8
F	210.8	GI3	$a = 0$	140.0
G	350.8	S1	$a < 0$	1.2

Table 5.11: *Points of importance for case C using the detailed simulation with a differential drag lower than the nominal value.*

Figure 5.26: x_1 vs. x_2 for case C using the detailed simulation with a differential drag lower than the original value.

Figure 5.27: x_3n vs. x_4n for case C using the detailed simulation with a differential drag lower than the original value.
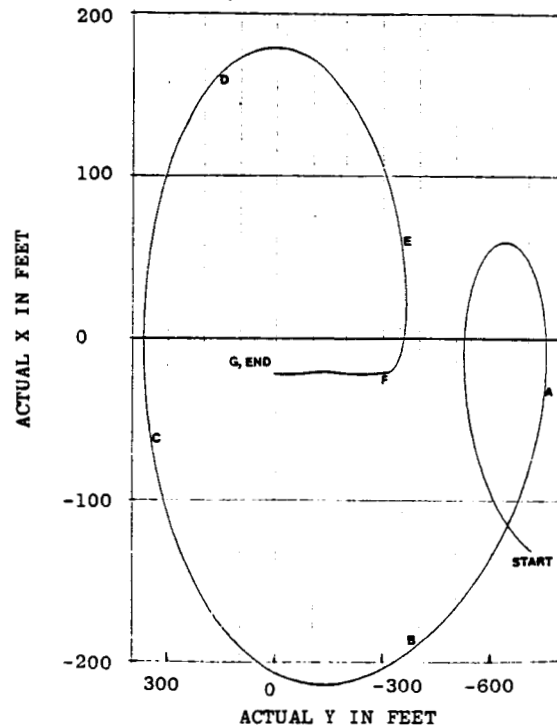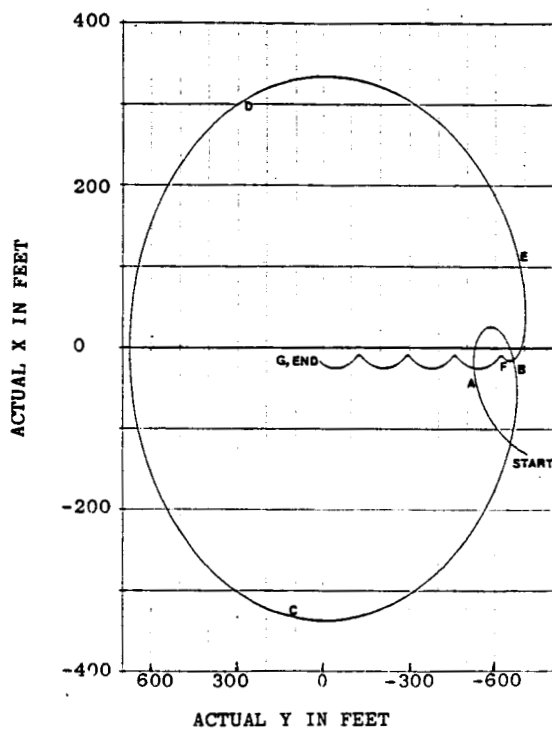
Figure 5.28: *y vs. x for case C using the detailed simulation with a differential drag higher than the original value.*

position	simulation time (min)	switch curve	commanded control	duration of control (min)
START	0.0	–	$a = 0$	16.8
A	16.8	S4	$a > 0$	331.2
B	42.8	S1	$a < 0$	189.6
C	74.0	GA	$a = 0$	93.2
D	112.8	GI1	$a < 0$	70.4
E	142.8	GI2	$a > 0$	5.6
F	174.8	GI3	$a = 0$	46.0
G	550.8	S1	$a < 0$	26.0

Table 5.12: *Points of importance for case C using the detailed simulation with a differential drag higher than the original value.*
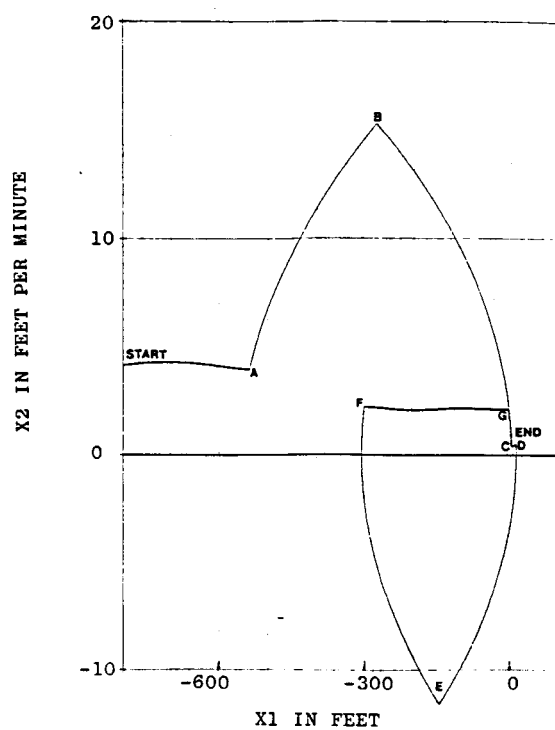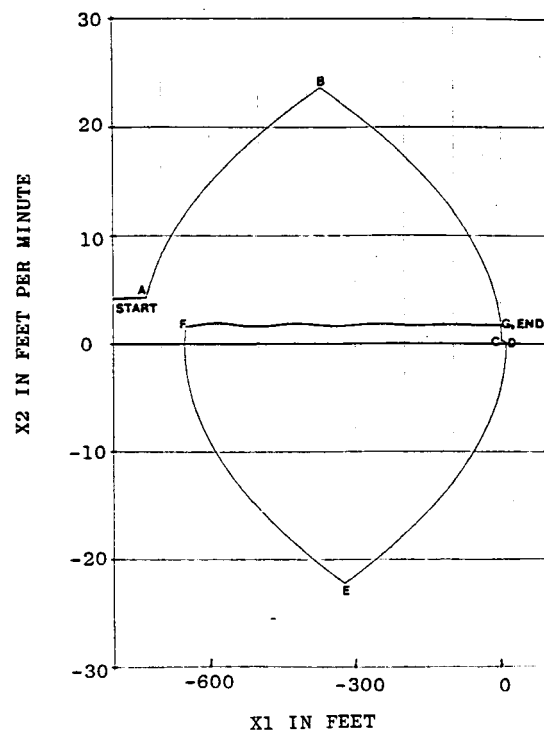
Figure 5.29: x_1 vs. x_2 for case C using the detailed simulation with a differential drag higher than the original value.
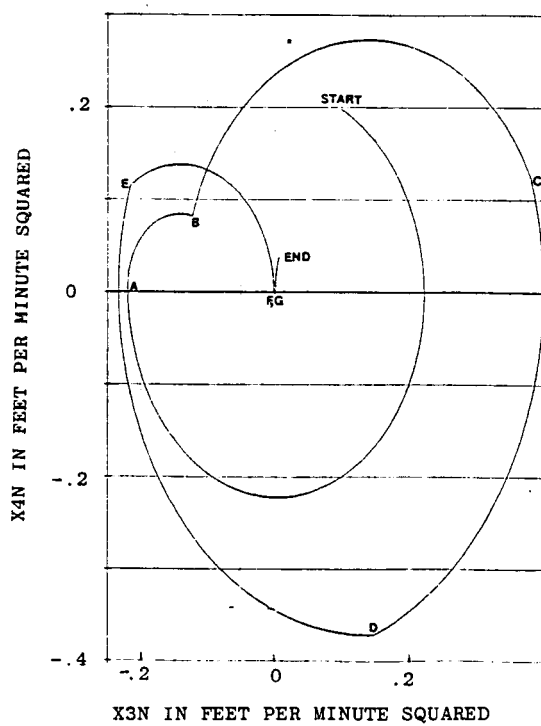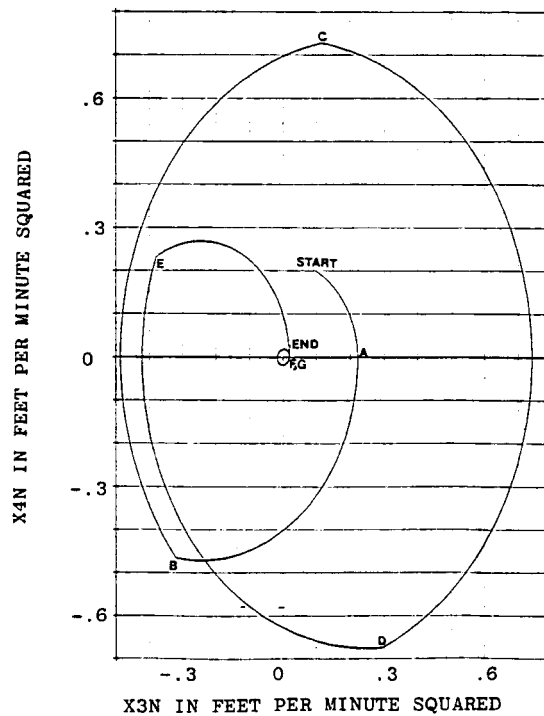

Figure 5.30: x_3n vs. x_4n for case C using the detailed simulation with a differential drag higher than the original value.
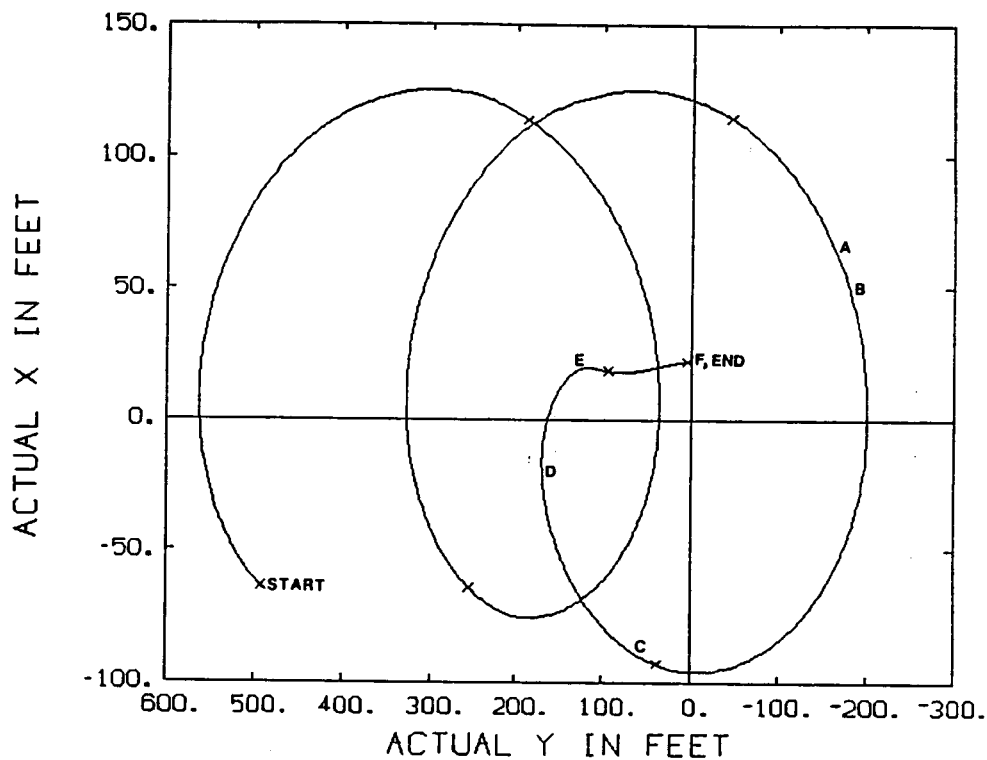
Figure 5.31: *y vs. x for case I which begins in the drift phase of a hat maneuver.*

position	simulation time (min)	switch curve	commanded control	duration of control (min)
START	0.0	–	$a = 0$	162.8
A	162.8	S2	$a > 0$	3.6
B	166.4	GA	$a = 0$	29.2
C	195.6	GI1	$a > 0$	15.2
D	210.8	GI2	$a < 0$	18.0
E	228.8	GI3	$a = 0$	55.6
F	284.4	S2	$a > 0$	4.8

Table 5.13: *Points of importance for case I which begins in the drift phase of a hat maneuver.*
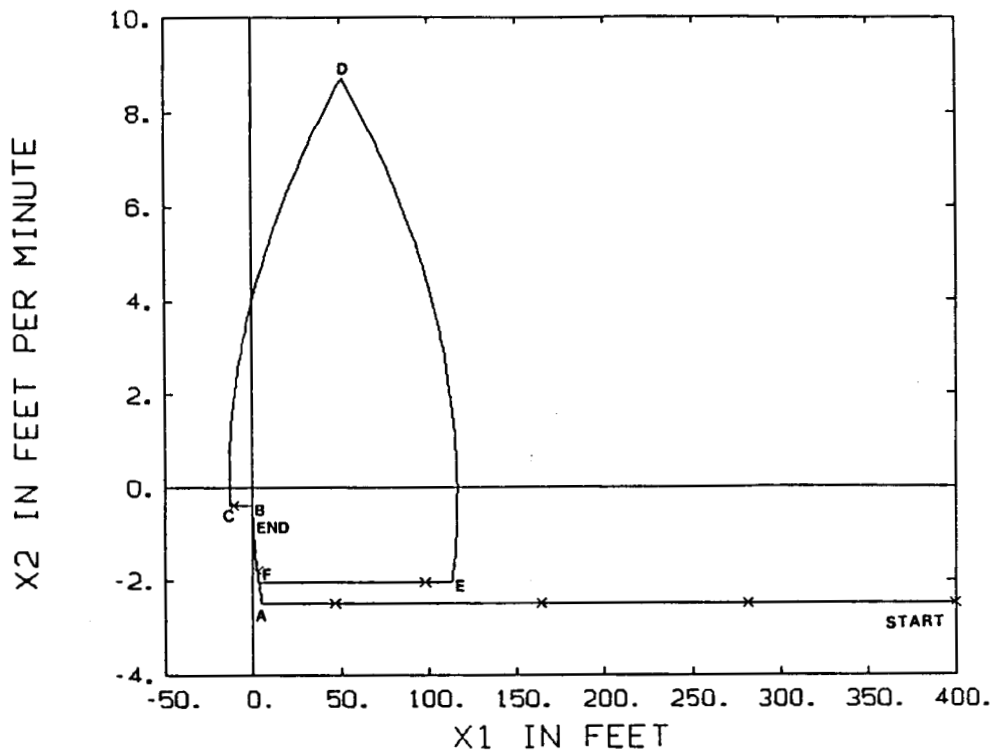
Figure 5.32: x_1 vs. x_2 for case I which begins in the drift phase of a hat maneuver.
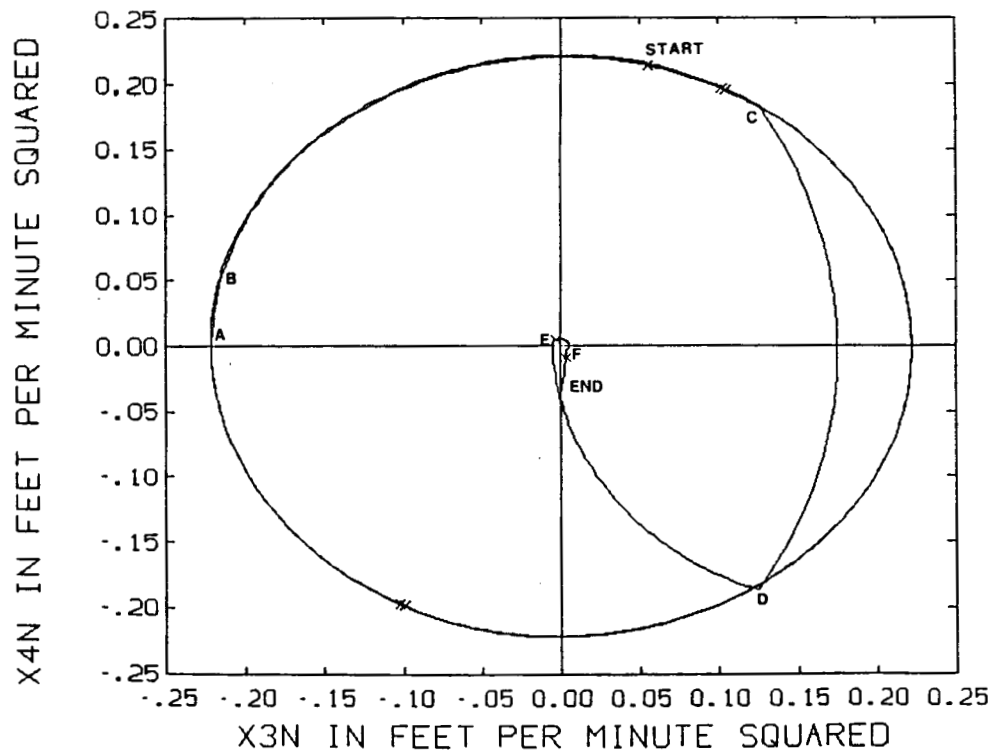
Figure 5.33: x_3n vs. x_4n for case I which begins in the drift phase of a hat maneuver.

Case I takes 194.8 minutes longer to reach the origin than does Case A; yet the duration of non-zero control for Case I is 41.6 minutes, less than half the 101.2 minutes of non-zero control in case A. Figure 5.32 shows that case I has two hat maneuver drift phases in the gamma control scheme while Figure 5.5 shows case A only having one; this accounts for the differences in total simulation time and duration of non-zero control.

Figure 5.34 shows y vs. x for case J. The plot of x_1 vs. x_2 is shown in Figure 5.35 while x_3n vs. x_4n is shown in Figure 5.36. Table 5.14 shows the important points of this simulation. The total simulation time is 2029.6 minutes. The durations of positive and negative drag are 62.4 and 57.6 minutes respectively; the total time of zero differential drag is 1909.6 minutes.

Case J takes 1438.8 more minutes to reach the origin than does case D; this is due mainly to the 1608.8 minutes of drift phase in a hat maneuver (associated with point E) in the case J simulation. The duration of non-zero control in case J is 120.0 minutes while for case D it is 287.2 minutes. Case J has one more drift phase in a hat maneuver than does case D.

For initial conditions in which it is possible to start the control law in the gamma control scheme, a case started in the gamma control scheme will have one more drift phase of a hat maneuver than if it were started at the beginning of the control scheme. The extra drift phase generally causes the slave to take longer to reach the origin and have a shorter duration of non-zero control than the case started at the beginning of the control law.

If time is to be minimized, then the control law should be started at the beginning for any initial position; if drag is to be minimized, then the control law should begin in the drift phase of a hat maneuver in the gamma control scheme whenever it is possible to do so. Two of the assumptions in the formulation of the control law are that drag is considered free and that the time to move the slave from its initial position to the origin should be minimized; thus in this formationkeeping problem, it is proper to initialize at the beginning of the control law for all cases.

5.4 Formationkeeping at the Origin

This section discusses how differential drag can be used to keep the slave at

the origin. Section 5.4.1 shows what happens to the slave if the control law is simply turned off once the slave reaches the origin. Section 5.4.2 explains what happens if the control law is turned off once the slave reaches the origin, and is then turned back on again once the slave drifts more than ten feet away. A controller that attempts to keep the slave within one foot of the origin in the y direction is discussed Section 5.4.3.

5.4.1   Slave Behavior When the Control Law is Turned Off

If the difference in $\bar{x}$ between the slave and the target is zero when the slave reaches the origin, then the slave will stay in place indefinitely. The original tolerances placed upon what is considered the origin in the control law were based upon the time step used in the simulations, and thus may allow the slave to drift away from the target at an unacceptable rate. The controller must drive the slave closer to the target if the control law is to be turned off when the slave reaches the origin. This section compares uncontrolled slave motion following the normal control law, and following the control law with tighter tolerances set for the origin.

All tests were run using the ideal simulation; the initial conditions of the tests where those at the start of the final gamma control scheme for cases A, B and C. The control law drives the slave to the origin after which the slave is allowed to drift for a total simulation time of 24 hours.

Normal Tolerance on Placement of Slave

Figure 5.37 shows y vs. x from the start of the final hat maneuver for   case A; Figure 5.38 shows x_1 vs. x_2 while x_3n vs. x_4n is shown in Figure 5.39. Table 5.15 explains the important points of this simulation. The control is turned off 233.0 minutes into the simulation. In the remaining 1267 minutes (21.2 hours) the slave drifts 494.7 feet away from the origin in the direction opposite to the velocity vector. The drift rate of the slave away from the target is .390 feet per minute.

Figure 5.40 shows y vs. x from the start of the final hat maneuver for case B, x_1 vs. x_2 is shown in Figure 5.41 and Figure 5.42 shows x_3n vs. x_4n.
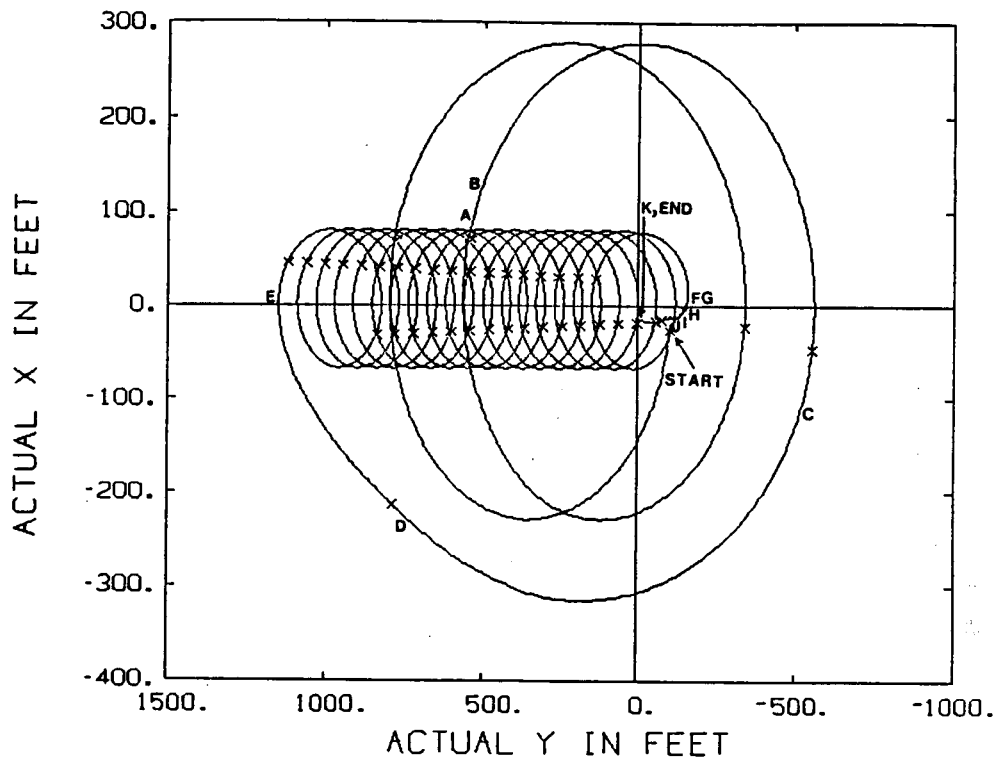
Figure 5.34: *y vs. x for case J which begins in the drift phase of a hat maneuver.*

position	simulation time (min)	switch curve	commanded control	duration of control (min)
START	0.0	–	$a = 0$	158.8
A	158.8	S2	$a > 0$	3.6
B	162.4	GA	$a = 0$	27.6
C	190.0	GO1	$a > 0$	42.4
D	238.4	GO2	$a < 0$	42.8
E	275.2	GO3	$a = 0$	1608.8
F	1884.0	S2	$a > 0$	0.4
G	1884.4	GA	$a = 0$	35.6
H	1920.0	GI1	$a < 0$	12.8
I	1932.8	GI2	$a > 0$	16.0
J	1948.8	GI3	$a = 0$	78.8
K	2027.6	S1	$a < 0$	2.0

Table 5.14: *Points of importance for case J which begins in the drift phase of a hat maneuver.*
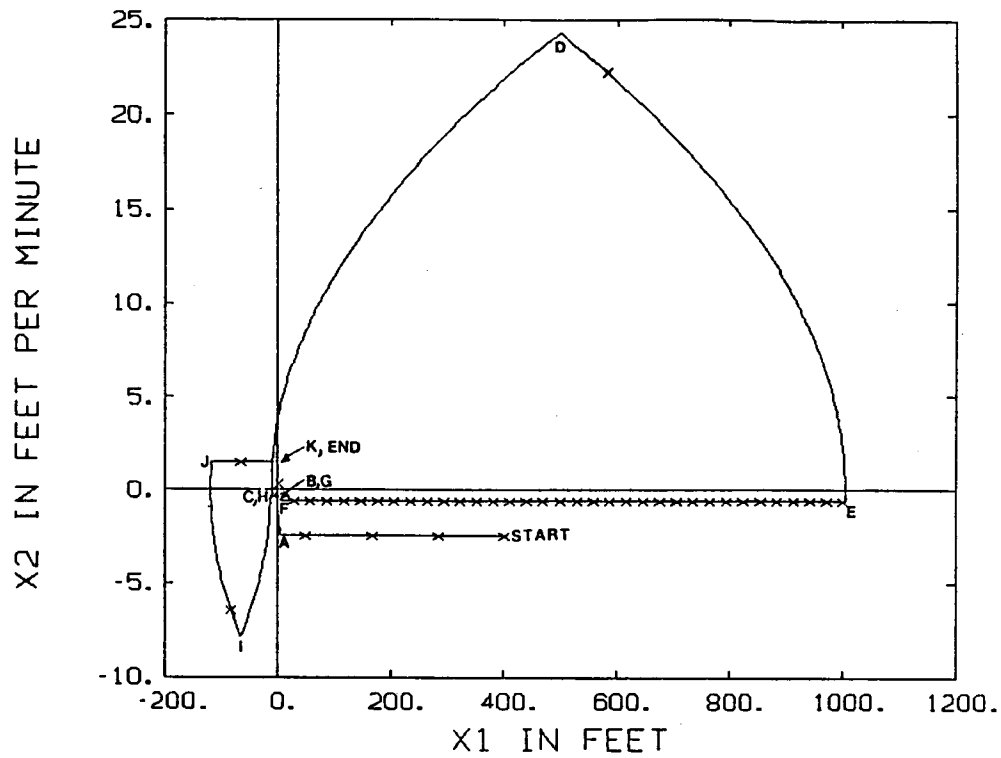
Figure 5.35: x_1 vs. x_2 for case J which begins in the drift phase of a hat maneuver.
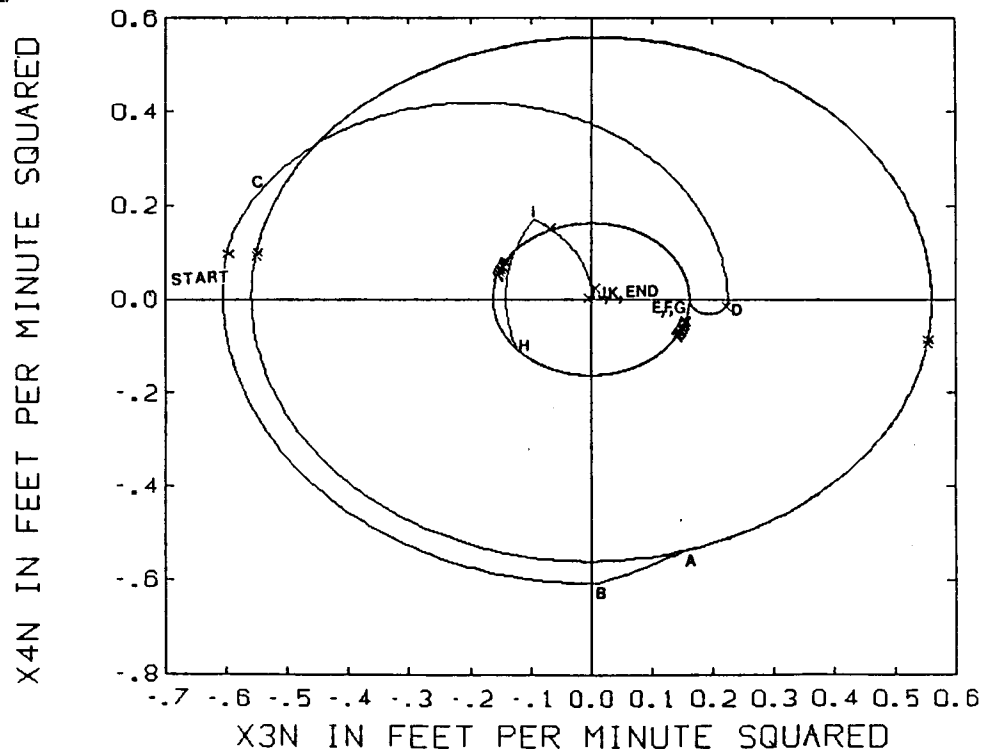
Figure 5.36: x_3n vs. x_4n for case J which begins in the drift phase of a hat maneuver.

Figure 5.37: *y vs. x for the case that begins at the start of the final hat maneuver of case A and turns the control off once the slave reaches the target.*

position	simulation time (min)	switch curve	commanded control	duration of control (min)
START	0.0	–	$a = 0$	37.2
A	37.2	GI1	$a > 0$	24.8
B	62.0	GI2	$a < 0$	28.0
C	90.0	GI3	$a = 0$	138.8
D	228.8	S2	$a > 0$	3.2

Table 5.15: *Points of importance for the case that begins at the start of the final hat maneuver of case A and turns the control off once the slave reaches the target.*

Figure 5.38: x_1 vs. x_2 for the case that begins at the start of the final hat maneuver of case A and turns the control off once the slave reaches the target.

Figure 5.39: x_3n vs. x_4n for the case that begins at the start of the final hat maneuver of case A and turns the control off once the slave reaches the target.
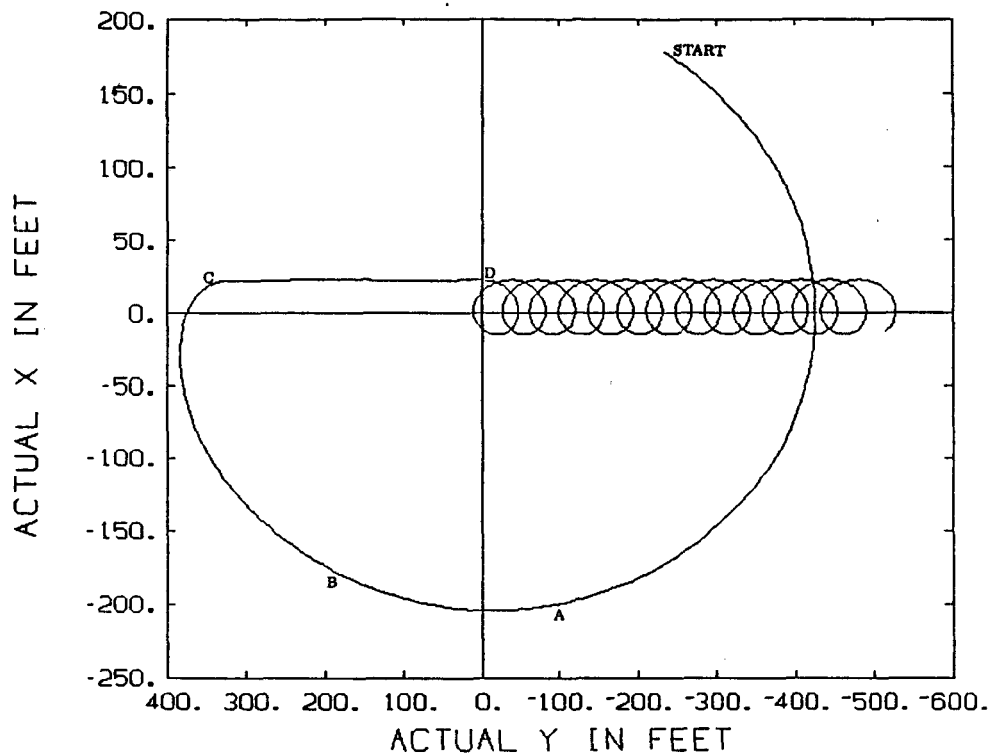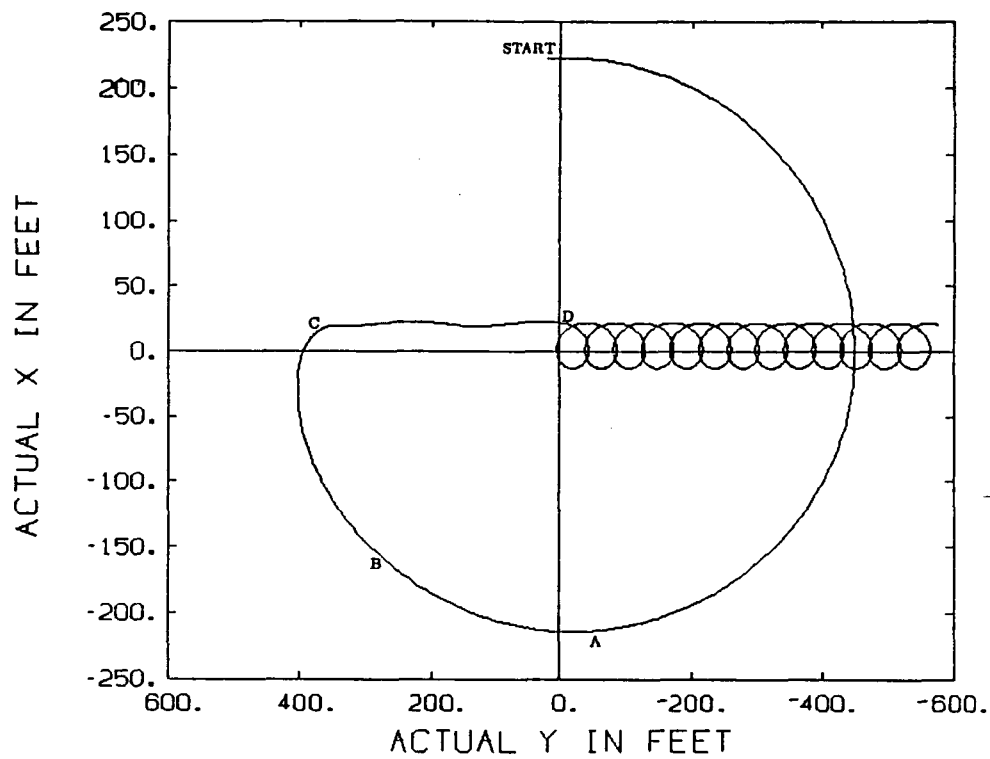
Figure 5.40: *y vs. x for the case that begins at the start of the final hat maneuver of case B and turns the control off once the slave reaches the target.*

position	simulation time (min)	switch curve	commanded control	duration of control (min)
START	0.0	–	$a = 0$	45.6
A	45.6	GI1	$a > 0$	26.0
B	71.6	GI2	$a < 0$	28.8
C	100.4	GI3	$a = 0$	163.2
D	263.6	S2	$a > 0$	2.8

Table 5.16: *Points of importance for the case that begins at the start of the final hat maneuver of case B and turns the control off once the slave reaches the target.*
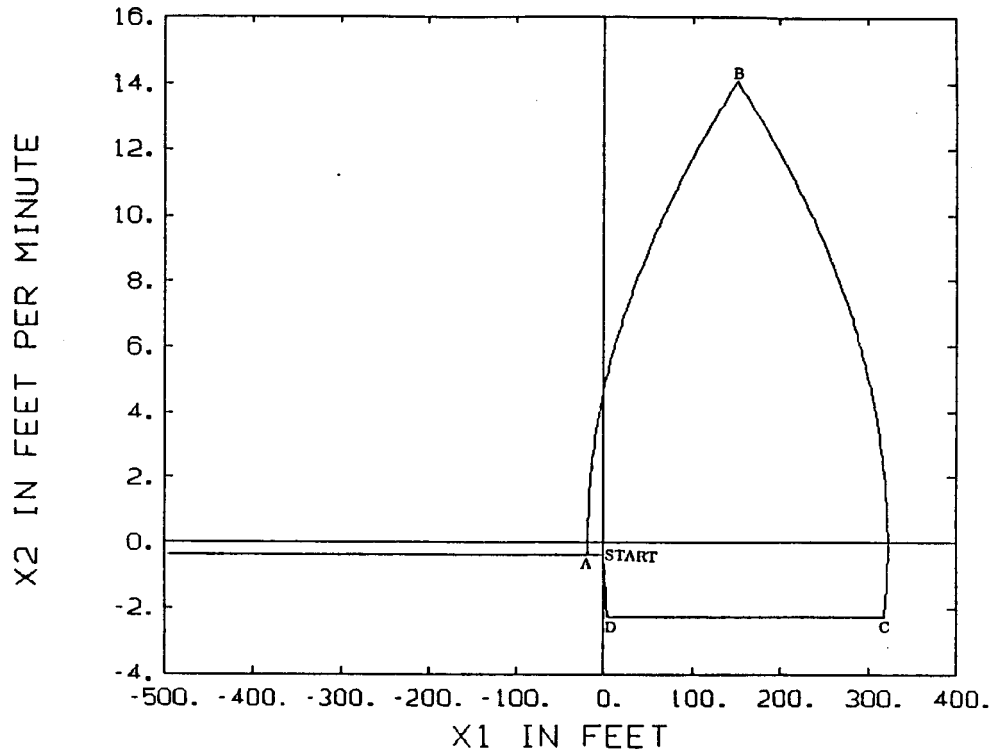
Figure 5.41: x_1 vs. x_2 for the case that begins at the start of the final hat maneuver of case B and turns the control off once the slave reaches the target.
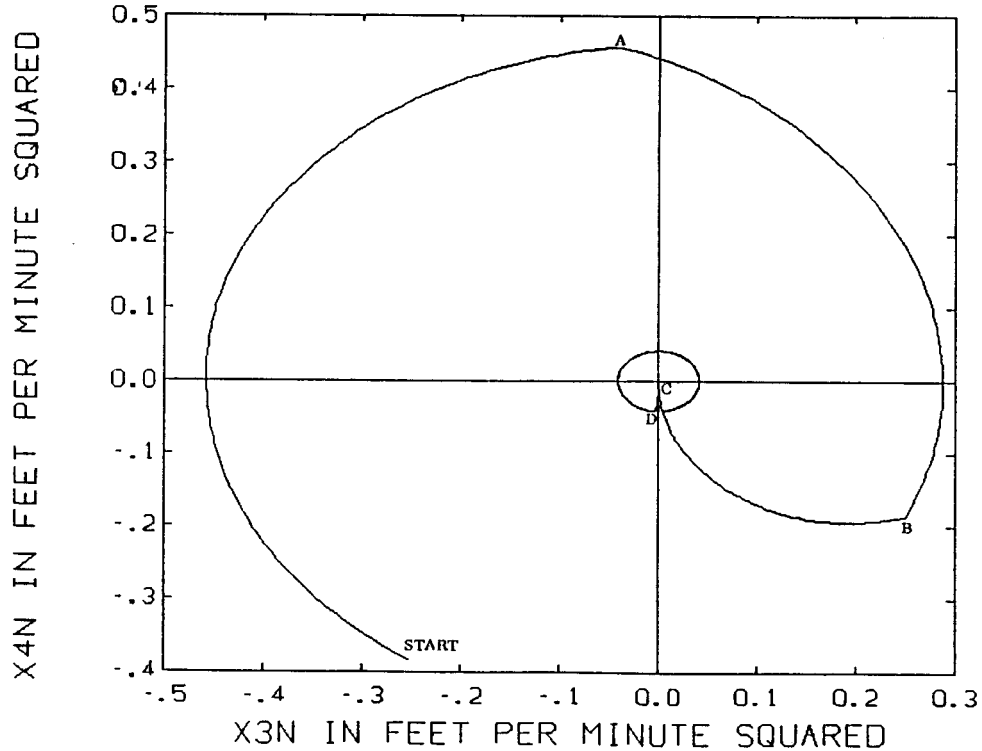

Figure 5.42: x_3n vs. x_4n for the case that begins at the start of the final hat maneuver of case B and turns the control off once the slave reaches the target.
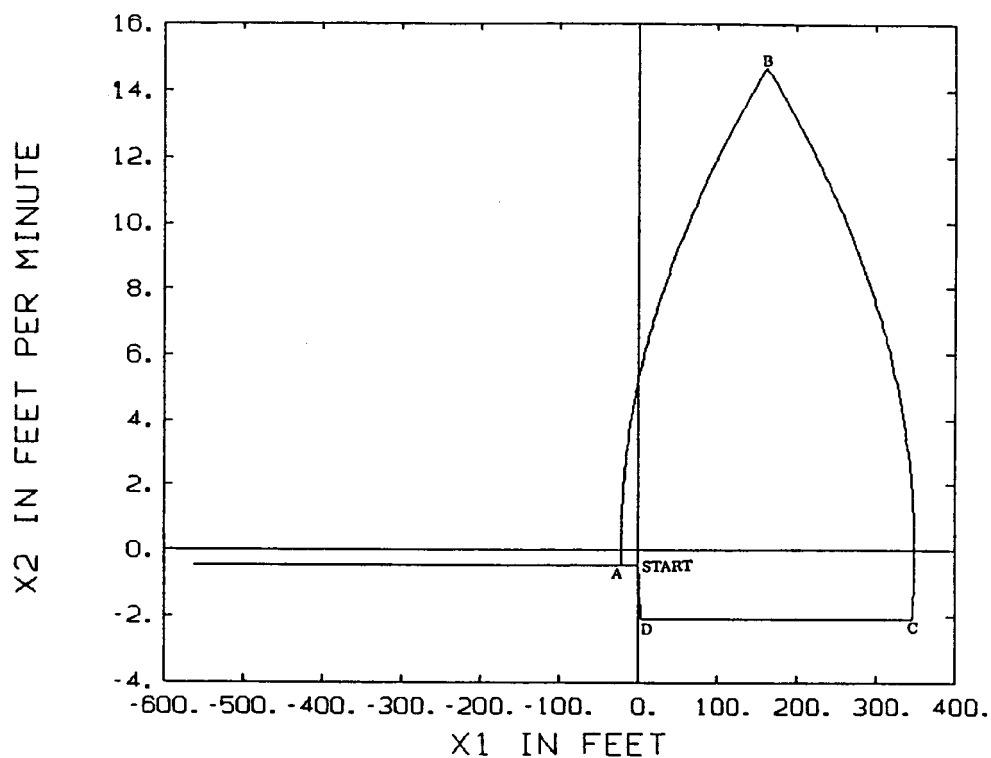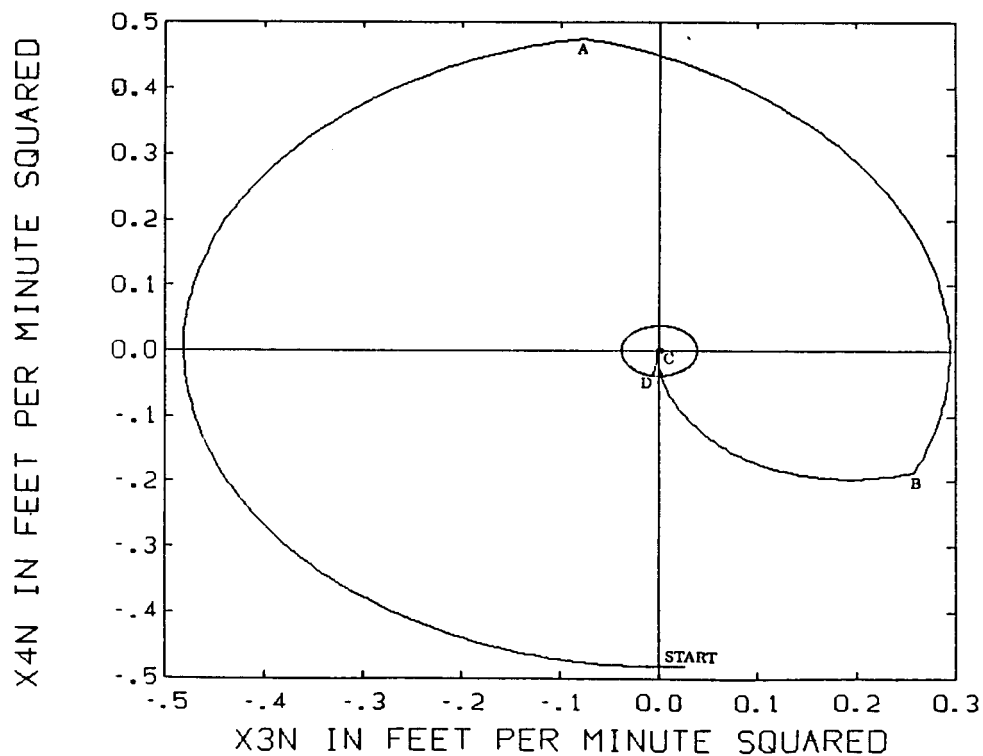
The important points of this simulation are explained in Table 5.16. The active control is turned off 266.4 minutes into the simulation allowing the slave to drift for 1234.0 minutes (20.6 hours). From the time that the control is turned off, the slave moves 561.8 feet away from the origin; the corresponding drift rate is .455 feet per minute.

Figure 5.43 shows y vs. x from the start of the final hat maneuver for case C; Figure 5.44 shows x_1 vs. x_2 and Figure 5.45 shows x_3n vs. x_4n. Table 5.17 explains the important points of this simulation. The end of the active control occurs after 784.0 minutes. The slave drifts 346.6 feet in the direction of the velocity vector in the remaining 715 minutes (11.9 hours); the corresponding drift rate is .488 feet per minute.

Precision Tolerance on the Placement of the Slave

The original tolerance on the origin allows an error of 3.0 ft in x_1 and .5 ft/min in x_2 at the end of the simulation. The more precise placement of the slave at the target allows the slave to have an error of 2.0 ft in x_1 and by 0.05 ft/min in x_2.

The changes necessary in the control law for the more precise placement of the slave at the origin are:

- the time step during the hat maneuver is changed from .4 minute to .1 minute.

- the time step while on the S1 or S2 switch curve is changed from .4 minute to .05 minute.

- the difference between Θ_1 and Θ_2 is changed from 10 to 0.5 degrees.

- the maximum allowable $\sqrt{(x_3n)^2 + (x_4n)^2}$ is changed from .05 ft/min^2 to .01 ft/min^2.

The ideal simulation with changes made to reduce error in the placement of the slave at the target will be referred to as the precise simulation.

Figure 5.46 shows y vs. x from the start of the final hat maneuver for case A using the precise simulation; Figure 5.47 shows x_1 vs. x_2 while x_3n vs. x_4n is shown in Figure 5.48. Table 5.18 explains the important points of this

simulation. The start of the final drift phase begins 292.45 minutes into the simulation and the origin is not reached until 655.20 minutes later; the drift rate corresponding to the uncontrolled movement of the slave is .047 *ft/min*. The slave is 25.87 feet away from the origin after a simulation time of 24 hours.

Figure 5.49 shows y vs. x from the start of the final hat maneuver for case B using the precise simulation, Figure 5.50 shows x_1 vs. x_2 and Figure 5.51 shows x_3n vs. x_4n. The important points of the simulation are explained in Table 5.19. The start of the final drift phase begins 306.15 minutes into the simulation and the origin is reached 799.00 minutes later; the drift rate corresponding to the uncontrolled movement of the slave is .040 *ft/min*. After a simulation time of 24 hours, the slave is 15.64 feet away from the origin.

Figure 5.52 shows the plot of y vs. x from the start of the final hat maneuver for case C using the precise simulation; Figure 5.53 shows x_1 vs. x_2, x_3n vs. x_4n is shown in Figure 5.54, and Table 5.20 explains the important points of the simulation. The start of the final drift phase begins 552.30 minutes into the simulation; the origin is reached 463.66 minutes later. The drift rate corresponding to the uncontrolled movement of the slave is .040 *ft/min*. The slave is 19.35 feet away from the origin after a simulation time of 24 hours.

For similar initial conditions, a test that uses the precision simulation has an extra hat maneuver compared to a test that uses the original ideal simulation. This extra hat maneuver causes the final eccentricity and $\bar{x}$ to be smaller than the corresponding values reached using the ideal simulation. The drift rate of the slave with respect to the origin using the precision simulation is approximately one-tenth the drift rate produced by the ideal simulation. As expected, for all cases, the values for $\bar{x}$ and eccentricity stay fixed once the control law is turned off.

5.4.2   Behavior of the Slave when the Control Law is Restarted

This section examines the behavior of the slave when the control law is cycled on and off as a function of the distance from the target; the control law is turned off when the slave reaches the target and is restarted once the slave drifts more than ten feet away from the origin.

Figure 5.43: *y vs. x for the case that begins at the start of the final hat maneuver of case C and turns the control off once the slave reaches the target.*

position	simulation time (min)	switch curve	commanded control	duration of control (min)
START	0.0	–	$a = 0$	20.8
A	20.8	GI1	$a < 0$	28.4
B	49.2	GI2	$a > 0$	30.4
C	79.6	GI3	$a = 0$	704.0
D	783.6	S1	$a < 0$	0.4

Table 5.17: *Points of importance for the case that begins at the start of the final hat maneuver of case C and turns the control off once the slave reaches the target.*

Figure 5.44: x_1 vs. x_2 for the case that begins at the start of the final hat maneuver of case C and turns the control off once the slave reaches the target.

Figure 5.45: x_3n vs. x_4n for the case that begins at the start of the final hat maneuver of case C and turns the control off once the slave reaches the target.
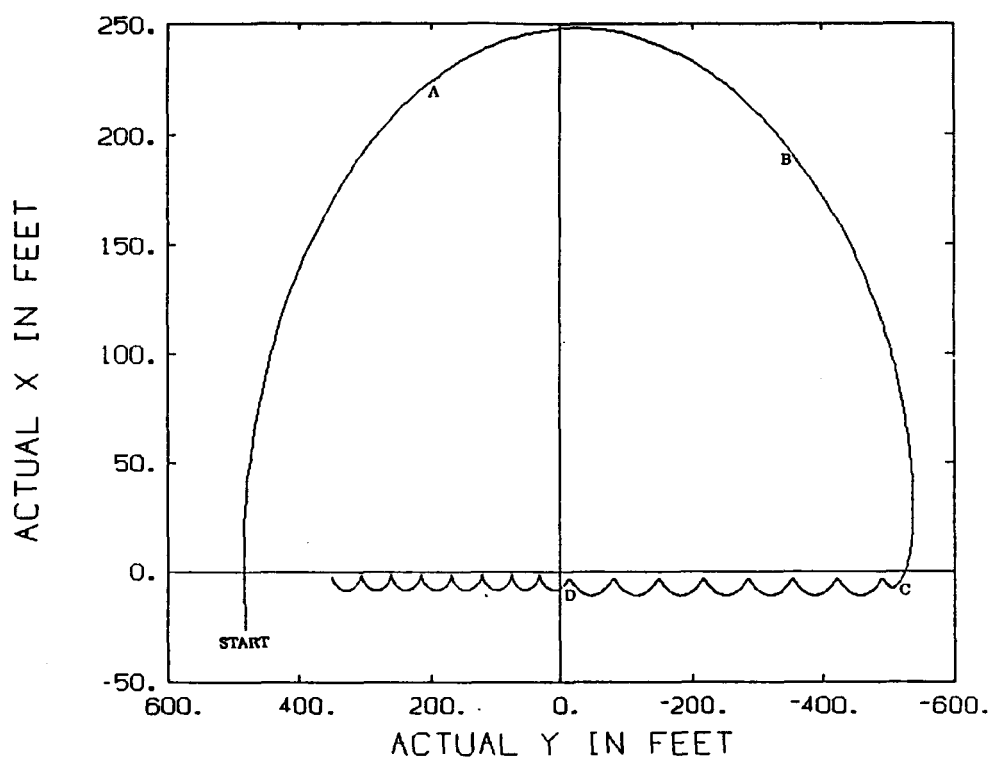
Figure 5.46: *y vs. x for the case that begins at the start of the final hat maneuver of case A and turns the control off once the slave reaches the target using the precise simulation.*

position	simulation time (min)	switch curve	commanded control	duration of control (min)
START	0.0	–	$a = 0$	37.0
A	37.0	GI1	$a > 0$	25.1
B	62.1	GI2	$a < 0$	27.7
C	89.8	GI3	$a = 0$	170.1
D	259.9	S2	$a > 0$	3.15
E	263.05	GA	$a = 0$	15.2
F	278.25	GI1	$a < 0$	7.0
G	285.25	GI2	$a > 0$	7.2

Table 5.18: *Points of importance for the case that begins at the start of the final hat maneuver of case A and turns the control off once the slave reaches the target using the precise simulation.*
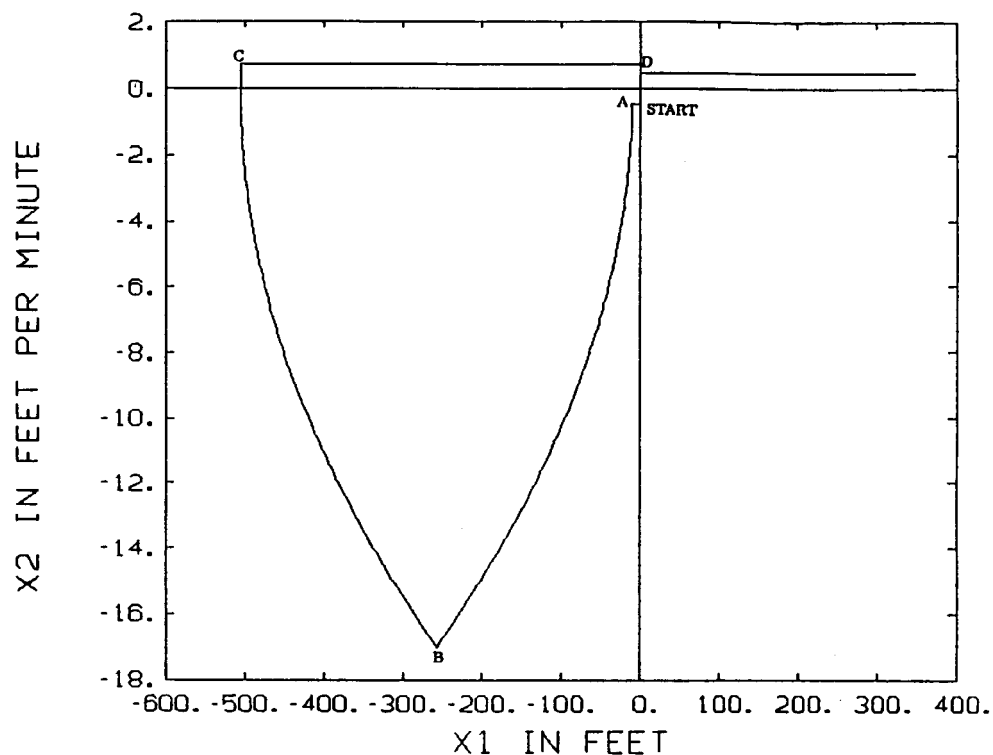
Figure 5.47: x_1 vs. x_2 for the case that begins at the start of the final hat maneuver of case A and turns the control off once the slave reaches the target using the precise simulation.
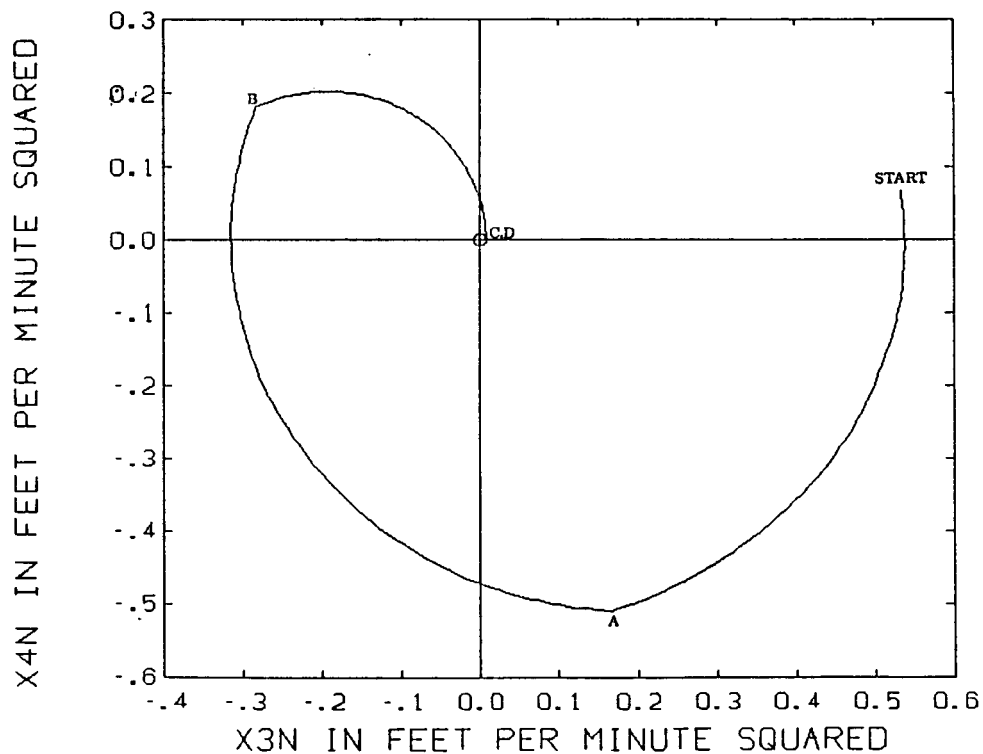

Figure 5.48: $x_{3}n$ vs. $x_{4}n$ for the case that begins at the start of the final hat maneuver of case A and turns the control off once the slave reaches the target using the precise simulation.
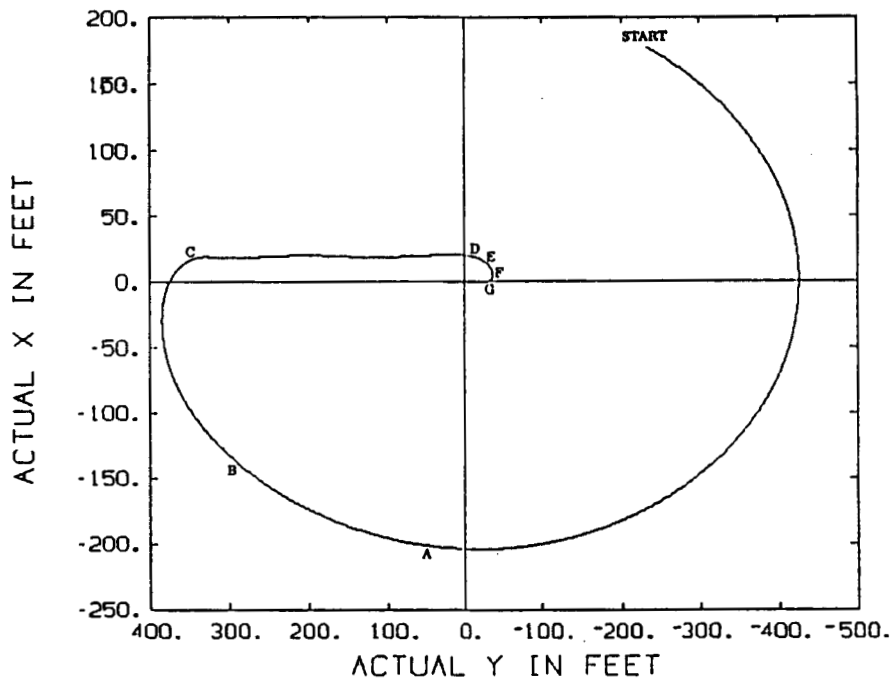
Figure 5.49: *y vs. x for the case that begins at the start of the final hat maneuver of case B and turns the control off once the slave reaches the target using the precise simulation.*

position	simulation time (min)	switch curve	commanded control	duration of control (min)
START	0.0	–	$a = 0$	45.6
A	45.6	GI1	$a > 0$	26.0
B	71.6	GI2	$a < 0$	28.6
C	100.2	GI3	$a = 0$	173.3
D	273.5	S2	$a > 0$	3.25
E	276.75	GA	$a = 0$	15.0
F	291.75	GI1	$a < 0$	7.1
G	298.85	GI2	$a > 0$	7.3

Table 5.19: *Points of importance for the case that begins at the start of the final hat maneuver of case B and turns the control off once the slave reaches the target using the precise simulation.*
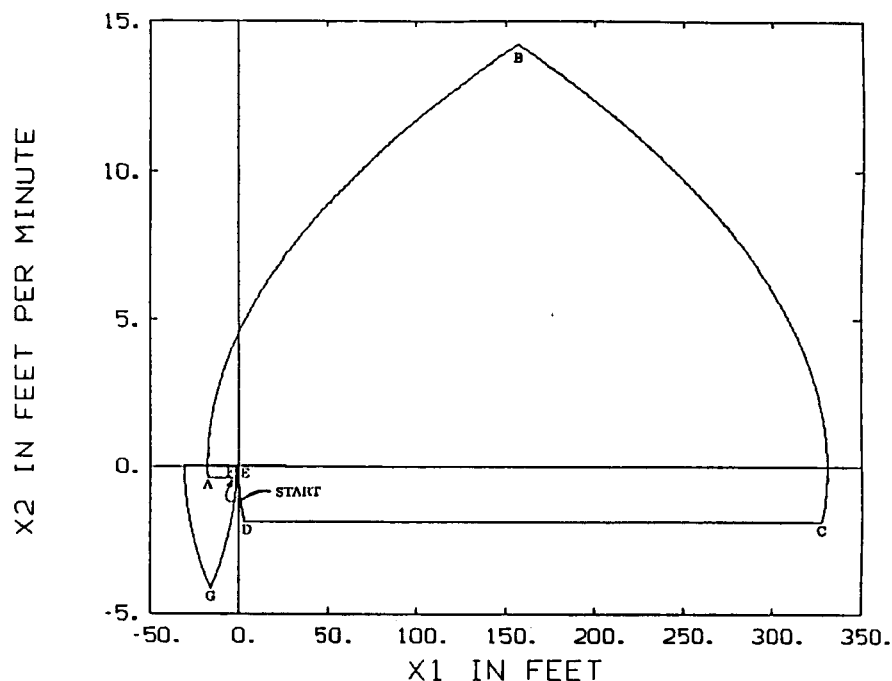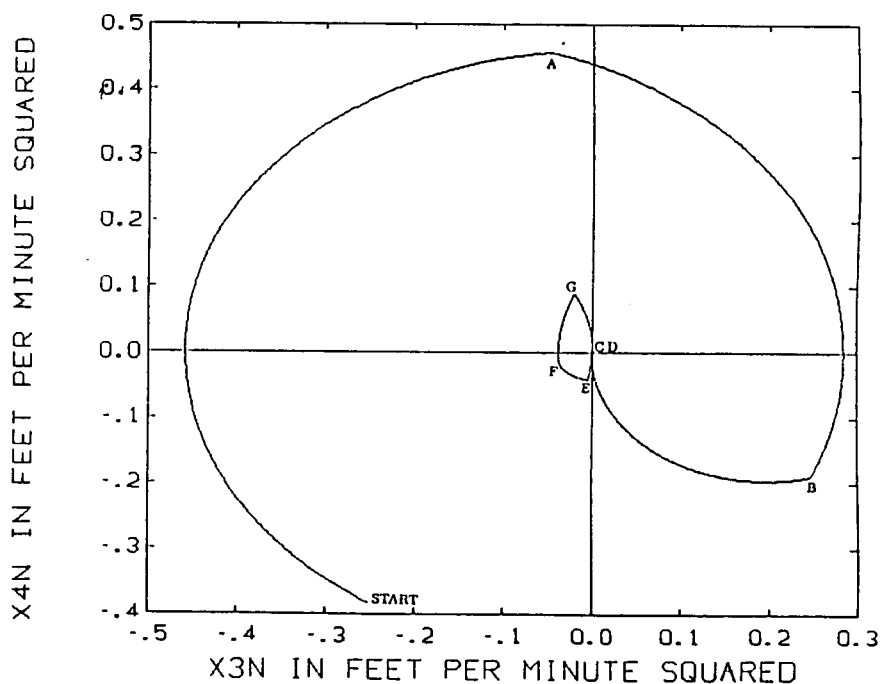
Figure 5.50: x_1 *vs.* x_2 *for the case that begins at the start of the final hat maneuver of case B and turns the control off once the slave reaches the target using the precise simulation.*
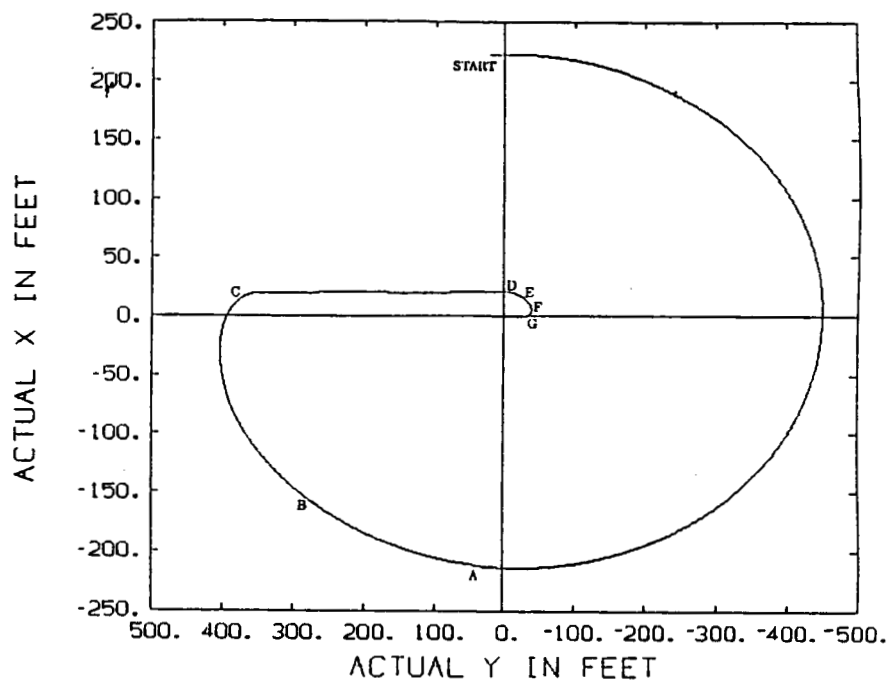

Figure 5.51: x_3n *vs.* x_4n *for the case that begins at the start of the final hat maneuver of case B and turns the control off once the slave reaches the target using the precise simulation.*
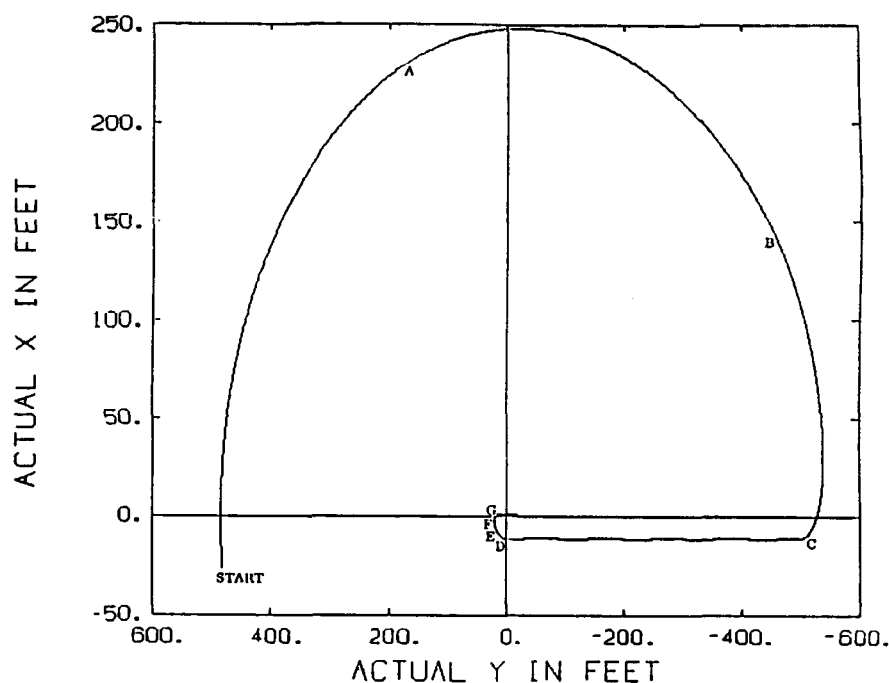
Figure 5.52: *y vs. x for the case that begins at the start of the final hat maneuver of case C and turns the control off once the slave reaches the target using the precise simulation.*

position	simulation time (min)	switch curve	commanded control	duration of control (min)
START	0.0	–	$a = 0$	20.7
A	20.7	GI1	$a < 0$	28.2
B	48.9	GI2	$a > 0$	30.9
C	79.8	GI3	$a = 0$	441.5
D	521.3	S1	$a < 0$	1.8
E	523.1	GA	$a = 0$	18.4
F	541.5	GI1	$a > 0$	5.3
G	546.8	GI2	$a < 0$	5.5

Table 5.20: *Points of importance for the case that begins at the start of the final hat maneuver of case C and turns the control off once the slave reaches the target using the precise simulation.*
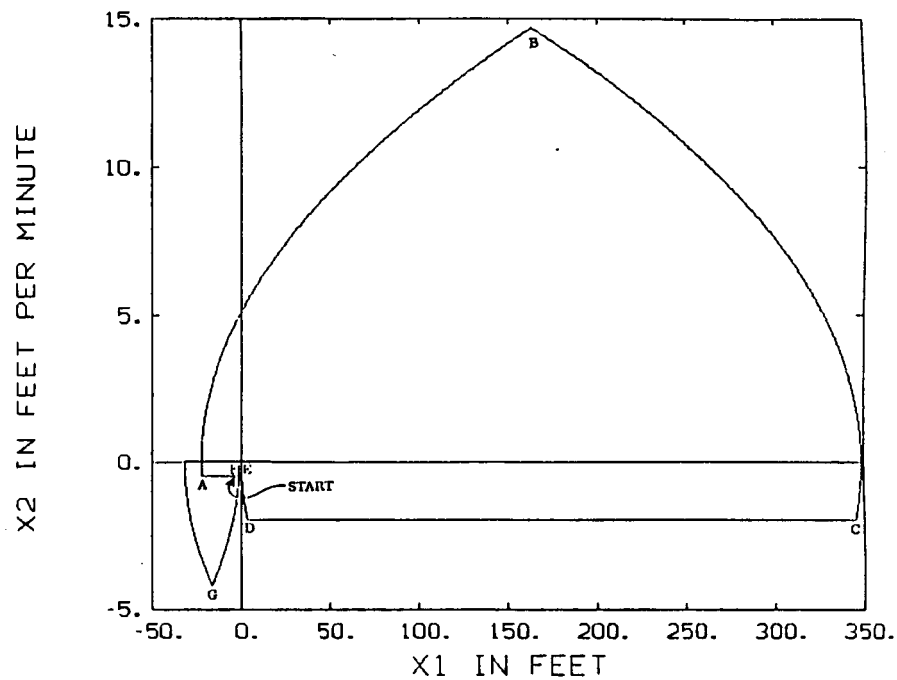
Figure 5.53: x_1 vs. x_2 for the case that begins at the start of the final hat maneuver of case C and turns the control off once the slave reaches the target using the precise simulation.
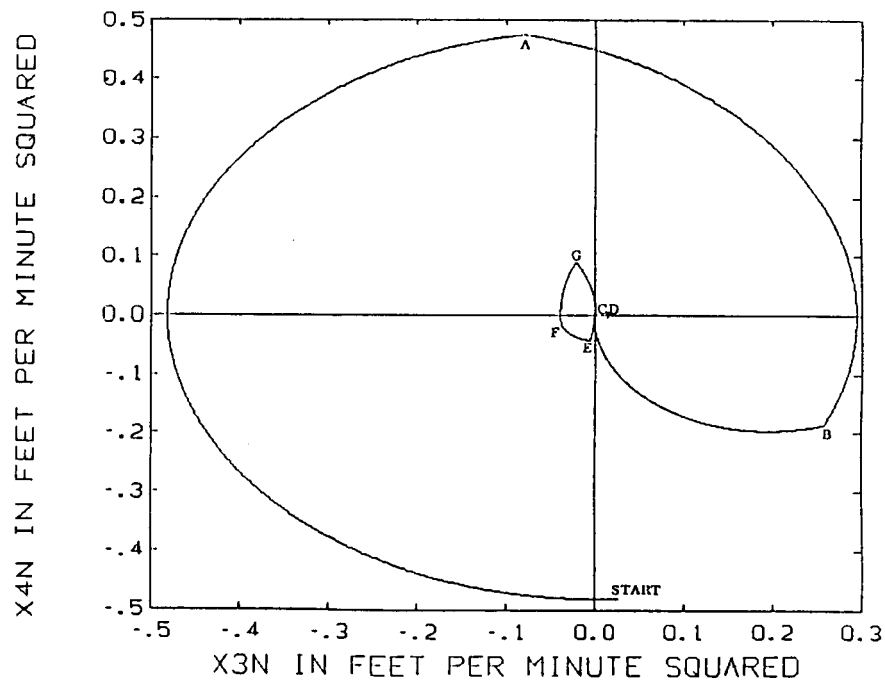

Figure 5.54: x_3n vs. x_4n for the case that begins at the start of the final hat maneuver of case C and turns the control off once the slave reaches the target using the precise simulation.
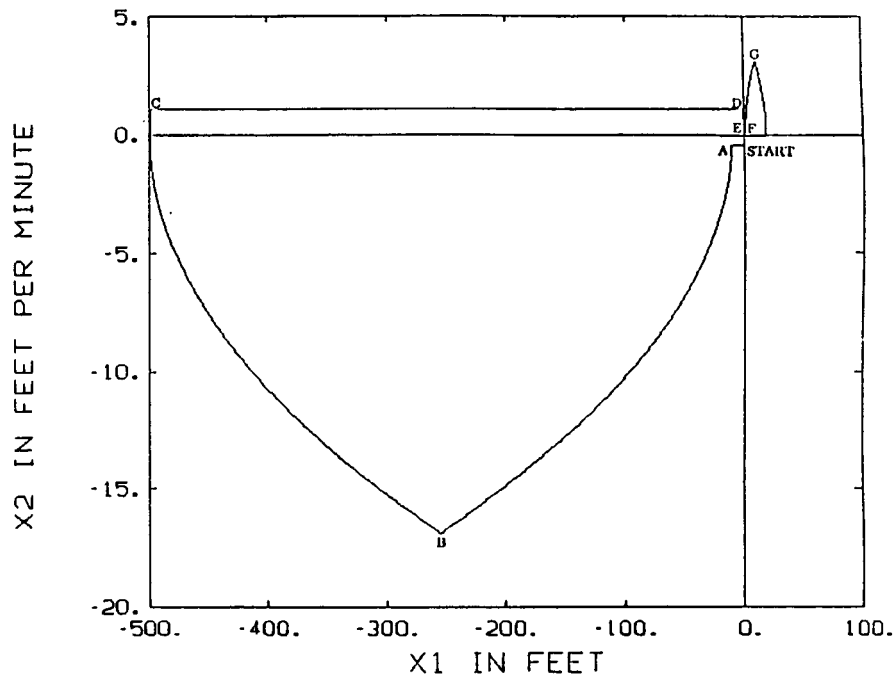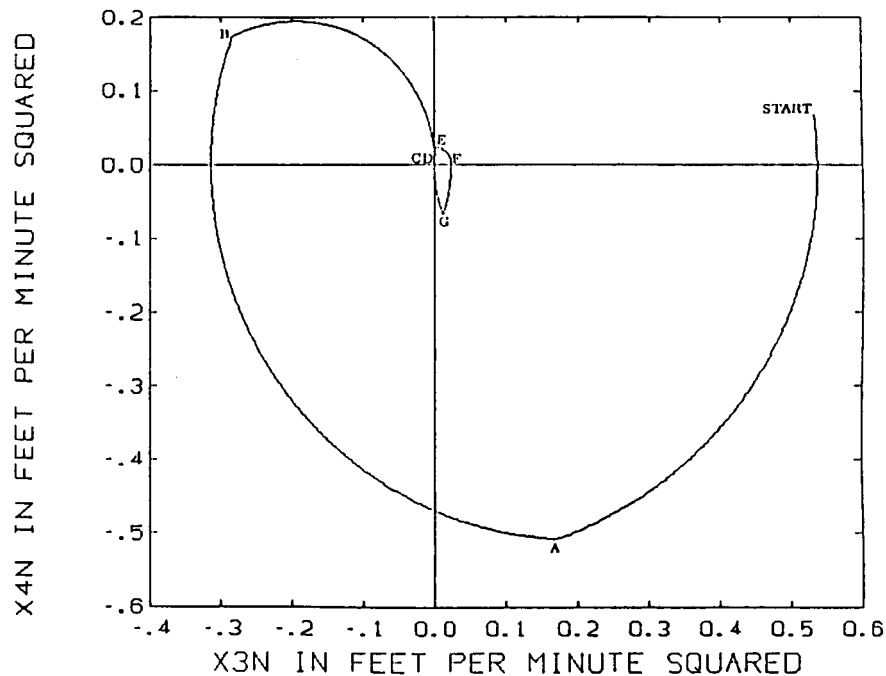
The initial conditions are derived from the simulations in Section 5.4.1 where the slave is is the uncontrolled phase of the simulation and 10 feet away from the origin. The initial conditions derived from the precision simulation of case A will be referred to as case K; the case using initial conditions from the simulation of case B will be called L, and case M will be taken from the simulation for case C. When the control law is restarted, it uses the precision simulation.

The plot of y vs. x is shown in Figure 5.55 for case K; x_1 vs. x_2 is shown in Figure 5.56 and x_3n vs. x_4n is plotted in Figure 5.57. Table 5.21 explains the important areas on the plots. After the slave reaches the vicinity of F, it commands its differential drag to be zero and drifts for 507.0 minutes until it is in the vicinity of A; the control sequence then repeats itself two more times during the simulation. In a 24 hour period the total duration of non-zero differential drag is 50.4 minutes. The maximum y is 12.79 feet and the minimum y is -16.45 feet; the maximum and minimum x are 7.26 and -0.95 feet respectively.

Figure 5.58 shows y vs. x for case L, x_1 vs. x_2 is shown in Figure 5.59 and x_3n vs. x_4n is plotted in Figure 5.60. The important areas on the plots are explained in Table 5.22. After the slave reaches the vicinity of F, it commands its differential drag to be zero and drifts for 608.0 minutes until it is in the vicinity of A; the control sequence then repeats itself two more times during the simulation. In a 24 hour period the total duration of non-zero differential drag is 51.0 minutes. The maximum y is 13.87 feet and the minimum y is -18.00 feet; the maximum and minimum x are 7.92 and -0.88 feet respectively.

For case M the plot of y vs. x is shown in Figure 5.61 while x_1 vs. x_2 is shown in Figure 5.62 and x_3n vs. x_4n is shown in Figure 5.63; important areas on the plots are explained in Table 5.23. The basic control sequence repeats itself three times during the simulation. In a 24 hour period the total duration of non-zero differential drag is 51.2 minutes. The maximum y is 17.88 feet and the minimum y is -13.78 feet; the maximum and minimum x are 0.89 and -7.89 feet respectively.

5.4.3 Controller to Keep Slave in Tight Limit Cycle About Origin

A control law designed to keep y within one foot of the origin, and the results from simulations of this control law, are examined in this section.

The Control Law

The control law to keep the slave in a tight limit cycle about the origin uses the facts that if $\bar{x}$ is negative the unforced slave will drift in the positive y direction, and if $\bar{x}$ is positive, the unforced motion of the slave will be in the negative y direction. The possible positions for $\bar{x}$ at the end of a precision simulation are such that the proper drag, commanded to last for 0.4 minutes, will send $\bar{x}$ to the other side of the x_1 axis; this maneuver will reverse the direction that the slave is drifting with respect to the target.

The control law to keep the slave in a tight limit cycle about the origin used the following principles:

- If $\bar{x}$ is negative when $\bar{y}$ becomes more than 1 foot away from the origin, a positive drag is commanded for one 0.4 minute time step.

- If $\bar{x}$ is as positive when $\bar{y}$ becomes more than 1 foot away from the origin, a negative drag is commanded for one 0.4 minute time step.

This control law will be referred to as the limit cycle control law. It was not sure if the eccentricity of the system would stay bound through a series of these maneuvers.

Test Cases and Results

Initial values for the test cases were taken from the precision simulations in Section 5.4.1. The position and eccentricity of the slave in the uncontrolled phase of the simulation and one foot away from the origin in cases A, B, and C, formed the initial values for test cases N, O, and P, respectively. The duration of the limit cycle simulations is 24 hours.

Figure 5.64 shows y vs. x for case N. The maximum y is 2.26 feet and the minimum y is -2.17 feet. The maximum and minimum values for x are 1.14 and -1.28 feet respectively. Over a 24 hour period, the total duration of non-zero drag is 20.6 minutes.

Figure 5.65 shows the plot of y vs. x for case O. The maximum and minimum y are 4.02 and -4.17 feet; the maximum and minimum x are 2.09 and -2.27 feet. The duration of non-zero drag is 17.5 minutes over a 24 hour period.
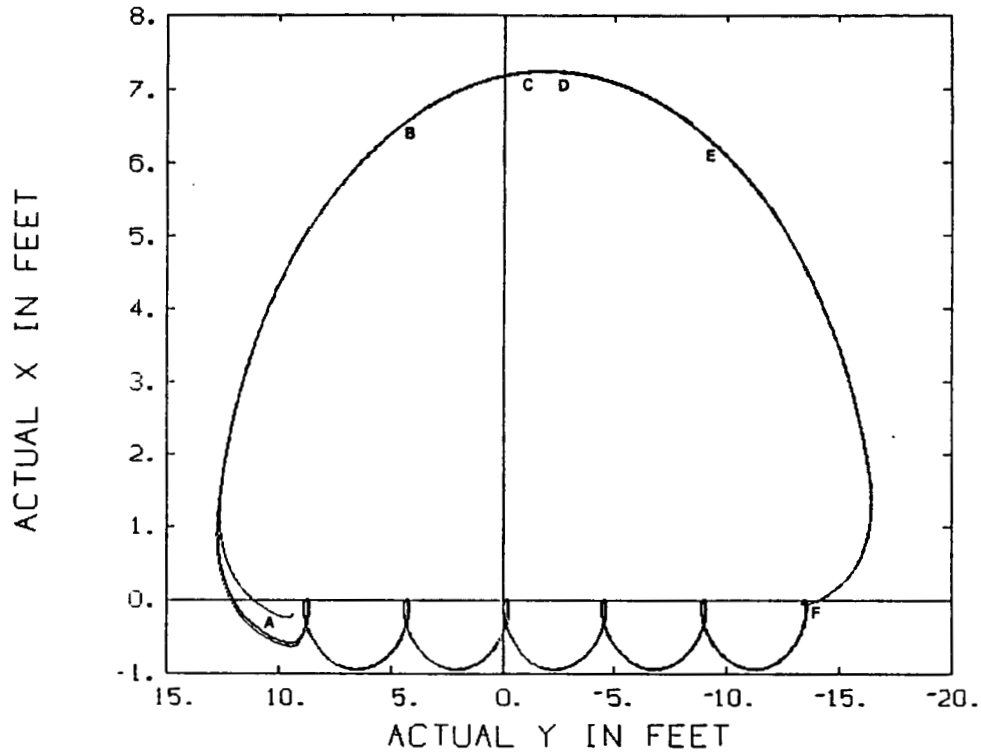
Figure 5.55: *y vs. x for case K in which the precision control law is restarted once the slave drifts more than 10 feet away from the origin.*

position	simulation time (min)	switch curve	commanded control	duration of control (min)
A	2.0	S3	$a < 0$	4.3
B	6.3	S2	$a > 0$	4.1
C	10.4	GA	$a = 0$	43.2
D	53.6	GI1	$a < 0$	4.1
E	57.7	GI2	$a > 0$	4.3
F	62.0	GI3	$a = 0$	507.0

Table 5.21: *Points of importance for case K in which the precision control law is restarted once the slave drifts more than 10 feet away from the origin.*

Figure 5.56: x_1 vs. x_2 for case K in which the precision control law is restarted once the slave drifts more than 10 feet away from the origin.

Figure 5.57: x_3n vs. x_4n for case K in which the precision control law is restarted once the slave drifts more than 10 feet away from the origin.

Figure 5.58: *y vs. x for case L in which the precision control law is restarted once the slave drifts more than 10 feet away from the origin.*

position	simulation time (min)	switch curve	commanded control	duration of control (min)
A	2.0	S3	$a < 0$	4.3
B	6.3	S2	$a > 0$	4.1
C	10.4	GA	$a = 0$	42.6
D	53.0	GI1	$a < 0$	4.1
E	57.1	GI2	$a > 0$	4.3
F	61.4	GI3	$a = 0$	608.0

Table 5.22: *Points of importance for case L in which the precision control law is restarted once the slave drifts more than 10 feet away from the origin.*
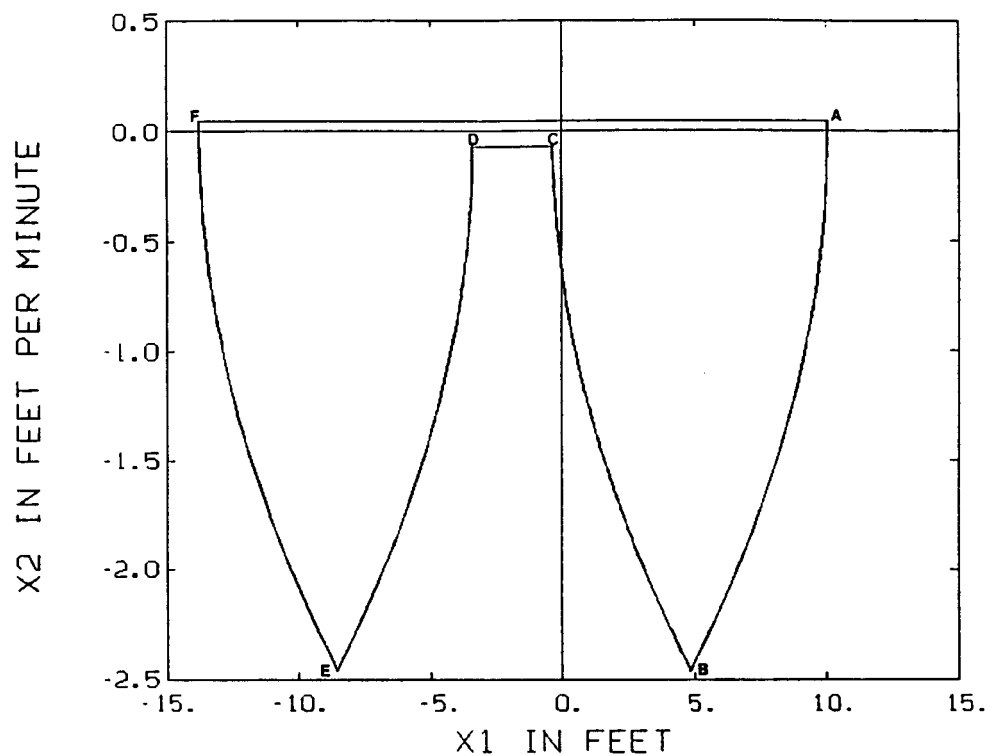
Figure 5.59: x_1 vs. x_2 for case L in which the precision control law is restarted once the slave drifts more than 10 feet away from the origin.
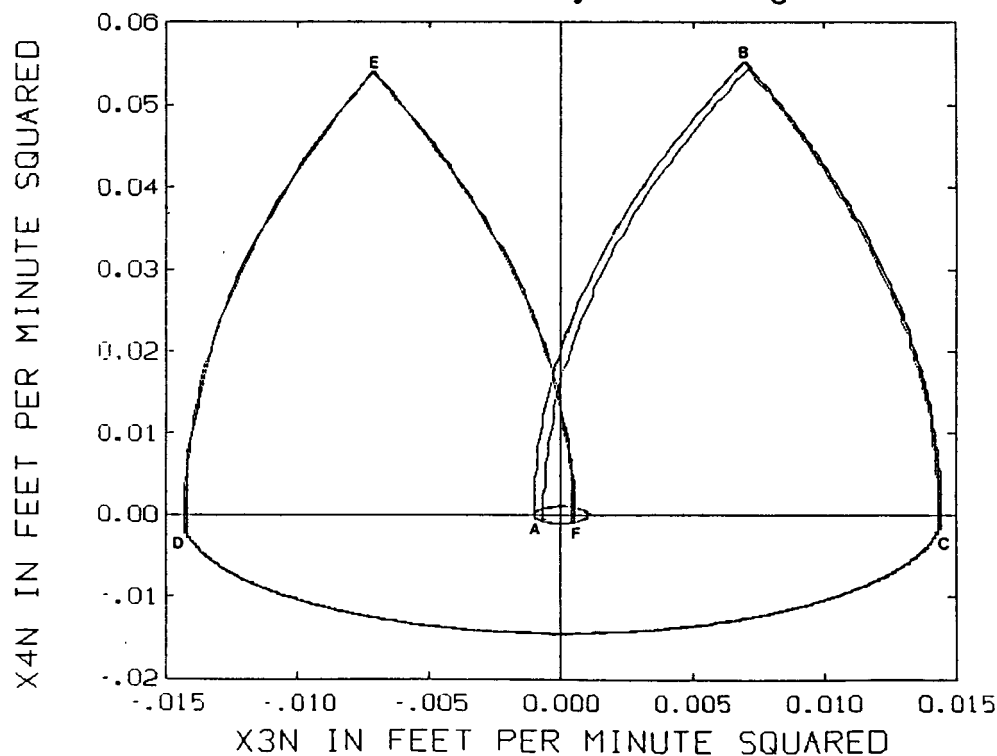

Figure 5.60: x_3n vs. x_4n for case L in which the precision control law is restarted once the slave drifts more than 10 feet away from the origin.
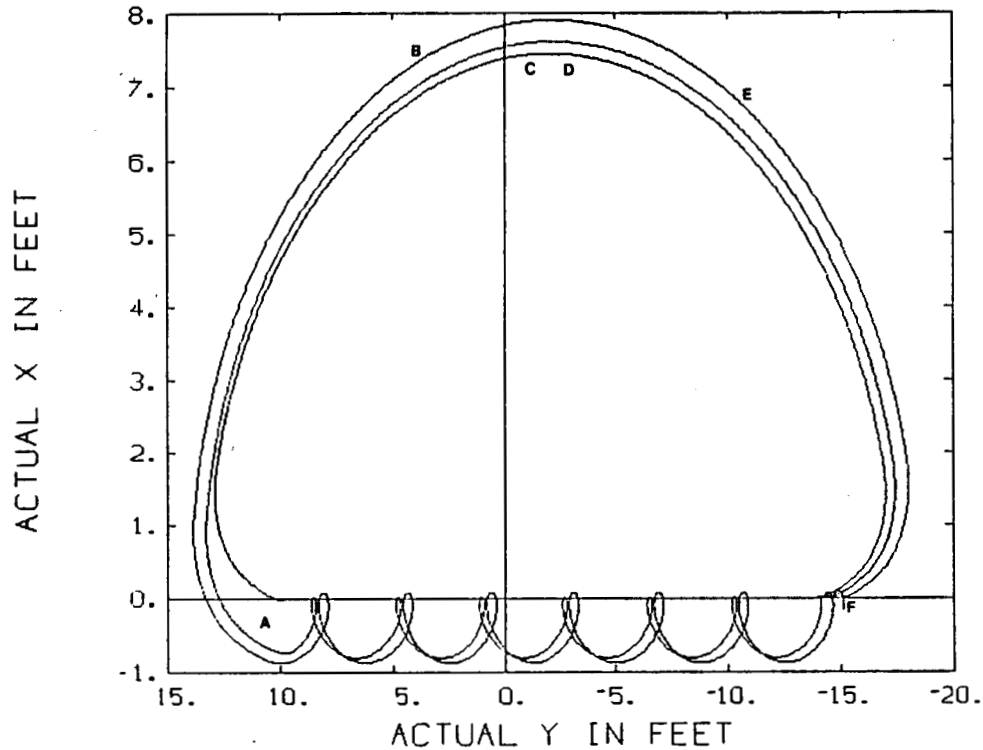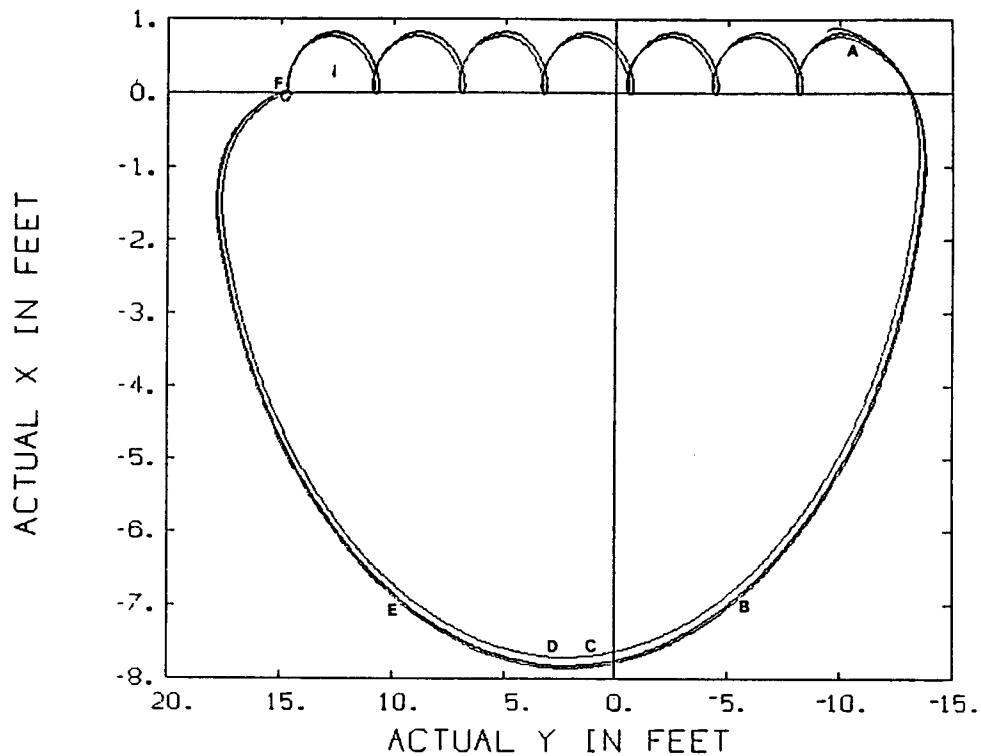
Figure 5.61: *y vs. x for case M in which the precision control law is restarted once the slave drifts more than 10 feet away from the origin.*

position	simulation time (min)	switch curve	commanded control	duration of control (min)
A	2.0	S4	$a > 0$	4.3
B	6.3	S1	$a < 0$	4.1
C	10.4	GA	$a = 0$	44.3
D	54.7	GI1	$a > 0$	4.1
E	58.9	GI2	$a < 0$	4.4
F	63.3	GI3	$a = 0$	618.0

Table 5.23: *Points of importance for case M in which the precision control law is restarted once the slave drifts more than 10 feet away from the origin.*
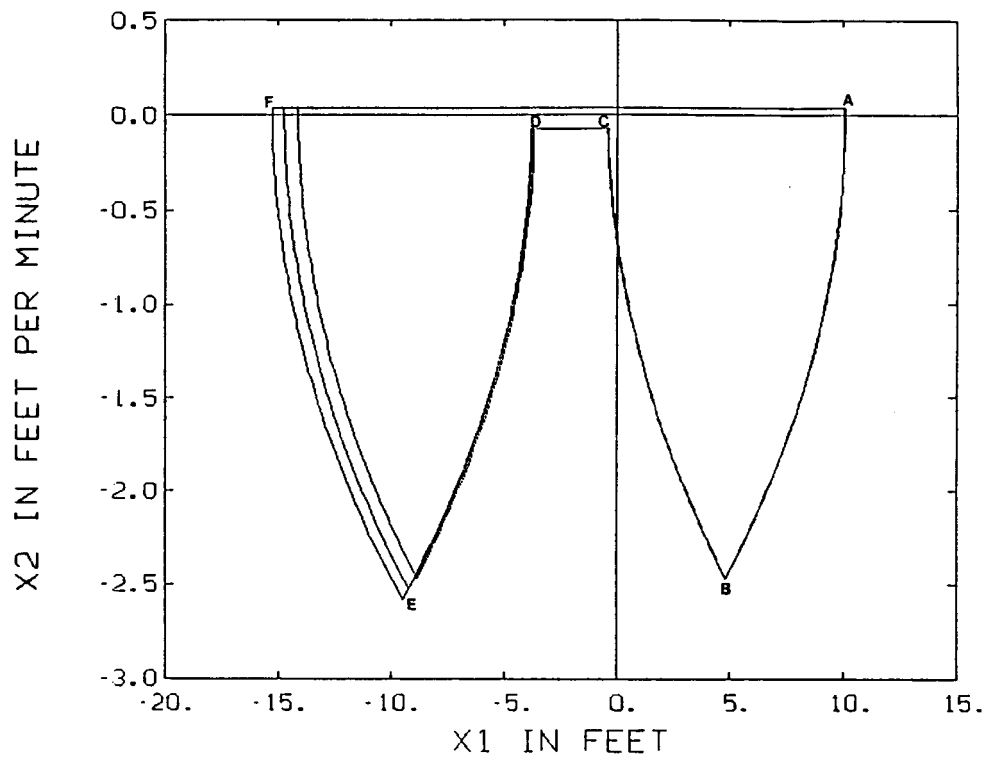
Figure 5.62: x_1 vs. x_2 for case M in which the precision control law is restarted once the slave drifts more than 10 feet away from the origin.
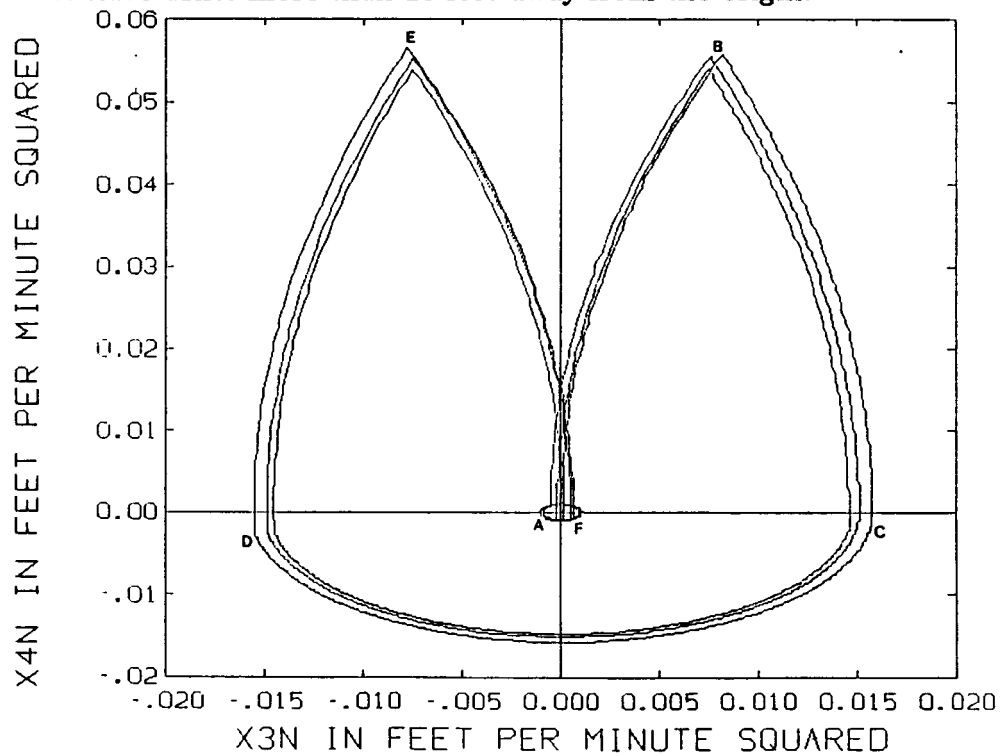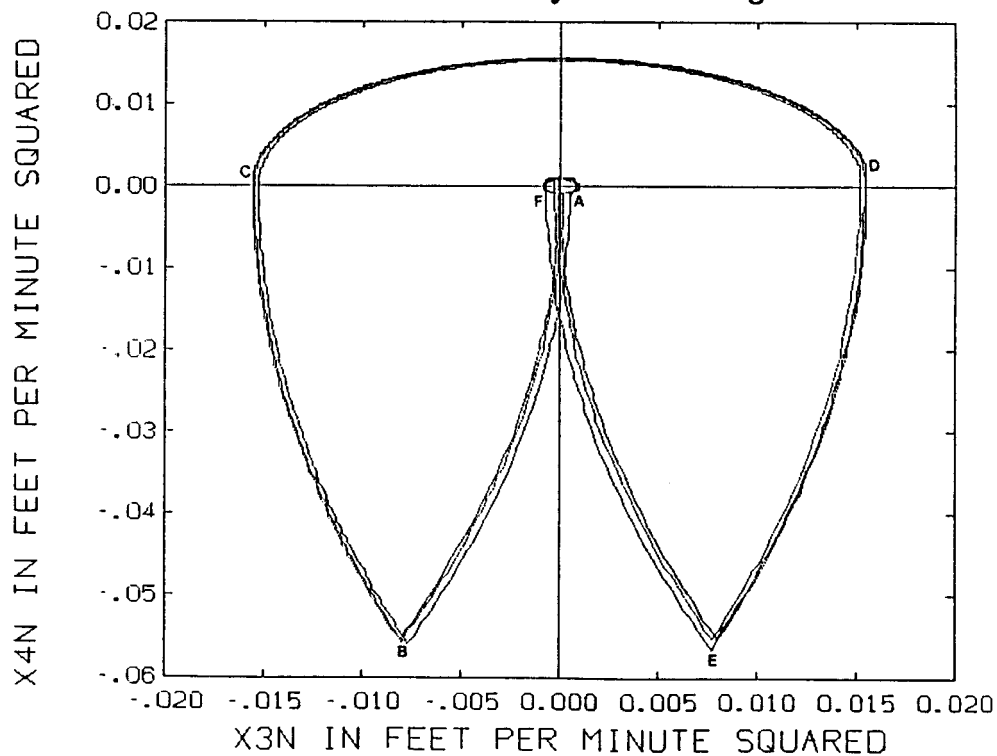

Figure 5.63: x_{3n} vs. x_{4n} for case M in which the precision control law is restarted once the slave drifts more than 10 feet away from the origin.
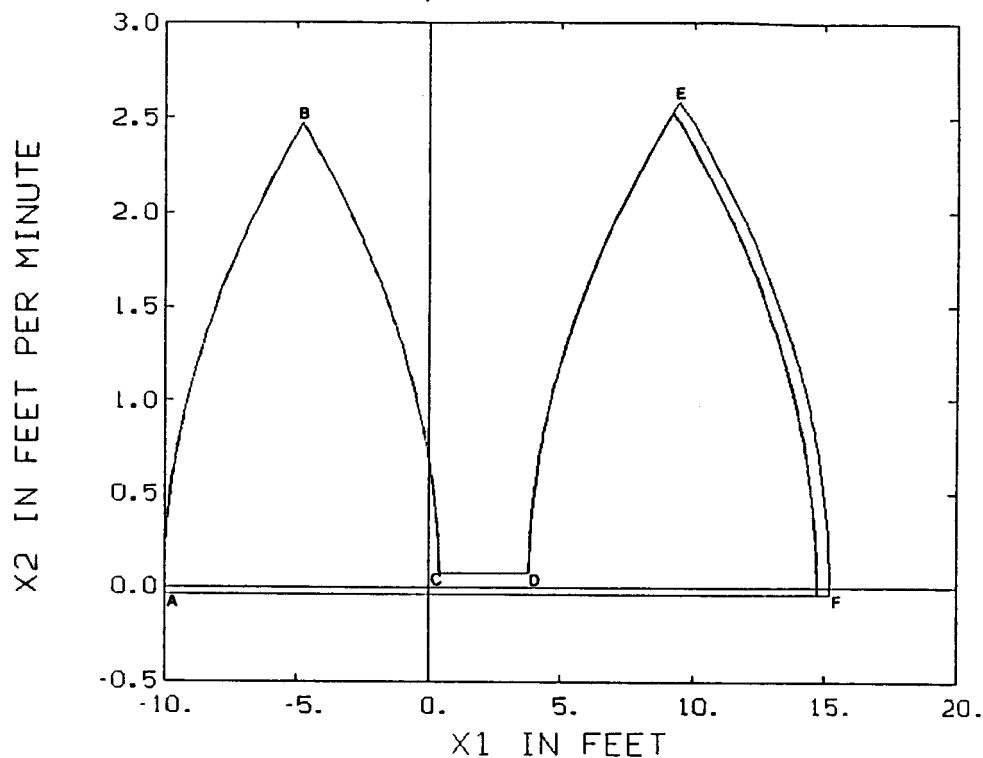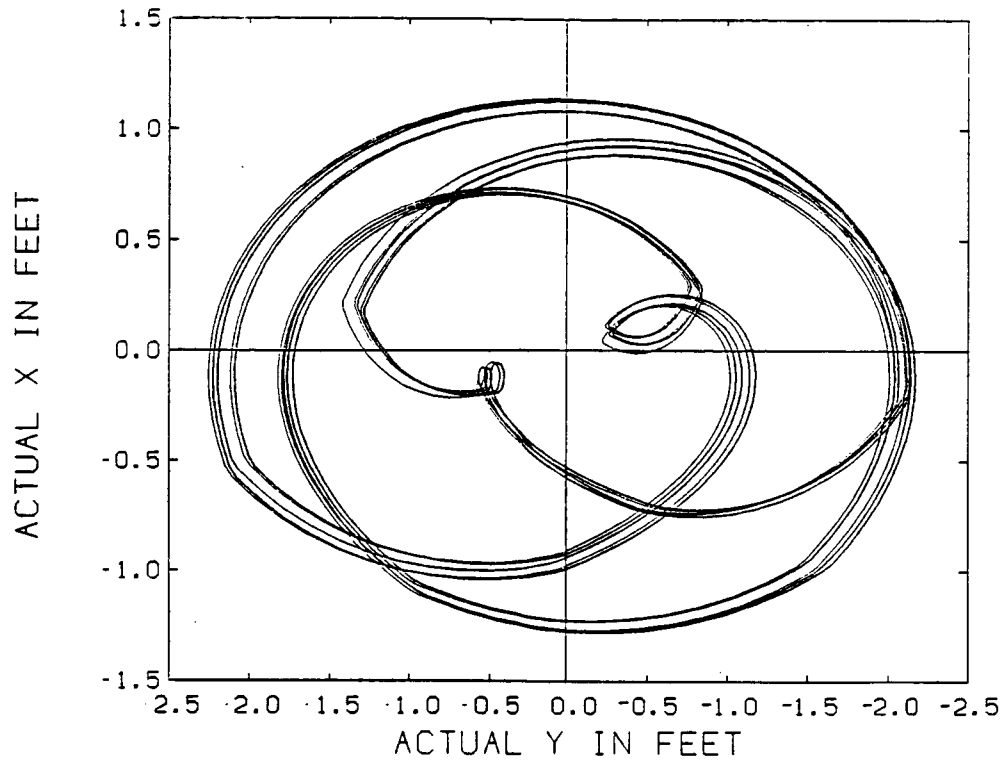
Figure 5.64: *y vs. x using the limit cycle control law for case N.*
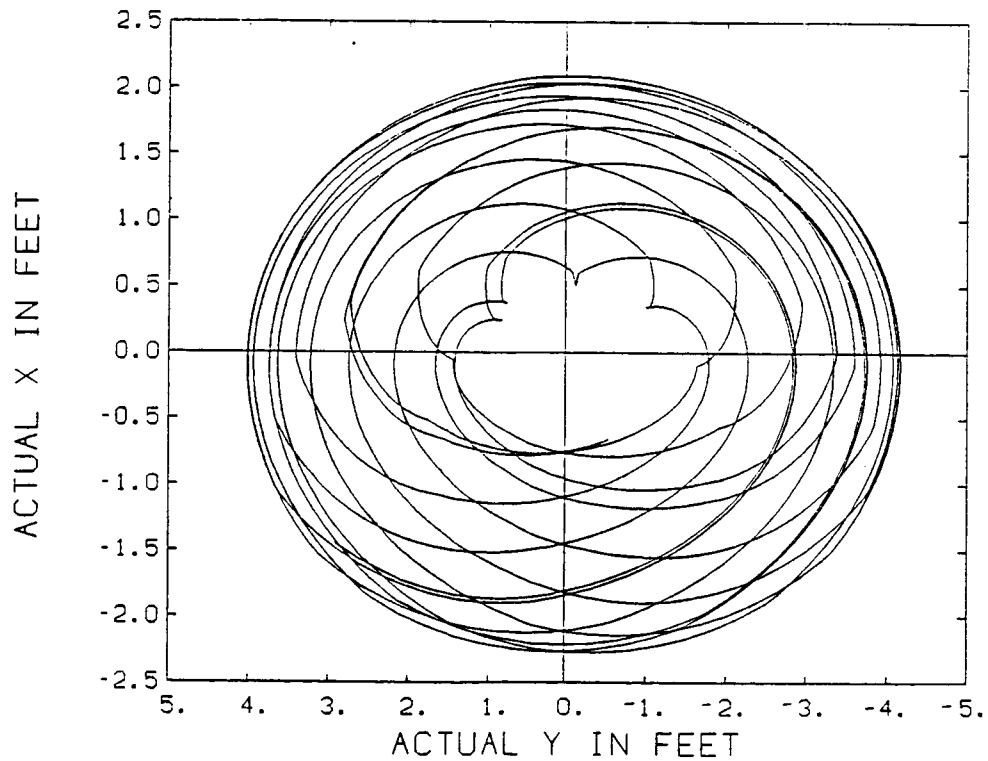
Figure 5.65: *y vs. x using the limit cycle control law for case O.*
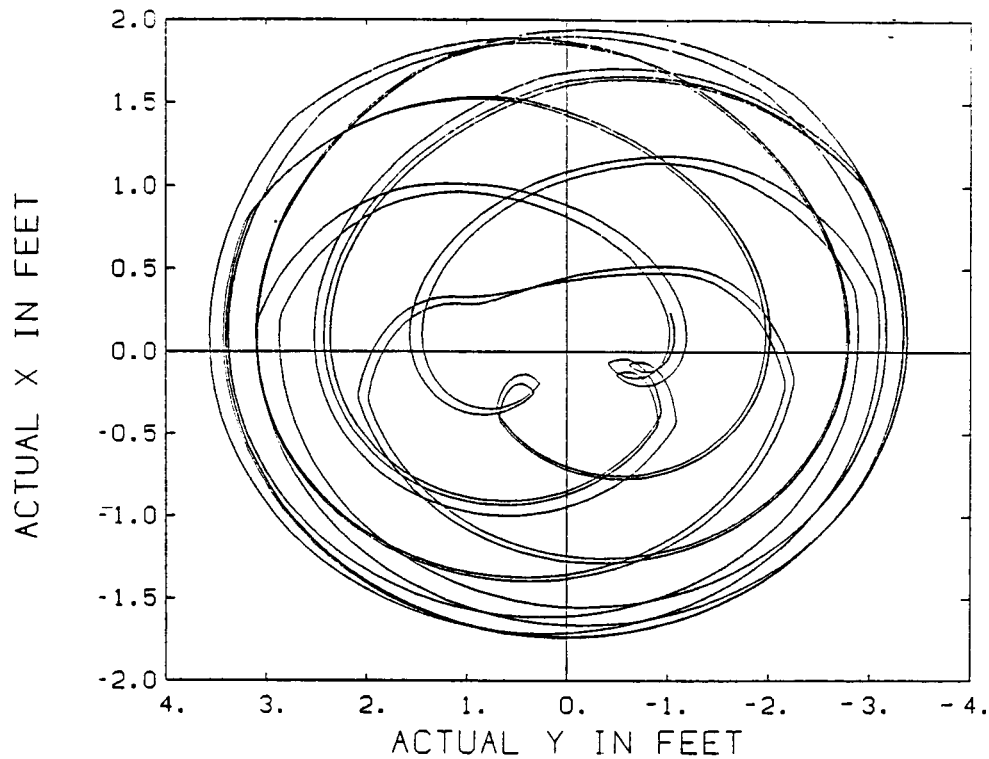
Figure 5.66: *y vs. x using the limit cycle control law for case P.*

The plot of y vs. x for case P is shown in Figure 5.66. The maximum and minimum y are 3.56 and -3.37 feet; the maximum and minimum x are 1.94 and -1.74 feet. Over a 24 hour simulation time, the duration of non-zero drag is 17.6 minutes.

In all cases y becomes greater than 1 foot away from the origin, this is caused by the eccentricity of the slave. The largest distance that the slave is away from the origin was 4.17 feet.

Chapter 6

Conclusions and Recommendations

6.1 Thesis Findings

The formationkeeping problem is reformulated as the simultaneous solution of both a double integrator and a harmonic oscillator. The double integrator models the average position of the slave relative to the target. The harmonic oscillator models the eccentricity of the slave; the target is assumed to be in a circular orbit. Solving the double integrator and harmonic oscillator concurrently leads to the positioning of the slave at the target. A phase plane approach is used in the development of the control law.

The control law consists of two parts: the main control law and the gamma control scheme. The commanded differential drag depends solely on the previous and present eccentricity and average position. The main control law drives the average position of the slave to that of the target while minimizing eccentricity as much as possible. The gamma control scheme is activated once the average position of the slave is at the target; its purpose is to reduce the eccentricity of the slave as much as possible without jeopardizing its final average position.

The control law was tested using eight sets of initial conditions and two different simulations; the first simulation is based on the assumptions formed in the development of the control law, the other is is based on a pre-existing Space Systems Simulator at the Charles Stark Draper Laboratory. Differences in the plots generated by the two separate simulations for a specific test case provide a measure of the validity of the assumptions in the formulation of the control

law. Although the control law was initially formulated in terms of relative position in rectilinear coordinates, the curvature of the orbit made it necessary to reformulate the control in curvilinear coordinates. Over sufficiently small displacements, the rectilinear formulation is adequate, but over several thousand feet, the orbit curvature is sufficiently large to significantly impact performance.

The control law is capable of moving a slave satellite from an arbitrary initial position to a specified final position with respect to an orbiting reference. The time it takes to drive a slave satellite to a target position depends upon its initial position and eccentricity; all of the cases tested were driven to the target in less than 24 hours. The control law uses previous and current eccentricity and average position to determine the commanded differential drag at each instant of the formation flying maneuver. The control for formation flying developed in reference [2] computes an open-loop maneuver from the current to the desired position and follows either a straight line constrained trajectory or a two-burn coasting trajectory; disturbance rejection is accomplished by an optimal linear quadratic regulator which employs the nominal open loop trajectory as set points for feedback control. Since the basis and goals of the two control laws are so different, no immediate comparison between the two maneuvers can be made.

A comparison was made of the main control law and the gamma control scheme using identical initial conditions. In order to minimize the time to reach the target, the control law should be started in the main control scheme. On the other hand, to minimize the interval of non-zero differential drag, it may be preferable to initialize in the gamma control scheme.

Two strategies were examined for formationkeeping. One activates the controller when the slave drifts a certain distance from the origin, the other uses the limit cycle control law developed in Section 5.4.4. The first keeps the slave within 18 feet of the origin, while the limit cycle control law keeps the slave within 4.17 feet of the origin. The main control law uses approximately 50.4 minutes of non-zero differential drag in a 24 hour period; the limit cycle control law uses an average of 18.6 minutes of non-zero drag over a 24 hour period.

The maximum error produced in formationkeeping by the control scheme developed by Vassar and Sherwood was 7.5 meters (24.606 feet). The slave stayed within 20 feet of the origin for the control law created by Redding, Adams, and Kukiak, but could have been controlled to approximately 2 feet if a better sensor

had been used. No immediate comparison can be made between the efficiency of the formationkeeping methods developed in this thesis and by references [1] and [2]; that analysis is recommended for future work.

6.2 Recomendations for Further Work

Research of a fairly new concept often leads to more questions than it answers; this is true with the problem of formationkeeping via differential drag.

An in-depth comparison should be made between the concept of formationkeeping with differential drag and with chemical thrusters. It is important to quantify the trade-off between fuel saved using differential drag rather than jets for formationkeeping and the additional fuel required to reboost the system more often due to the differential drag. Control laws presented in references [1] , [2] and [12] could serve as a valid basis of comparison for the new control law. It is not claimed that the control law developed in this thesis is either time optimal or minimal in its use of drag; an optimal time control law can be developed as can a control law to minimize the duration of non-zero drag.

The control law derived in Chapter 4 assumed a constant density atmosphere. The effect of variations in the atmosphere on formationkeeping with differential drag should be examined. Changes in density from the light to dark side of the earth should be examined as well as changes in density due to altitude. Other causes of non-uniformity in atmospheric density should be examined, such as non-uniform gravity and solar disturbances, and their effect on formationkeeping quantified. Shadowing and its effects should be studied; shadowing occurs when a spacecraft downwind from another spacecraft encounters reduced drag due to the upwind satellite's deflection of molecules.

The effect of changing the angle of attack on the attitude of the satellite should be researched. The change of angle of attack of the drag plate was assumed to be instantaneous in this study; the effect of limits in the plate rotation rate should be determined. The control law used a, 0 and $-a$ as the available values for differential drag; a controller that uses continuous variation in the angle of attack of the drag plate should be designed. The use of differential drag to affect motion in the out-of-plane direction should be examined; a control law for plane changes should be developed.

The minimum value of differential drag for which the control law will work should be found; this will place the upper limit on the altitude at which this method can be used for formationkeeping. The use of differential drag in the formationkeeping of several vehicles to the space station should be studied. The effect of errors in the measurement of relative position, velocity, and acceleration requires examination.

References

[1] Vassar, R.H. and Sherwood, R.B. "Formationkeeping for a Pair of Satellites in a Circular Orbit." *AIAA Journal of Guidance and Control*, March-April 1985: 235-242.

[2] Redding, David C., Adams, Neil J., and Kubiak, Edward T. "Linear-Quadratic Stationkeeping for the STS Orbiter," Charles Stark Draper Laboratory Report CSDL-R-1879, June 1986.

[3] Hollister, Walter M. *The Design of a Control System for the Terminal Phase of a Satellite Rendezvous*. Master of Science Thesis, M.I.T., June 1959.

[4] Hill, George W. "Researches in the Lunar Theory." *American Journal of Mathematics*. Vol. 1, No. 1, 1878: 5-26.

[5] Wheelon, Albert D. "Midcourse and Terminal Guidance." In *Space Technology*. Ed. Seifert, Howard. New York: John Wiley & Sons, 1959.

[6] Clohessy, W.H. and Wiltshire R.S. "Terminal Guidance System for Satellite Rendezvous." *Journal of the Aerospace Science* Sept. 1980: 653-658, 674.

[7] Brockett, Roger W. *Finite Dimensional Linear Systems*. New York: John Wiley & Sons, 1970.

[8] Bryson, A.E. and Ho, Y.C. *Applied Optimal Control*. Waltham, MA: Blaisdell Publishing Company, 1969.

[9] Athans, M. and Falb, P.L. *Optimal Control*. New York: McGraw-Hill, 1966.

[10] Skylab Program Operational Data Books Vols II and IV, NASA MSC-01549, 1971.

[11] Vargas, Tina F. *Attitude Control Augmentation of Spacecraft in Low Earth Orbit Utilising Aerodynamic Forces.* Master of Science Thesis, M.I.T., December 1982.

[12] Gustafson, D. E. and Kriegsman, B. A., "A Guidance and Navigation System for Automatic Stationkeeping in Near-Earth Orbit," Charles Stark Draper Laboratory Report E-2534, August 1970.

Appendix A

Test Results

Case D

The total simulation time for the ideal case is 590.8 minutes; non-zero drag accounts for 287.2 minutes of that time. The detailed simulation took 1061.6 minutes to complete; 267.6 minutes of that time was spent with non-zero drag.

The plots for y vs. x for the ideal and detailed simulations are shown in Figures A.1 and A.2; table A.1 explains the important points for the detailed case while table A.2 does so for the detailed case. The significant differences in the plots are due to the different directions taken by, and the drift rates associated with, the first hat maneuver. Slight differences in the states when the gamma control scheme is entered cause the hat maneuver to move in opposite directions.

Figures A.3 and A.4 show x_1 vs. x_2 for the ideal and detailed cases. These plots show the differences in the first hat maneuver. The oscillation in x_1 in the drift phase of the first hat for the ideal case is caused by the assumption of a linear coordinate system as discussed for case B in Chapter 5.

x_3n vs. x_4n for the ideal and detailed cases are shown in Figures A.5 and A.6. The difference in the apperance between the two plots is mainly due to the longer periods of zero differential drag between points D and E, and H and I on the ideal plot. The control sequence E-F-G, relating to the first hat maneuver in the ideal case, is different by 180 degrees from that of the detailed case; this is expected from hat maneuvers of opposite direction.
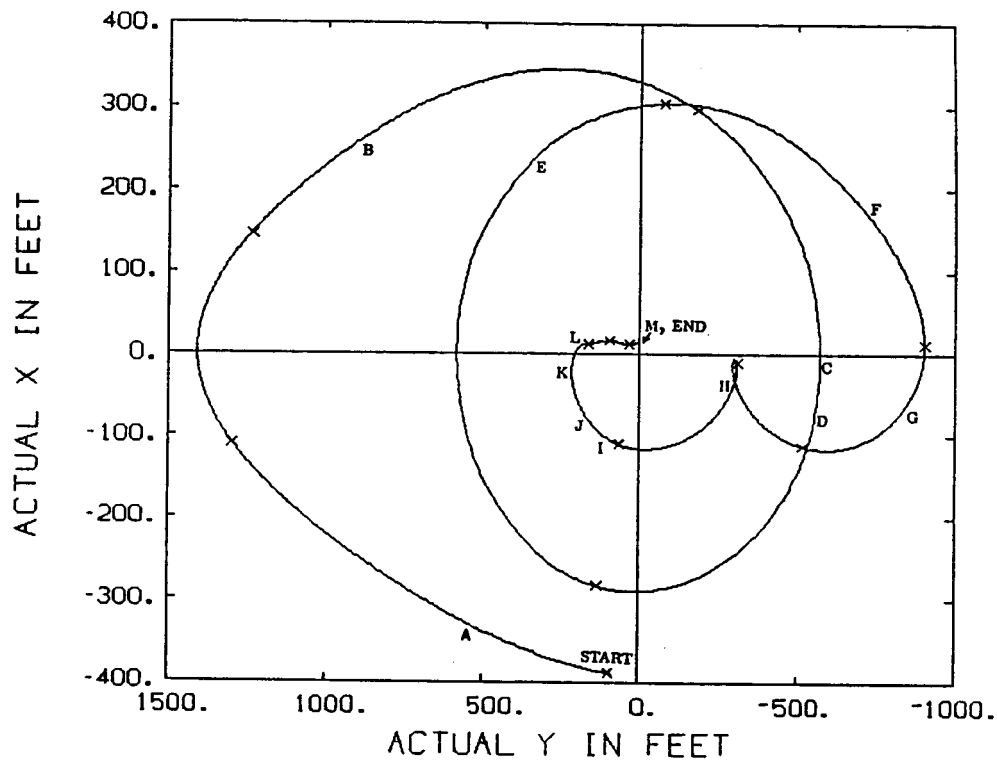
116

Figure A.1: y vs. x for the ideal simulation for case D.

. . .

position	simulation time (min)	switch curve	commanded control	duration of control (min)
START	0.0	–	a=0	16.8
A	16.8	S3	$a < 0$	98.0
B	114.8	S2	$a > 0$	52.4
C	167.2	S1	$a < 0$	4.8
D	172.0	GA	$a = 0$	44.4
E	216.4	GO1	$a < 0$	37.6
F	254.0	GO2	$a > 0$	47.2
G	301.2	GO3	$a = 0$	115.6
H	416.8	S1	$a < 0$	9.6
I	426.4	GA	$a = 0$	2.4
J	428.8	GI1	$a > 0$	16.4
K	445.2	GI2	$a < 0$	19.6
L	464.8	GI3	$a = 0$	124.4
M	589.2	S2	$a > 0$	1.6

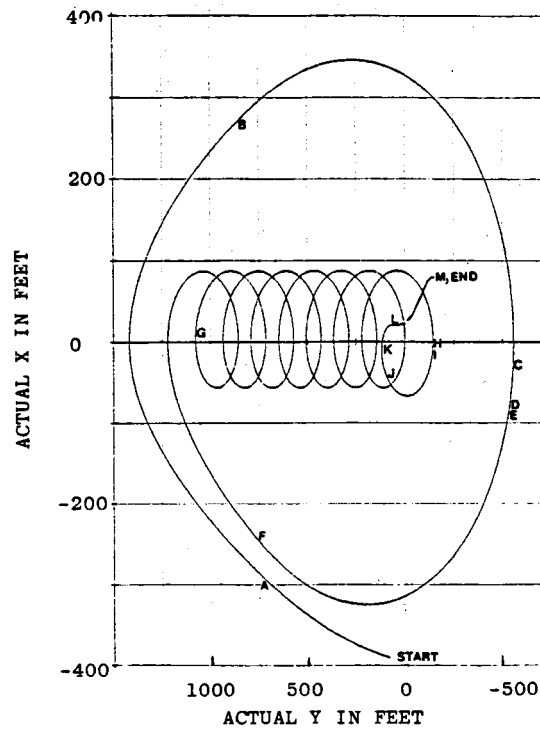Table A.1: Points of importance in the ideal simulation for case D.

Figure A.2: *y vs. x for the detailed simulation for case D.*

position	simulation time (min)	switch curve	commanded control	duration of control (min)
START	0.0	–	$a=0$	16.8
A	16.8	S3	$a < 0$	98.0
B	114.8	S2	$a > 0$	49.2
C	164.0	S1	$a < 0$	1.6
D	165.6	GA	$a = 0$	0.4
E	166.0	GO1	$a > 0$	42.0
F	208.0	GO2	$a < 0$	45.6
G	253.6	GO3	$a = 0$	714.0
H	967.6	S2	$a > 0$	2.0
I	969.6	GA	$a = 0$	35.2
J	1004.8	GI1	$a > 0$	12.4
K	1017.2	GI2	$a < 0$	15.6
L	1032.8	GI3	$a = 0$	27.6
M	1060.4	S2	$a > 0$	1.2

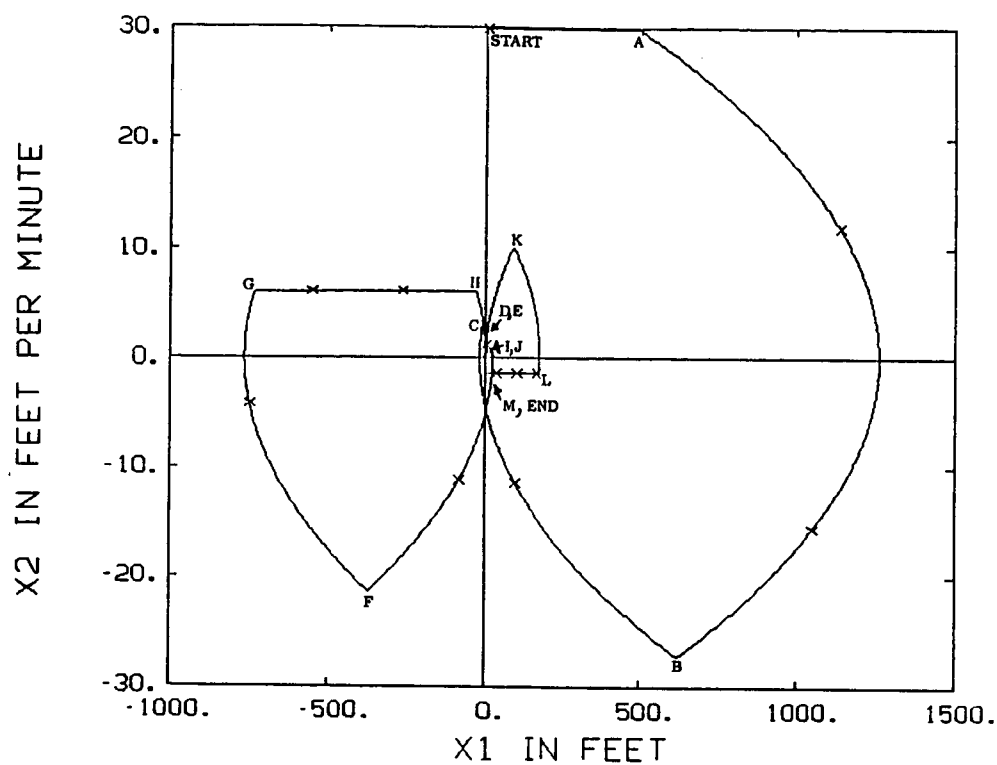Table A.2: *Points of importance in the detailed simulation for case D.*

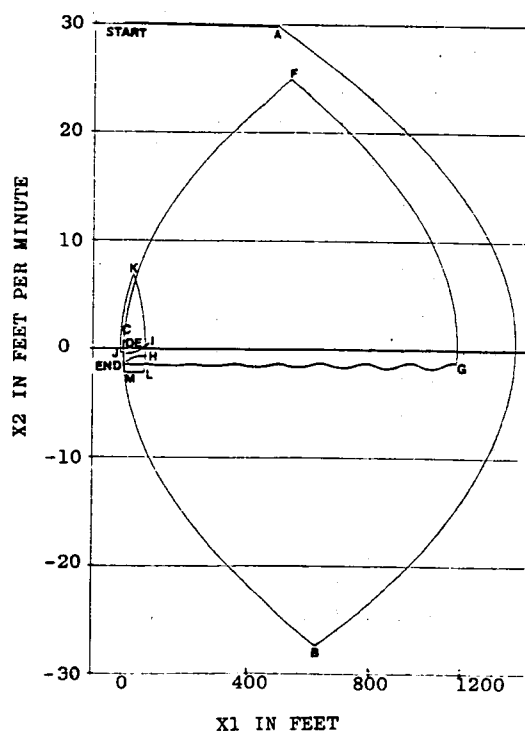**Figure A.3:** x_1 vs. x_2 for the ideal simulation for case D.

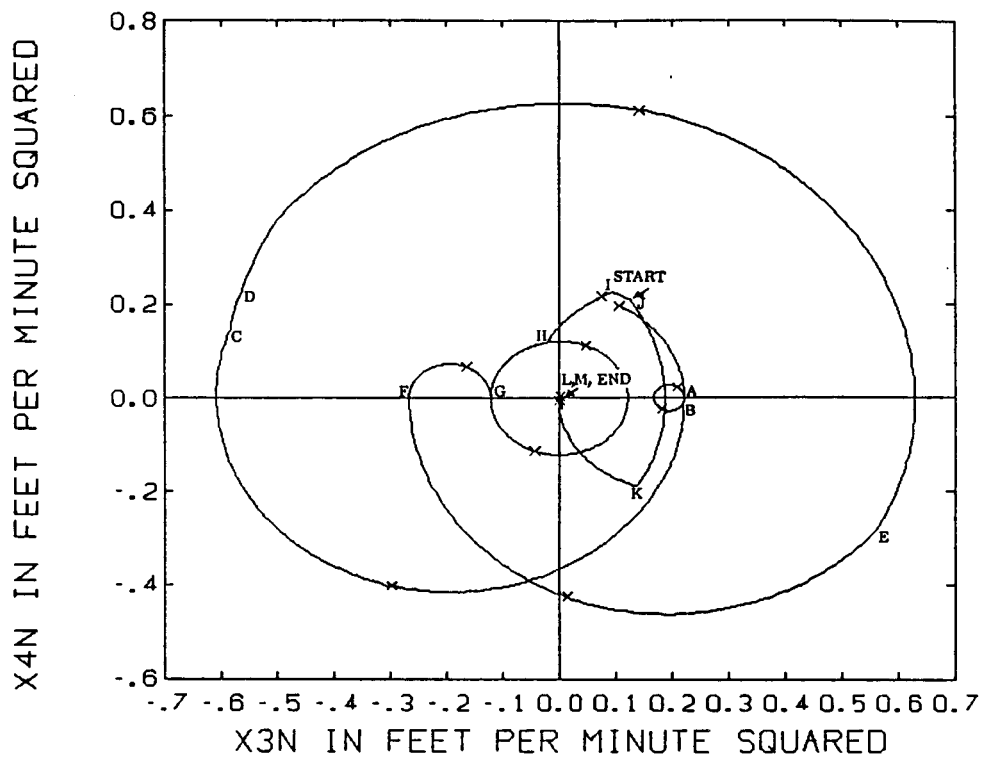**Figure A.4:** x_1 vs. x_2 for the detailed simulation for case D.

119

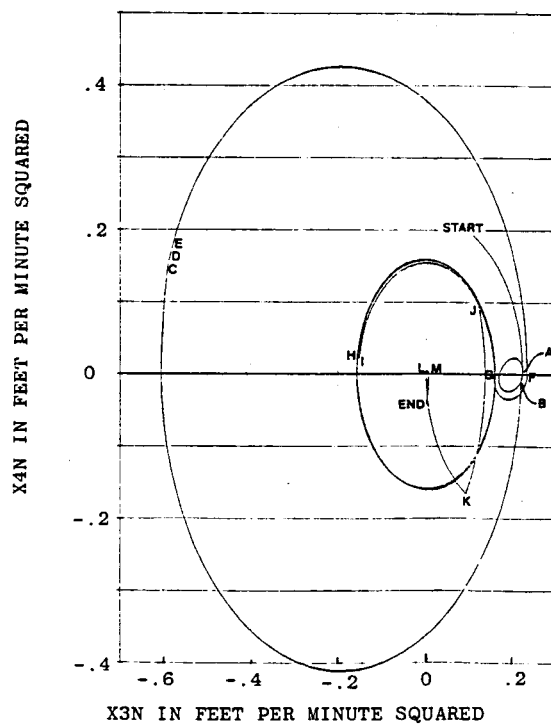Figure A.5: x_3n vs. x_4n for the ideal simulation for case D.

Figure A.6: x_3n vs. x_4n for the detailed simulation for case D.

120

Case E

The ideal simulation has 138.8 minutes of commanded non-zero drag in a total simulation time of 723.2 minutes; the detailed simulation requires the same duration of non-zero drag but has a shorter simulation time of 617.2 minutes.

Figures A.7 and A.8 of y vs. x for the ideal and detailed cases match nicely. The slightly longer duration of the drift phase of the hat maneuver accounts for the extra oscillation between points G and H in the ideal plot. Tables A.3 and A.4 explain the important points of the ideal and detailed simulations.

Figures A.9 and A.10 show x_1 vs. x_2 for the ideal and detailed simulations; x_3n vs. x_4n is plotted for the ideal and detailed cases in Figures A.11 and A.12. All corresponding plots match well.
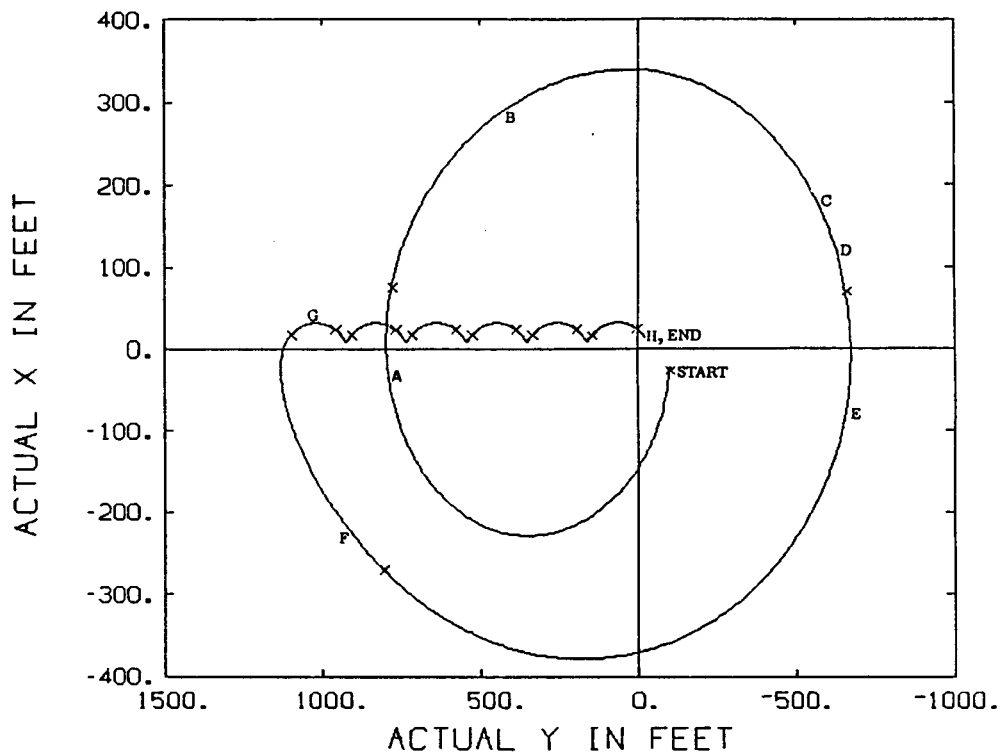
Figure A.7: *y vs. x for the ideal simulation for case E.*

position	simulation time (min)	switch curve	commanded control	duration of control (min)
START	0.0	–	$a=0$	44.8
A	44.8	S3	$a < 0$	18.4
B	63.2	S2	$a > 0$	26.0
C	89.2	S1	$a < 0$	2.8
D	92.0	GA	$a = 0$	10.0
E	102.0	GO1	$a > 0$	42.4
F	144.4	GO2	$a < 0$	46.4
G	190.8	GO3	$a = 0$	529.6
H	720.4	S2	$a > 0$	2.8

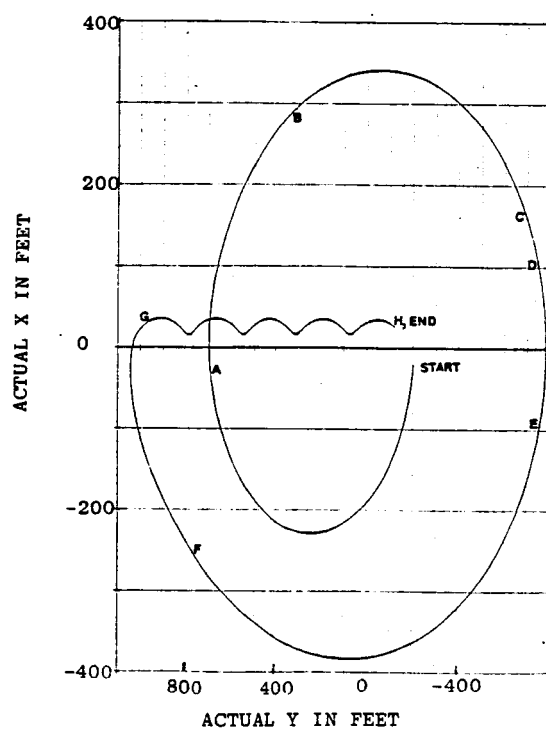Table A.3: *Points of importance in the ideal simulation of case E.*

Figure A.8: *y vs. x for the detailed simulation for case E.*

position	simulation time (min)	switch curve	commanded control	duration of control (min)
START	0.0	–	a=0	44.8
A	44.8	S3	$a < 0$	18.4
B	63.2	S2	$a > 0$	26.8
C	90.0	S1	$a < 0$	3.2
D	93.2	GA	$a = 0$	9.2
E	102.4	GO1	$a > 0$	42.0
F	144.4	GO2	$a < 0$	47.2
G	191.6	GO3	$a = 0$	424.4
H	616.0	S2	$a > 0$	1.2

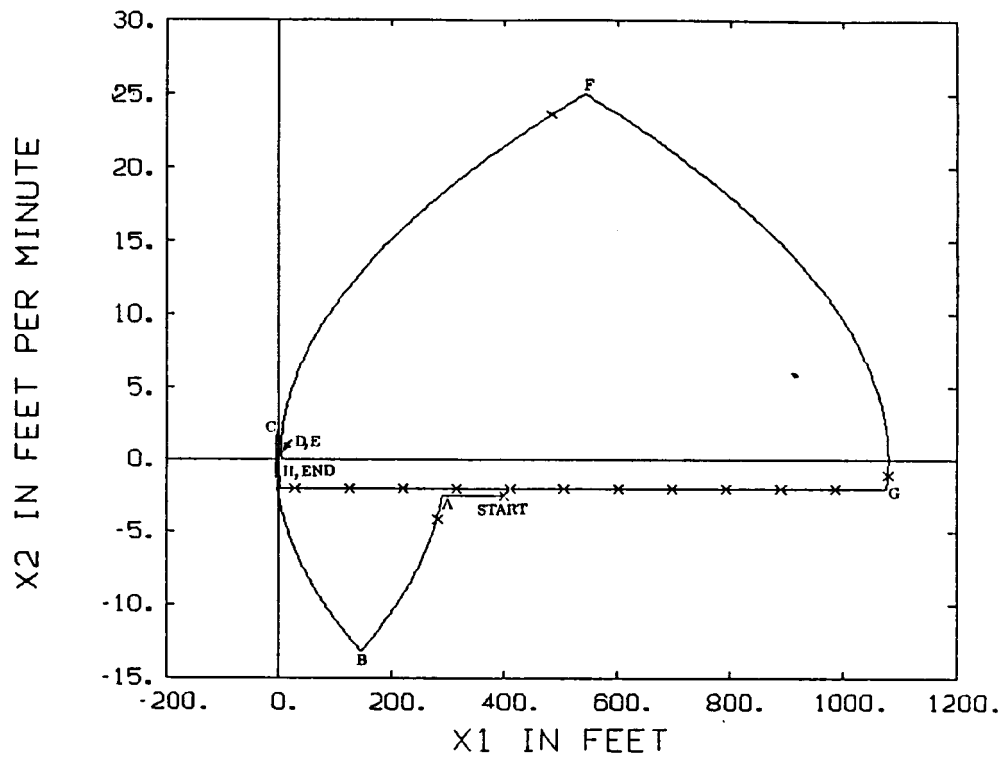Table A.4: *Points of importance in the detailed simulation of case E.*

123

Figure A.9: x_1 vs. x_2 for the ideal simulation for case E.
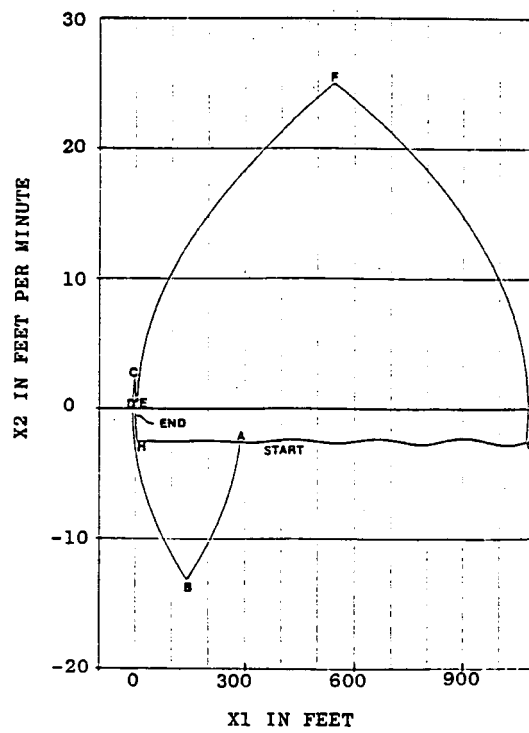

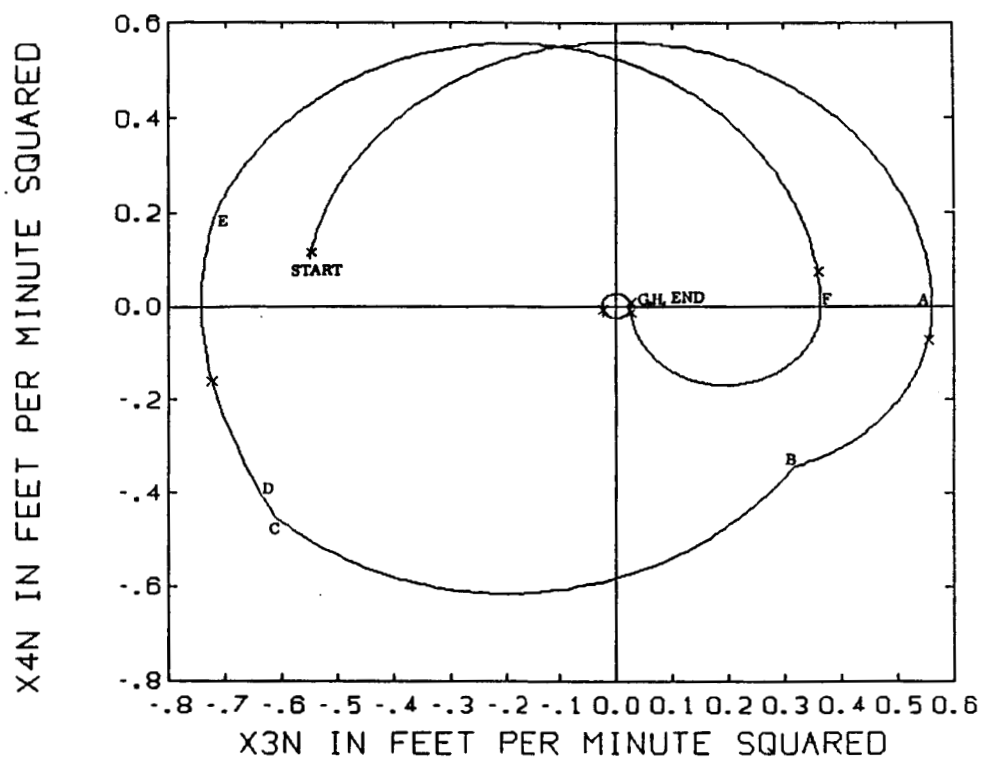Figure A.10: x_1 vs. x_2 for the detailed simulation for case E.

124

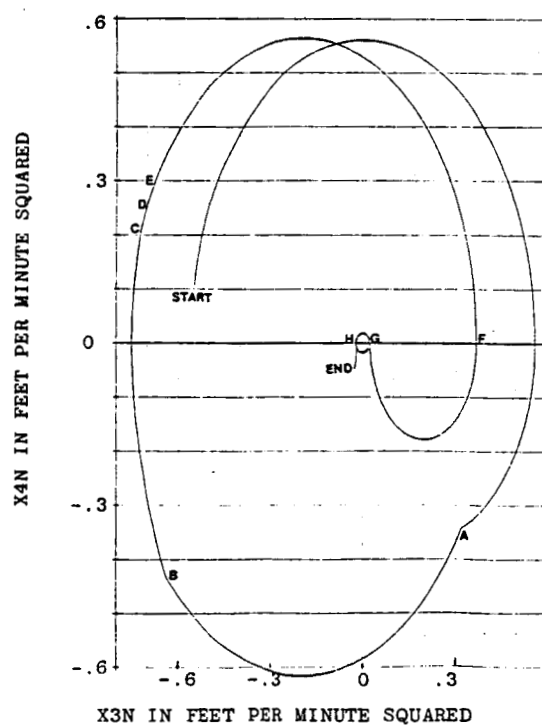Figure A.11: x_3n vs. x_4n for the ideal simulation for case E.

Figure A.12: x_3n vs. x_4n for the detailed simulation for case E.

125

Case F

The total simulation time of the ideal case is 1406.8 minutes with 796.4 minutes of non-zero drag. The total simulation time of the detailed simulation is 1245.2 minutes where 939.6 minutes use non-zero differential drag.

The plots of x vs. y for the ideal and detailed simulations are shown in Figures A.13 and A.14. The overall shape of the two plots is similar, though there are differences from point C to the end of the test run. The important points of the ideal and detailed simulations are explained in tables A.5 and A.6.

Figures A.15 and A.16 show the plots of x_1 vs. x_2 for the ideal and detailed simulations. The plot for the detailed simulation is not smooth in its trajectory from the start of the simulation almost to point C; these are removed with a switch to a curvilinear coordinate system as explained in Section 5.2.1. The detailed simulation also allows two sawtooth maneuvers compared to one allowed by the ideal simulation.

The plots of x_3n vs. x_4n for the ideal and detailed simulations are shown in Figures A.17 and A.18. These plots do not match. The plot for the ideal case has the tilted ellipse as explained in Section 5.2.1 for case B.

Case F was tested using the detailed simulation with curvilinear coordinates. The plot of x vs. y is shown in Figure A.19, x_1 vs. x_2 is plotted in Figure A.20, and x_3n vs. x_4n is depicted in Figure A.21. The important points of this simulation are explained in table A.7. The total simulation time for this case is 1253.2 minutes with 822.8 of those minutes using non-zero differential drag.

The plots of y vs. x for the ideal and curvilinear detailed simulation match exactly. The plots for x_1 vs. x_2 are also extremely similar. The plots of x_3n vs. x_4n would look very close if not for the scaling factors of the different plotting routines.

Figure A.13: *y vs. x for the ideal simulation for case F.*

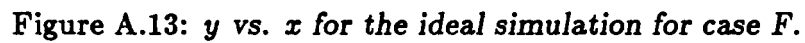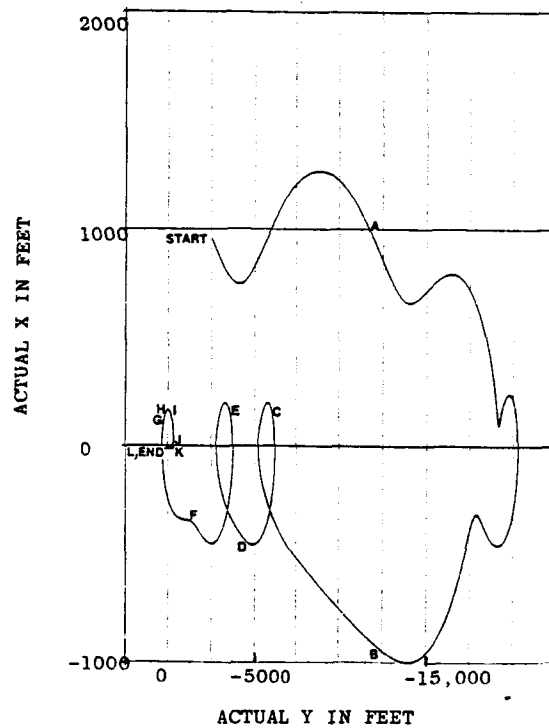| position	simulation time (min)	switch curve	commanded control	duration of control (min)
START	0.0	–	a=0	92.0
A	92.0	S4	$a > 0$	331.2
B	423.2	S3	$a < 0$	190.8
C	614.0	S4	$a > 0$	124.8
D	738.8	S1	$a < 0$	93.6
E	832.4	GA	$a = 0$	33.6
F	866.0	GI1	$a > 0$	26.4
G	892.4	GI2	$a < 0$	28.8
H	921.2	GI3	$a = 0$	484.8
I	1406.0	S2	$a > 0$	0.8

Table A.5: *Points of importance in the ideal simulation of case F.*

128

Figure A.14: *y vs. x for the detailed simulation for case F.*

position	simulation time (min)	switch curve	commanded control	duration of control (min)
START	0.0	–	a=0	92.4
A	92.4	S4	$a > 0$	330.0
B	422.4	S3	$a < 0$	184.0
C	606.4	S4	$a > 0$	95.2
D	701.6	S3	$a < 0$	95.2
E	796.8	S4	$a > 0$	102.4
F	899.2	S1	$a < 0$	81.6
G	980.8	S2	$a > 0$	4.8
H	985.6	GA	$a = 0$	11.6
I	997.2	GI1	$a < 0$	21.2
J	1018.4	GI2	$a > 0$	24.0
K	1042.4	GI3	$a = 0$	201.6
L	1244.0	S1	$a < 0$	1.2

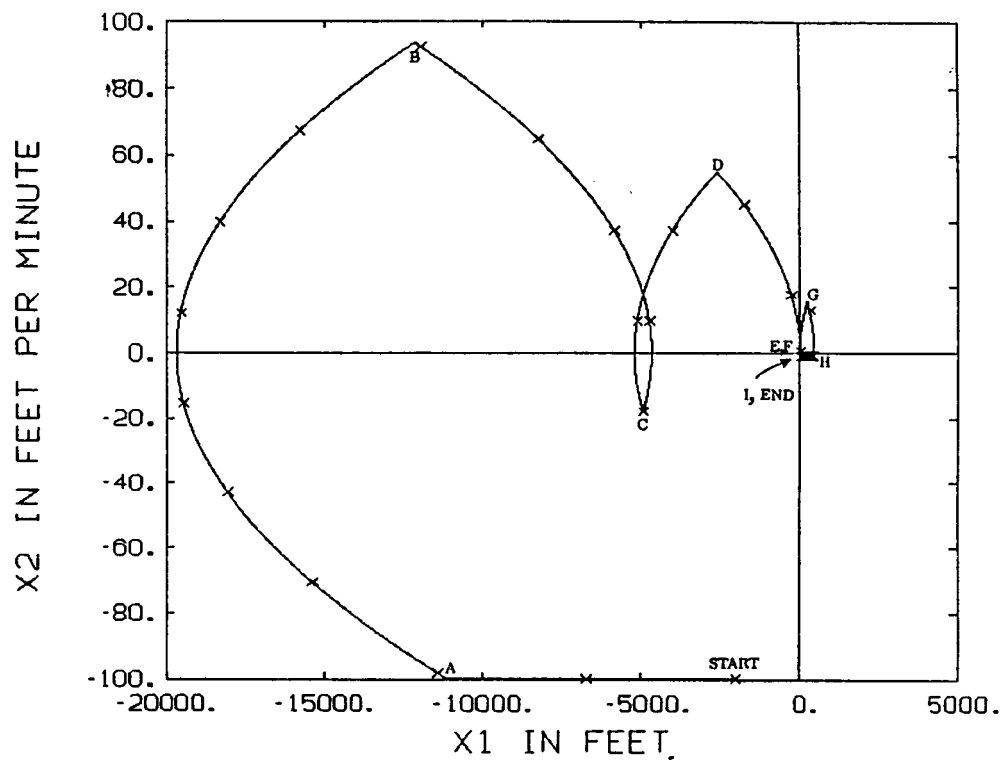Table A.6: *Points of importance in the detailed simulation of case F.*

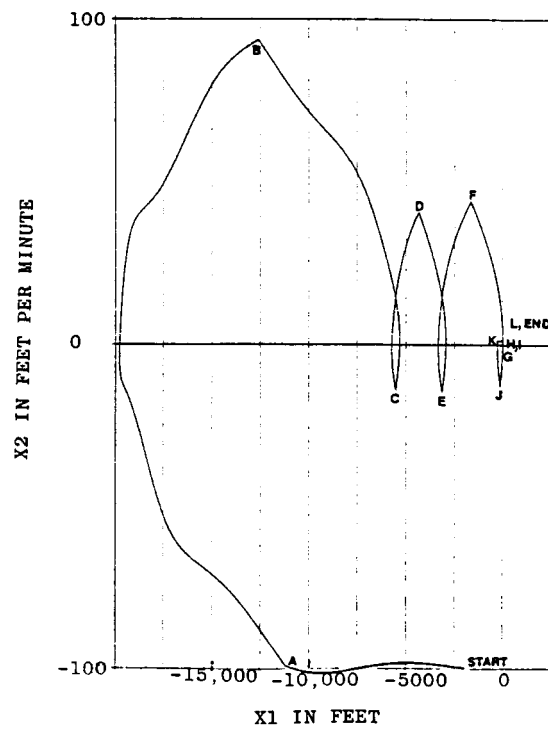Figure A.15: x_1 vs. x_2 for the ideal simulation for case F.

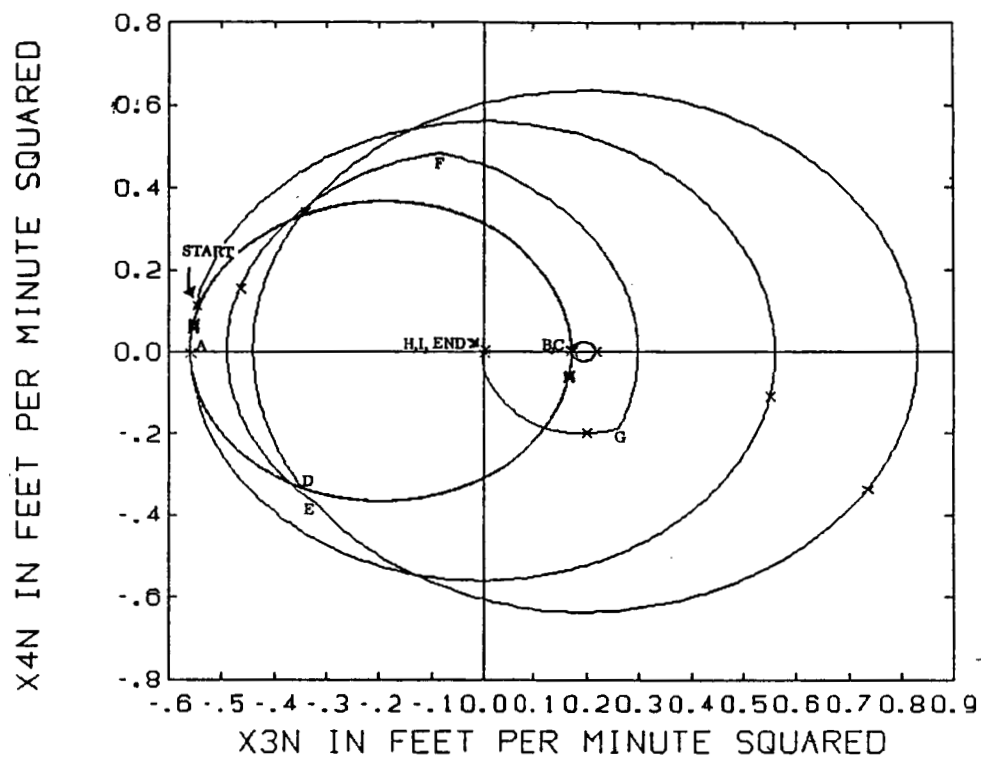Figure A.16: x_1 vs. x_2 for the detailed simulation for case F.

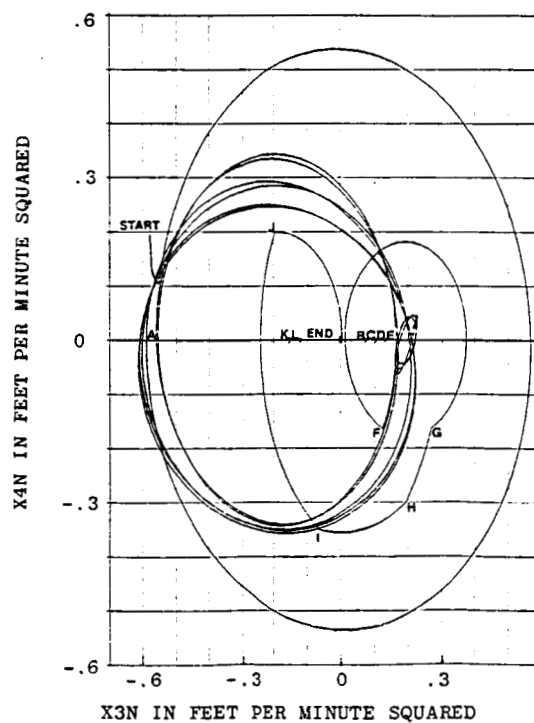Figure A.17: x_3n vs. x_4n for the ideal simulation for case F.

Figure A.18: x_3n vs. x_4n for the detailed simulation for case F.
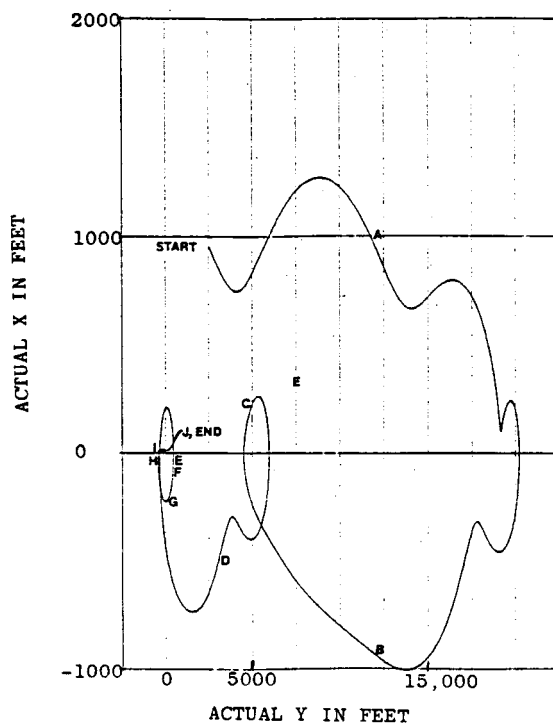
131

Figure A.19: *y vs. x for the for case F using the detailed simulation with curvilinear coordinates.*

position	simulation time (min)	switch curve	commanded control	duration of control (min)
START	0.0	–	a=0	92.4
A	92.4	S4	$a > 0$	331.6
B	424.0	S3	$a < 0$	196.4
C	620.4	S4	$a > 0$	132.4
D	752.8	S1	$a < 0$	101.2
E	854.0	S2	$a > 0$	4.0
F	858.0	GA	$a = 0$	15.6
G	873.6	GI1	$a > 0$	27.2
H	900.8	GI2	$a < 0$	28.8
I	929.6	GI3	$a = 0$	322.4
J	1252.0	S2	$a > 0$	1.2

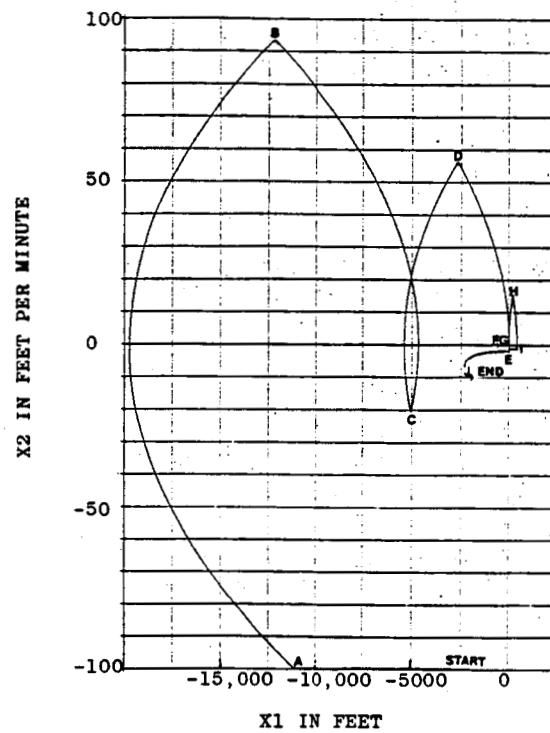Table A.7: *Points of importance in the detailed simulation using curvilinear coordinates for case F.*

132

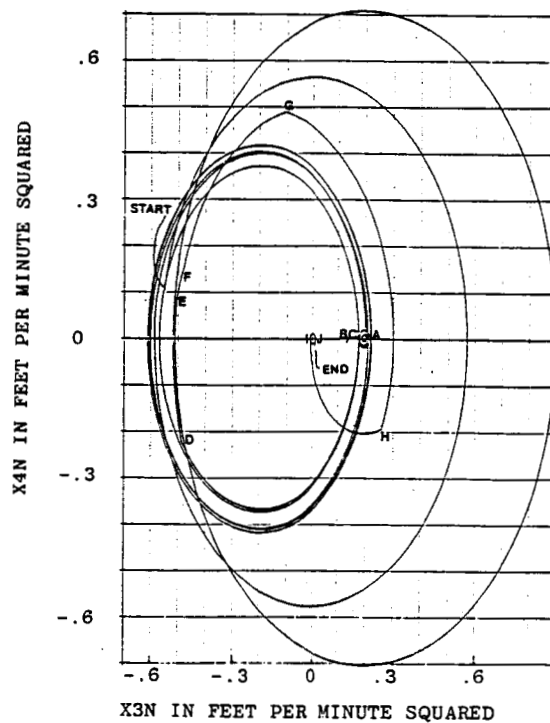Figure A.20: x_1 vs. x_2 for case F using the detailed simulation with curvilinear coordinates.

Figure A.21: x_3n vs. x_4n for case F using the detailed simulation with curvilinear coordinates.

Case G

The ideal simulation ended after 542.8 minutes; 170.0 of those minutes were spent with a commanded non-zero drag. The detailed simulation ended after 508.0 minutes with 168.8 minutes of non-zero drag.

The plots of y vs. x for the ideal and detailed simulations are similar and are shown in Figures A.22 and A.23. The corresponding important points of these simulations are explained in tables A.8 and A.9.

The plots of x_1 vs. x_2 for the different simulations are similar, though the trajectory for the detailed simulation is not smooth between the start of the simulation and point A, and from point G to mid-way to point F. These plots are shown in Figures A.24 and A.25.

Figures A.26 and A.27 show x_3n vs. x_4n for the ideal and detailed simulations. The plots are similar.
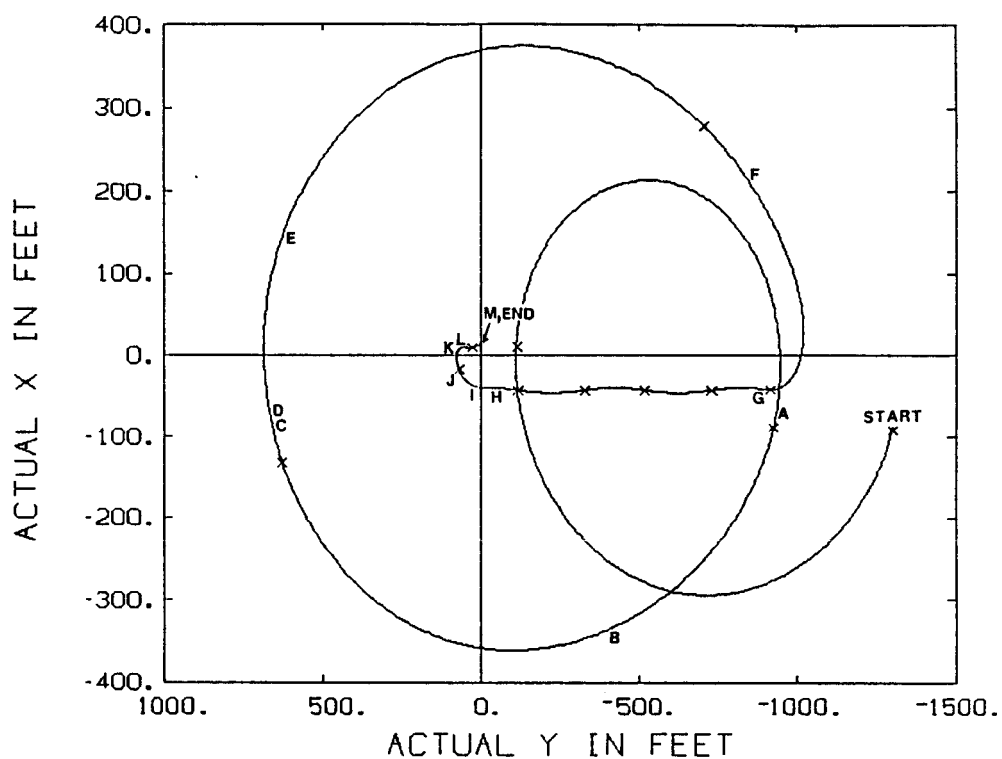
Figure A.22: *y vs. x for the ideal simulation for case G.*

position	simulation time (min)	switch curve	commanded control	duration of control (min)
START	0.0	–	$a=0$	92.0
A	92.0	S4	$a > 0$	21.2
B	113.2	S1	$a < 0$	32.8
C	146.0	S2	$a > 0$	4.0
D	150.0	GA	$a = 0$	4.8
E	154.8	GO1	$a < 0$	38.8
F	193.6	GO2	$a > 0$	46.8
G	240.4	GO3	$a = 0$	210.4
H	450.8	S1	$a < 0$	6.4
I	457.2	GA	$a = 0$	19.2
J	476.4	GI1	$a > 0$	8.0
K	484.4	GI2	$a < 0$	10.8
L	495.2	GI3	$a = 0$	46.4
M	541.6	S2	$a > 0$	1.2

Table A.8: *Points of importance in the ideal simulation of case G.*
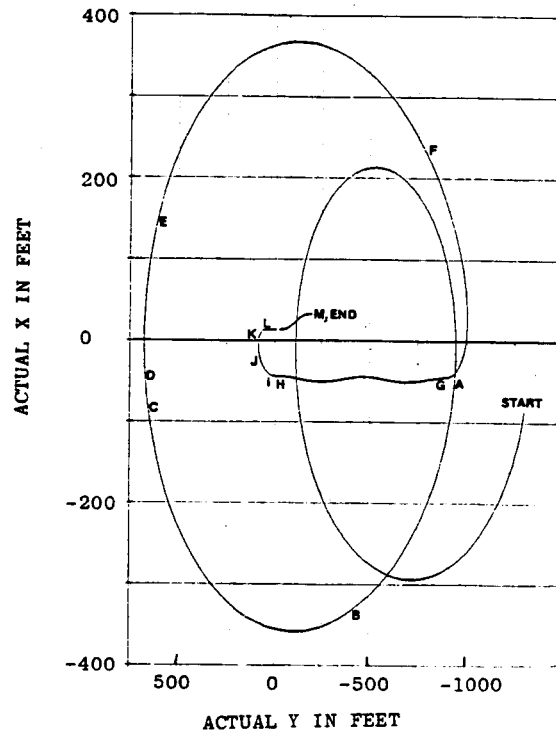
136

Figure A.23: *y vs. x* for the detailed simulation for case *G*.

position	simulation time (min)	switch curve	commanded control	duration of control (min)
START	0.0	–	$a=0$	92.4
A	92.4	S4	$a > 0$	20.8
B	113.2	S1	$a < 0$	30.8
C	144.0	S2	$a > 0$	2.4
D	146.4	GA	$a = 0$	8.8
E	155.2	GO1	$a < 0$	38.4
F	193.6	GO2	$a > 0$	47.2
G	240.8	GO3	$a = 0$	181.2
H	422.0	S1	$a < 0$	7.6
I	429.6	GA	$a = 0$	16.4
J	446.0	GI1	$a > 0$	8.8
K	454.8	GI2	$a < 0$	11.6
L	466.4	GI3	$a = 0$	40.4
M	506.8	S2	$a > 0$	1.2

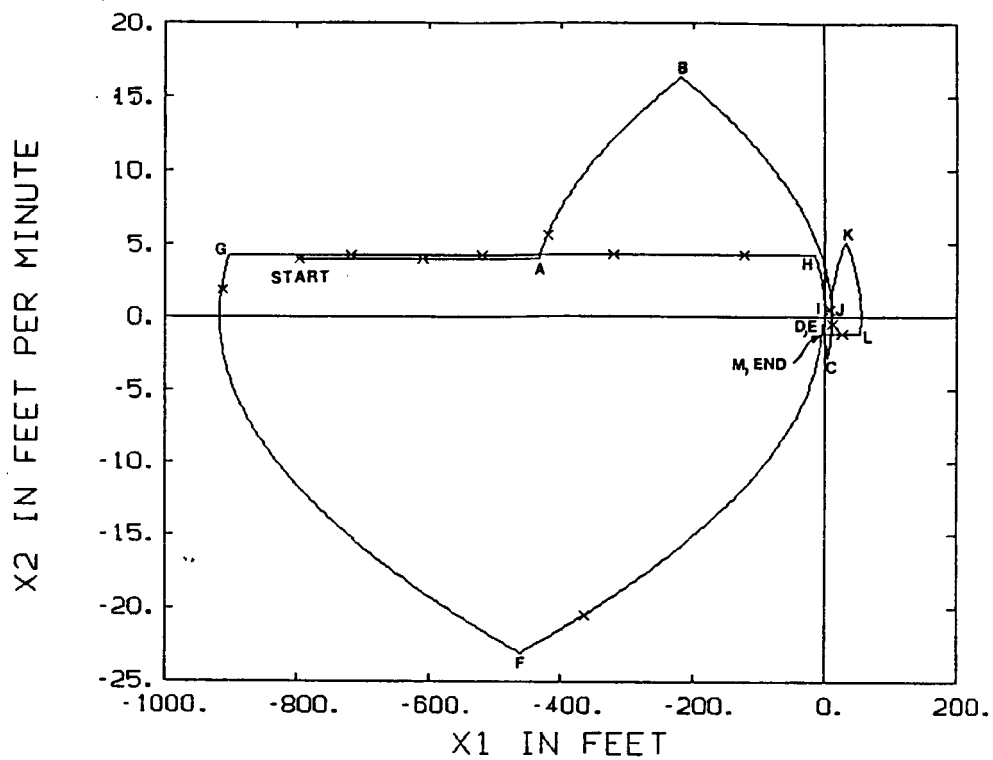Table A.9: *Points of importance in the detailed simulation of case G.*

137

Figure A.24: x_1 vs. x_2 for the ideal simulation for case G.
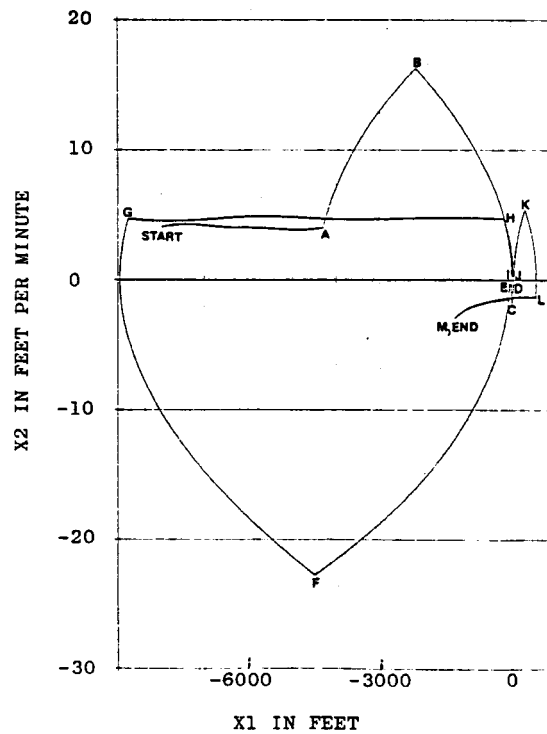

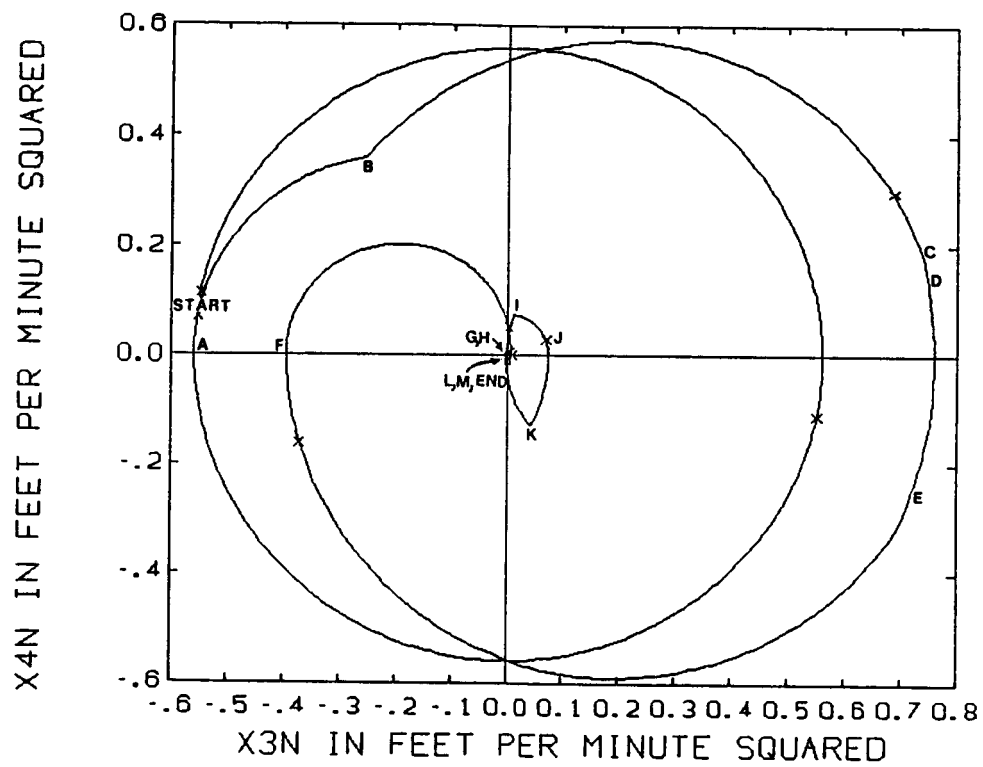**Figure A.25:** x_1 vs. x_2 for the detailed simulation for case G.

138

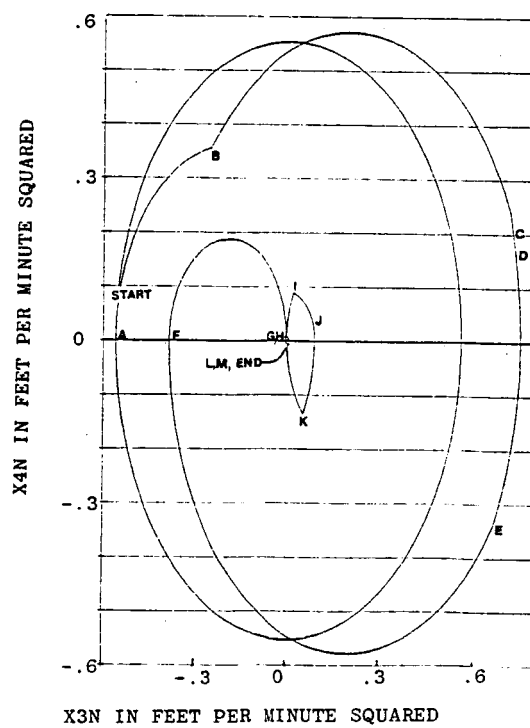Figure A.26: x_3n vs. x_4n for the ideal simulation for case G.

Figure A.27: x_3n vs. x_4n for the detailed simulation for case G.

Case H

The ideal simulation ended after 632.8 minutes; the time of commanded non-zero differential drag is 284.8 minutes. The total detailed simulation time is 637.2 minutes with 307.2 minutes spent with non-zero differential drag.

Figures A.28 and A.29 plot y vs. x for the ideal and detailed simulations. Tables A.10 and A.11 explain the important points of these plots. The y vs. x values for the ideal and detailed simulations match well. The same is true for the plots of x_1 vs. x_2 shown in Figures A.30 and A.31.

The differences in the plots of x_3n vs. x_4n shown in Figures A.32 and A.33 relate to C being the arrival point at the gamma control scheme for the ideal simulation, and D being the arrival point for the detailed simulation. A slight difference in position causes the detailed simulation to miss the origin when it is on the switch curve S1, and thereby use the switch curve S2 to reach the origin.
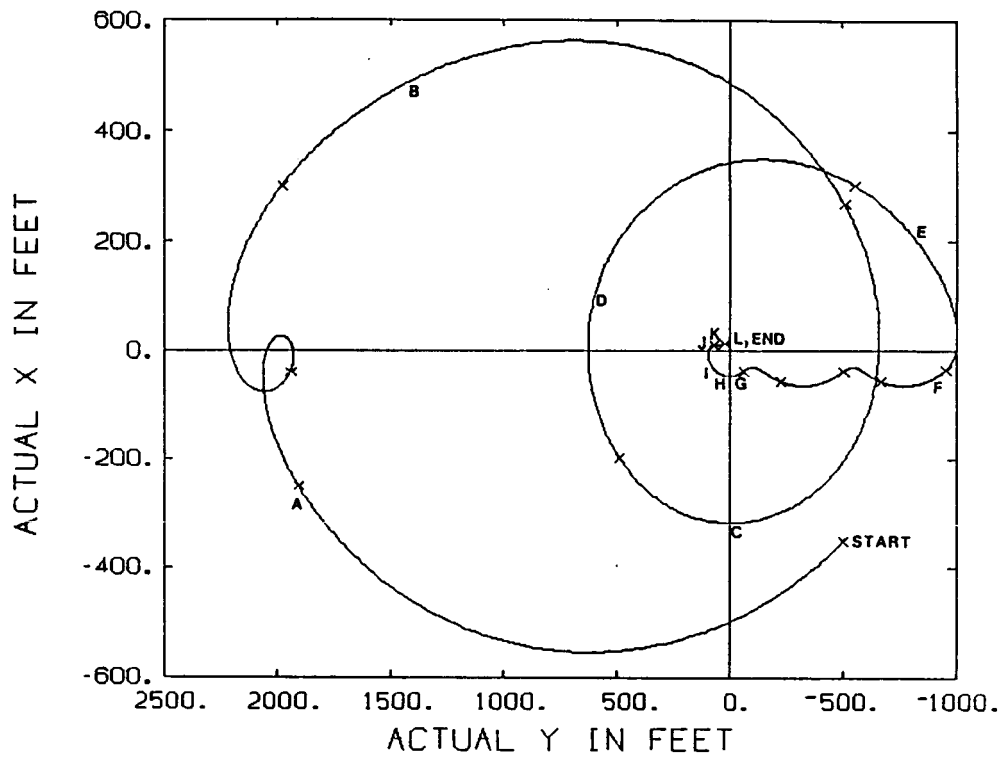
Figure A.28: *y vs. x for the ideal simulation for case H.*

position	simulation time (min)	switch curve	commanded control	duration of control (min)
START	0.0	–	a=0	44.8
A	44.8	S3	$a < 0$	111.2
B	156.0	S2	$a > 0$	59.2
C	215.2	GA	$a = 0$	38.4
D	253.6	GO1	$a < 0$	38.0
E	291.6	GO2	$a > 0$	46.8
F	338.4	GO3	$a = 0$	183.6
G	522.0	S1	$a < 0$	7.2
H	529.2	GA	$a = 0$	21.6
I	550.8	GI1	$a > 0$	9.2
J	560.0	GI2	$a < 0$	12.0
K	572.0	GI3	$a = 0$	59.6
L	631.6	S2	$a > 0$	1.2

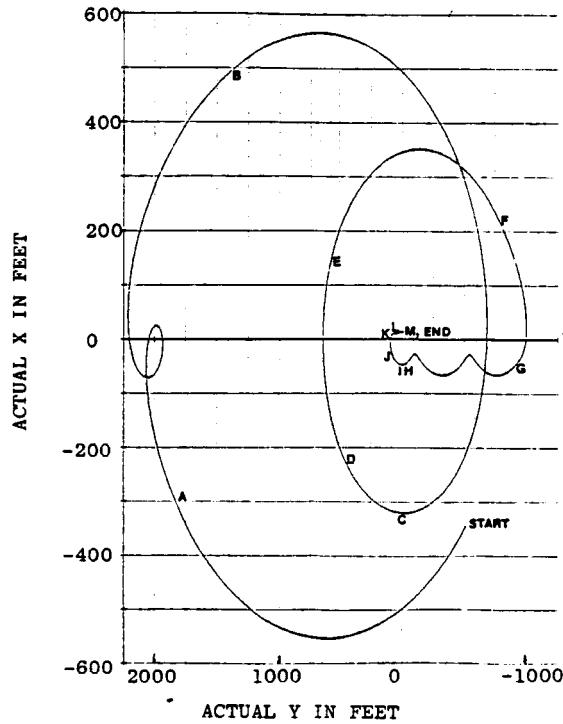Table A.10: *Points of importance in the ideal simulation of case H.*

142

Figure A.29: *y vs. x for the detailed simulation for case H.*

position	simulation time (min)	switch curve	commanded control	duration of control (min)
START	0.0	–	a=0	44.8
A	44.8	S3	$a < 0$	111.6
B	156.4	S2	$a > 0$	68.0
C	224.4	S1	$a < 0$	12.4
D	236.8	GA	$a = 0$	18.4
E	255.2	GO1	$a < 0$	38.4
F	293.6	GO2	$a > 0$	47.2
G	340.8	GO3	$a = 0$	184.4
H	525.2	S1	$a < 0$	7.2
I	532.4	GA	$a = 0$	22.4
J	554.8	GI1	$a > 0$	9.2
K	564.0	GI2	$a < 0$	12.0
L	576.0	GI3	$a = 0$	60.0
M	636.0	S2	$a > 0$	1.2

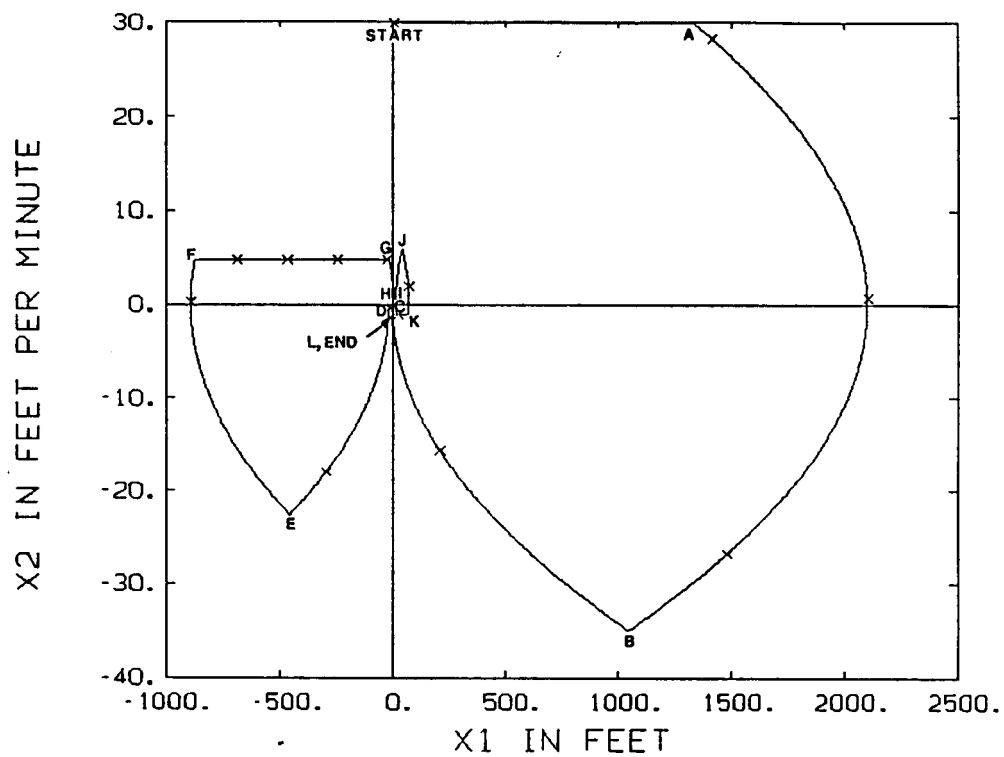Table A.11: *Points of importance in the detailed simulation of case H.*

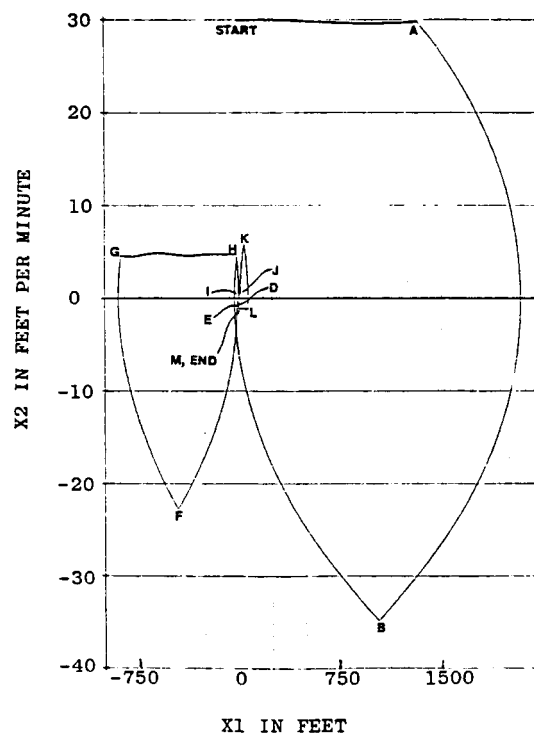Figure A.30: x_1 vs. x_2 for the ideal simulation for case H.

Figure A.31: x_1 vs. x_2 for the detailed simulation for case H.
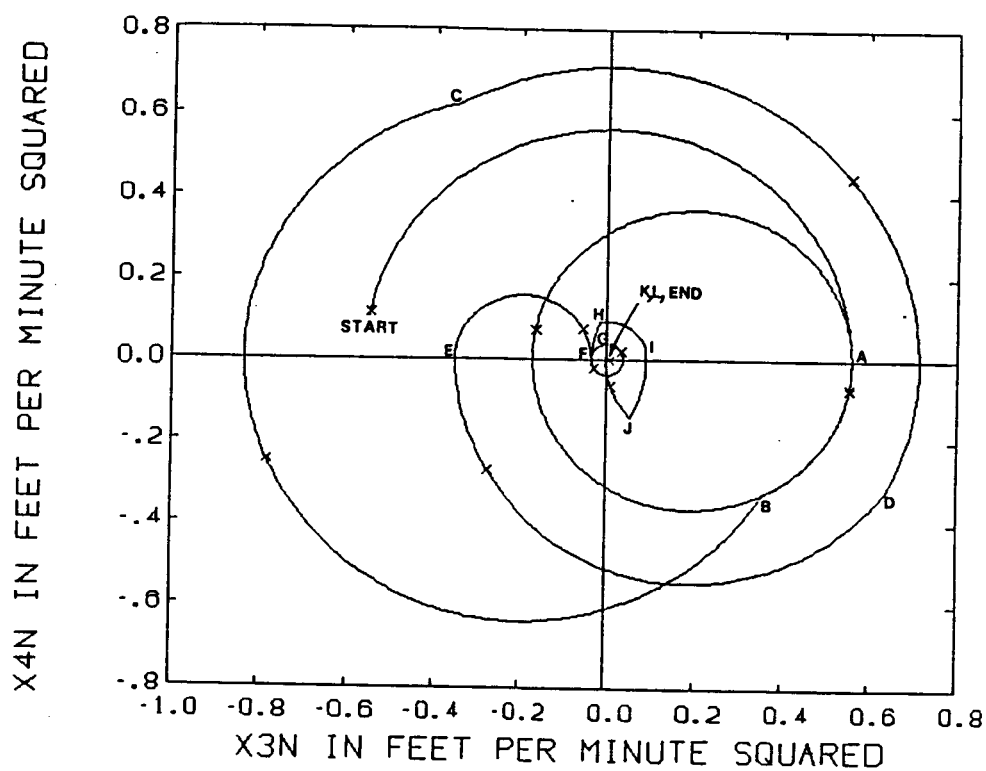
144

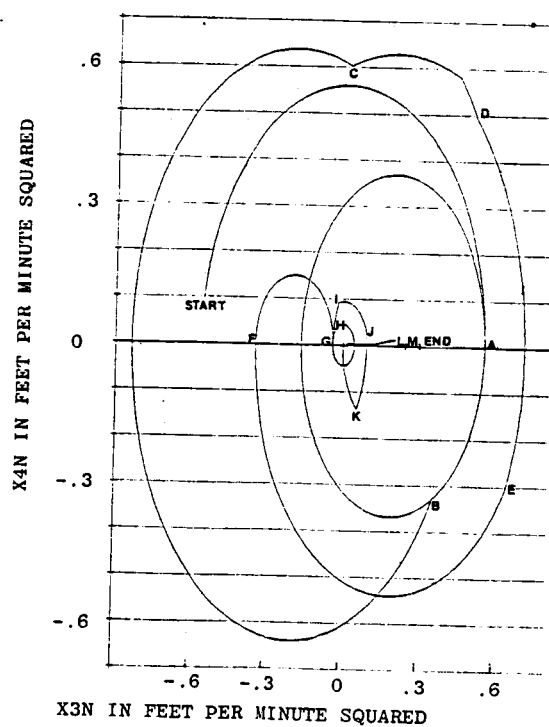Figure A.32: x_3n vs. x_4n for the ideal simulation for case H.

Figure A.33: x_3n vs. x_4n for the detailed simulation for case H.